Supporting Information

An Electrophilic Natural Product Provides a Safe and Robust Odor Neutralization Approach to Counteract Malodorous Organosulfur Metabolites Encountered in Skunk Spray

Lin Du,[†,] Charissa Munteanu,[‡] Jarrod B. King,[†] Doug E. Frantz, [‡] Robert H. Cichewicz[*,†]

[†]Natural Products Discovery Group, Institute for Natural Products Applications and Research Technologies, Department of Chemistry & Biochemistry, Stephenson Life Science Research Center, University of Oklahoma, 101 Stephenson Parkway, Norman, Oklahoma 73019, United States.

[§]Department of Chemistry, The University of Texas at San Antonio, San Antonio, Texas 78249, United States.

List of Contents

	Synthesis of the pericosine A analogs **19** and **20**	S5
Table S1	Crystal data and structure refinement for compound **3**	S9
Table S2	Calculated carbon chemical shifts of selected carbon atoms for the C-6 epimers of **7**, **8**, and **12**	S10
Table S3	The results of the AMES II™ assay of **4**	S11
Figure S1	Structures of compounds **1**-**36**	S12
Figure S2	Comparison of the ^{1}H (A) and ^{13}C (B) NMR spectra of Chloramine-T (blue) and Product A (red, residue after total evaporation of solvent was measured	S13
Figure S3	The fungal metabolite pericosine A (**4**) reacts with natural and synthetic nucleophiles to form pericosine-nucleophile adducts	S14
Figure S4	LCMS analysis for the reactions of pericosine A (**4**) with selected sulfur-containing compounds (**1**, **2**, **5**, and **6**)	S15
Figure S5	Determining the absolute configuration of **7**, **8**, and **12**	S16
Figure S6	Investigating the mechanism of the formation of **7**	S17
Figure S7	The mechanism of Et_3N-catalyzed formation of **8** from the reaction between pericosine A (**4**) and 4-bromo-alpha-toluene thioacetate (**2**)	S18
Figure S8	LCMS analysis of the pericosine analogs **4**, **19** and **20** (A) and the reactions of **19** and **20** with sulfur-containging compounds **1** and **2** in 50% MeOH with the presence of Et_3N (B)	S19
Figure S9	Comparison (A) and principle components analysis (PCA) (B) of the $^{3}J_{H,H}$ coupling constants of **19**, **20**, **6-*epi*-19**, **6-*epi*-20**, and **22**-**28**.	S20
Figure S10	Comparing the ^{13}C chemical shifts of **19**, **20**, **6-*epi*-19**, **6-*epi*-20**, and **23**-**28**	S21
Figure S11	Comparing the $^{3}J_{H,H}$ coupling constants of **21** with selected model compounds	S22
Figure S12	Investigating the mechanism of Et_3N-catalyzed formation of **23**-**25** from the reactions between **19** and **1**	S23
Figure S13	Catalytic effectts of selected basic compounds in the reactions between **4** and **2**	S24
Figure S14	Spermine (**29**)-catalyzed reactions of pericosine A (**4**)	S25
Figure S15	Generating the TFA salt of **30** (**TFA-30**)	S26
Figure S16	Investigating the mechanism of spermine-catalyzed reaction between **4** and **2** in 50% PG	S27
Figure S17	LCMS analysis of the reactions between skunk essence and thiol-reactive compounds (**4**, **19**, **20**, and chloramine-T)	S28
Figure S18	Optimized geometries, relative energies, and Boltzmann populations of the calculated lowest-energy conformers of **7a** at the 6-311+G(2d,p) level in gas phase	S29
Figure S19	Optimized conformers of **7b** at the 6-311+G(2d,p) level in gas phase	S30
Figure S20	Optimized conformers of **8a** at the 6-311+G(2d,p) level in gas phase	S31
Figure S21	Optimized conformers of **8b** at the 6-311+G(2d,p) level in gas phase	S32
Figure S22	Optimized conformers of **12a** at the 6-31G(d,p) level in gas phase	S33
Figure S23	Optimized conformers of **12b** at the 6-31G(d,p) level in gas phase	S34
Figure S24	^{1}H NMR (400 MHz, methanol-d_4, 25 ℃) spectrum of compound **3**	S35
Figure S25	^{13}C NMR (100 MHz, methanol-d_4, 25 ℃) spectrum of compound **3**	S36
Figure S26	^{1}H NMR (400 MHz, $CDCl_3$, 25 ℃) spectrum of compound **7**	S37
Figure S27	^{13}C NMR (100 MHz, $CDCl_3$, 25 ℃) spectrum of compound **7**	S38
Figure S28	^{1}H-^{1}H COSY (400 MHz, $CDCl_3$, 25 ℃) spectrum of compound **7**	S39
Figure S29	HSQC (400 MHz, $CDCl_3$, 25 ℃) spectrum of compound **7**	S40
Figure S30	HMBC (400 MHz, $CDCl_3$, 25 ℃) spectrum of compound **7**	S41
Figure S31	^{1}H NMR (400 MHz, $CDCl_3$, 25 ℃) spectrum of compound **8**	S42
Figure S32	^{13}C NMR (100 MHz, $CDCl_3$, 25 ℃) spectrum of compound **8**	S43
Figure S33	^{1}H-^{1}H COSY (400 MHz, $CDCl_3$, 25 ℃) spectrum of compound **8**	S44

Figure S34	HSQC (400 MHz, $CDCl_3$, 25 ℃) spectrum of compound **8**	S45
Figure S35	HMBC (400 MHz, $CDCl_3$, 25 ℃) spectrum of compound **8**	S46
Figure S36	^{1}H NMR (500 MHz, methanol-d_4, 25 ℃) spectrum of compound **11**	S47
Figure S37	^{13}C NMR (125 MHz, methanol-d_4, 25 ℃) spectrum of compound **11**	S48
Figure S38	^{1}H-^{1}H COSY (500 MHz, methanol-d_4, 25 ℃) spectrum of compound **11**	S49
Figure S39	HMBC (500 MHz, methanol-d_4, 25 ℃) spectrum of compound **11**	S50
Figure S40	^{1}H NMR (500 MHz, methanol-d_4, 25 ℃) spectrum of compound **12**	S51
Figure S41	^{13}C NMR (500 MHz, methanol-d_4, 25 ℃) spectrum of compound **12**	S52
Figure S42	^{1}H-^{1}H COSY (500 MHz, methanol-d_4, 25 ℃) spectrum of compound **12**	S53
Figure S43	HMBC (500 MHz, methanol-d_4, 25 ℃) spectrum of compound **12**	S54
Figure S44	^{1}H NMR (500 MHz, D_2O, 25 ℃) spectrum of (-)-methylshikimate	S55
Figure S45	^{1}H NMR (300 MHz, $CDCl_3$, 25 ℃) spectrum of **13**	S56
Figure S46	^{1}H NMR (300 MHz, $CDCl_3$, 25 ℃) spectrum of **14**	S57
Figure S47	^{1}H NMR (500 MHz, $CDCl_3$, 25 ℃) spectrum of **15**	S58
Figure S48	^{1}H NMR (500 MHz, $CDCl_3$, 25 ℃) spectrum of **16**	S59
Figure S49	^{1}H NMR (500 MHz, $CDCl_3$, 25 ℃) spectrum of **17**	S60
Figure S50	^{1}H NMR (500 MHz, $CDCl_3$, 25 ℃) spectrum of **18**	S61
Figure S51	^{1}H NMR (400 MHz, methanol-d_4, 25 ℃) spectrum of **19**	S62
Figure S52	^{13}C NMR (100 MHz, methanol-d_4, 25 ℃) spectrum of **19**	S63
Figure S53	^{1}H NMR (400 MHz, methanol-d_4, 25 ℃) spectrum of **20**	S64
Figure S54	^{13}C NMR (100 MHz, methanol-d_4, 25 ℃) spectrum of **20**	S65
Figure S55	^{1}H NMR (400 MHz, methanol-d_4, 25 ℃) spectrum of **21**	S66
Figure S56	^{13}C NMR (100 MHz, methanol-d_4, 25 ℃) spectrum of **21**	S67
Figure S57	^{1}H-^{1}H COSY (400 MHz, methanol-d_4, 25 ℃) spectrum of **21**	S68
Figure S58	HSQC (400 MHz, methanol-d_4, 25 ℃) spectrum of **21**	S69
Figure S59	^{1}H NMR (500 MHz, methanol-d_4, 25 ℃) spectrum of **22**	S70
Figure S60	^{13}C NMR (125 MHz, methanol-d_4, 25 ℃) spectrum of **22**	S71
Figure S61	^{1}H-^{1}H COSY (500 MHz, methanol-d_4, 25 ℃) spectrum of **22**	S72
Figure S62	HSQC (500 MHz, methanol-d_4, 25 ℃) spectrum of **22**	S73
Figure S63	^{1}H NMR (400 MHz, methanol-d_4, 25 ℃) spectrum of **23**	S74
Figure S64	^{13}C NMR (100 MHz, methanol-d_4, 25 ℃) spectrum of **23**	S75
Figure S65	^{1}H-^{1}H COSY (400 MHz, methanol-d_4, 25 ℃) spectrum of **23**	S76
Figure S66	HSQC (400 MHz, methanol-d_4, 25 ℃) spectrum of **23**	S77
Figure S67	^{1}H NMR (400 MHz, methanol-d_4, 25 ℃) spectrum of **24**	S78
Figure S68	^{13}C NMR (100 MHz, methanol-d_4, 25 ℃) spectrum of **24**	S79
Figure S69	^{1}H-^{1}H COSY (400 MHz, methanol-d_4, 25 ℃) spectrum of **24**	S80
Figure S70	HSQC (400 MHz, methanol-d_4, 25 ℃) spectrum of **24**	S81
Figure S71	^{1}H NMR (400 MHz, methanol-d_4, 25 ℃) spectrum of **25**	S82
Figure S72	^{13}C NMR (400 MHz, methanol-d_4, 25 ℃) spectrum of **25**	S83
Figure S73	^{1}H-^{1}H COSY (400 MHz, methanol-d_4, 25 ℃) spectrum of **25**	S84
Figure S74	HSQC (400 MHz, methanol-d_4, 25 ℃) spectrum of **25**	S85
Figure S75	^{1}H NMR (400 MHz, methanol-d_4, 25 ℃) spectrum of **26**	S86
Figure S76	^{13}C NMR (100 MHz, methanol-d_4, 25 ℃) spectrum of **26**	S87
Figure S77	^{1}H-^{1}H COSY (400 MHz, methanol-d_4, 25 ℃) spectrum of **26**	S88
Figure S78	HSQC (400 MHz, methanol-d_4, 25 ℃) spectrum of **26**	S89
Figure S79	^{1}H NMR (400 MHz, methanol-d_4, 25 ℃) spectrum of **27**	S90
Figure S80	^{13}C NMR (100 MHz, methanol-d_4, 25 ℃) spectrum of **27**	S91
Figure S81	^{1}H-^{1}H COSY (400 MHz, methanol-d_4, 25 ℃) spectrum of **27**	S92
Figure S82	HSQC (400 MHz, methanol-d_4, 25 ℃) spectrum of **27**	S93

Figure S83	^{1}H NMR (400 MHz, methanol-d_4, 25 ℃) spectrum of **28**	S94
Figure S84	^{13}C NMR (100 MHz, methanol-d_4, 25 ℃) spectrum of **28**	S95
Figure S85	^{1}H-^{1}H COSY (400 MHz, methanol-d_4, 25 ℃) spectrum of **28**	S96
Figure S86	HSQC (400 MHz, methanol-d_4, 25 ℃) spectrum of **28**	S97
Figure S87	^{1}H NMR (500 MHz, methanol-d_4, 25 ℃) spectrum of **30**	S98
Figure S88	^{13}C NMR (100 MHz, methanol-d_4, 25 ℃) spectrum of **30**	S99
Figure S89	^{1}H-^{1}H COSY (400 MHz, methanol-d_4, 25 ℃) spectrum of **30**	S100
Figure S90	HSQC (400 MHz, methanol-d_4, 25 ℃) spectrum of **30**	S101
Figure S91	HMBC (400 MHz, methanol-d_4, 25 ℃) spectrum of **30**	S102
Figure S92	^{1}H NMR (400 MHz, methanol-d_4, 25 ℃) spectrum of TFA-**30**	S103
Figure S93	^{13}C NMR (100 MHz, methanol-d_4, 25 ℃) spectrum of TFA-**30**	S104
Figure S94	^{1}H-^{1}H COSY (400 MHz, methanol-d_4, 25 ℃) spectrum of TFA-**30**	S105
Figure S95	HSQC (400 MHz, methanol-d_4, 25 ℃) spectrum of TFA-**30**	S106
Figure S96	HMBC (400 MHz, methanol-d_4, 25 ℃) spectrum of TFA-**30**	S107
Figure S97	^{13}C NMR (100 MHz, methanol-d_4, 25 ℃) spectrum of [^{13}C]-labeled **30**	S108
Figure S98	^{1}H NMR (400 MHz, $CDCl_3$, 25 ℃) spectrum of **31**	S109
Figure S99	^{1}H NMR (400 MHz, $CDCl_3$, 25 ℃) spectrum of **31**	S110
Figure S100	^{1}H-^{1}H COSY (400 MHz, $CDCl_3$, 25 ℃) spectrum of **31**	S111
Figure S101	HSQC (400 MHz, $CDCl_3$, 25 ℃) spectrum of **31**	S112
Figure S102	HMBC (400 MHz, $CDCl_3$, 25 ℃) spectrum of **31**	S113
Figure S103	^{1}H NMR (500 MHz, DMSO-d_6, 25 ℃) spectrum of **31**	S114
Figure S104	^{1}H-^{1}H COSY (500 MHz, DMSO-d_6, 25 ℃) spectrum of **31**	S115
Figure S105	HSQC (500 MHz, DMSO-d_6, 25 ℃) spectrum of **31**	S116
	References	S117

Synthesis of the pericosine A analogs 19 and 20

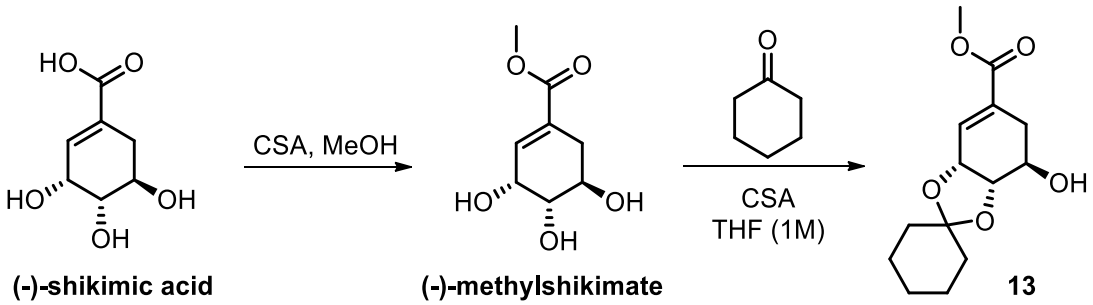

(-)-shikimic acid **(-)-methylshikimate**

To a round bottom flask with shikimic acid (50 mmol, 8.70 g) and camphorsulfonic acid (CSA) (10 mol %, 5 mmol, 1.16 g) was added methanol (100 mL). This solution was then refluxed overnight followed by concentration under reduced pressure. The residue was purified by recrystallization from ethyl acetate (125 mL) to yield (-)-methylshikimate (7.04 g, 75 % yield). To a solution of (-)-methylshikimate (37.4 mmol, 7.04 g) and cyclohexanone (1.5 equiv, 56.1 mmol, 5.8 mL) in THF (75 mL) was added CSA (10 mol %, 3.74 mmol, 868 mg). The reactant mixture was stirred overnight at room temperature. Upon completion, as judged by TLC, the reaction was then concentrated under reduced pressure and purified using a silica gel column, eluting with 5 % acetone/DCM to produce compound **13** (9.02 g, 90 % yield).

(-)-methylshikimate: white solid; ^{1}H NMR (500 MHz, D_2O) δ 6.76 (dt, *J* = 3.8, 1.8 Hz, 1H), 4.39 (td, *J* = 4.0, 1.9 Hz, 1H), 3.97 (ddd, *J* = 8.1, 6.2, 5.1 Hz, 1H), 3.72 (d, *J* = 4.3 Hz, 1H), 3.70 (s, 3H), 2.69 (ddt, *J* = 18.2, 5.2, 1.7 Hz, 1H), 2.18 (ddt, *J* = 18.1, 6.3, 1.7 Hz, 1H).

(3a*S*,4*R*,7a*R*)-methyl 4-hydroxy-3a,4,5,7a-tetrahydrospiro[benzo[*d*][1,3]dioxole-2,1'-cyclohexane]-6-carboxylate (15)[3]: white solid; ^{1}H NMR (300 MHz, $CDCl_3$) δ 6.97 (ddd, *J* = 3.5, 2.2, 1.1 Hz, 1H), 4.76 (t, *J* = 5.0 Hz, 1H), 4.10 (dd, *J* = 7.5, 6.2 Hz, 1H), 3.93 (td, *J* = 8.0, 4.6 Hz, 1H), 3.80 (s, 3H), 2.83 (dd, *J* = 17.4, 4.7 Hz, 1H), 2.35 – 2.16 (m, 1H), 2.08 (s, 1H), 1.78 – 1.29 (m, 10H).

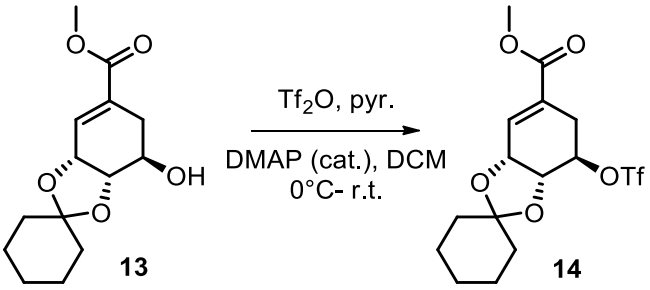

To a three-neck round bottom flask equipped with an addition funnel was added **13** (15 mmol, 4.02 g), and DCM (150 m). Pyridine (1 equiv, 15 mmol, 1.21 mL) was added followed by DMAP (3 mol %, 0.45 mmol, 55 mg). The solution was cooled down to 0°C. A solution of Tf_2O (1.2 equiv, 18 mmol, 3.04 m) in DCM (70 m) was then added dropwise over 15 min. The reactant mixture was stirred at 0°C

for 5 min. The ice bath was then removed and the mixture was warmed to room temperature. Upon completion as judged by TLC (5% acetone/DCM) the reaction was worked up by quenching with $NaHCO_3$, and partitioning with 3x EtOAc, drying over sodium sulfate, and concentrating under reduced pressure. Purification was performed using a silica gel column, eluting with 100% DCM to yield compound **14** (4.12 g, 69 % yield, containing 4 wt% DCM).

(3a*R*,4*R*,7a*R*)-methyl 4-(((trifluoromethyl)sulfonyl)oxy)-3a,4,5,7a-tetrahydrospiro[benzo[*d*][1,3]dioxole-2,1'-cyclohexane]-6-carboxylate (14)[4]: colorless oil; ^{1}H NMR (300 MHz,$CDCl_3$) δ 7.03 (ddd, *J* = 3.6, 2.2, 1.2 Hz, 1H), 5.04 (td, *J* = 8.0, 4.8 Hz, 1H), 4.89 – 4.79 (m, 1H), 4.33 (dd, *J* = 7.5, 6.2 Hz, 1H), 3.82 (s, 3H), 3.06 (ddt, *J* = 17.5, 4.9, 1.1 Hz, 1H), 2.63 (ddt, *J* = 17.5, 8.4, 1.8 Hz, 1H), 1.80 – 1.32 (m, 10H).

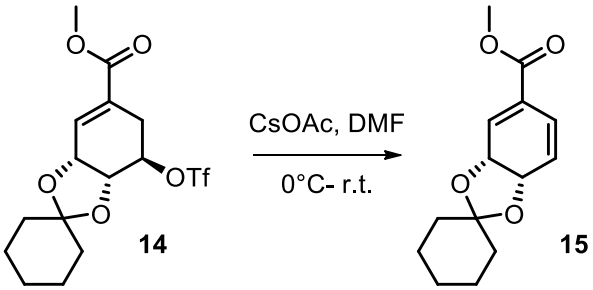

To a solution of 1**4** (9.46 mmol, 3.79 g) in DMF (10 mL) was added CsOAc (1 equiv, 9.46 mmol, 1.81 g) at 0°C. After complete addition, the ice/water bath was removed and the reaction was warmed to room temperature with stirring overnight. Upon completion as judged by TLC (100% DCM), the reaction was quenched with NH_4Cl. The aqueous layer was partitioned 3x with MTBE. The organic extracts were combined and washed once with brine, dried over sodium sulfate, and concentrated under reduced pressure. Purification was performed using a silica gel column, eluting with 100% DCM to produce compound **15** (1.02 g, 43 % yield, containing 2.6 wt% DCM). The diene decomposes readily and therefore was used immediately in the next step.

(3a*R*,7a*S*)-methyl 3a,7a-dihydrospiro[benzo[*d*][1,3]dioxole-2,1'-cyclohexane]-5-carboxylate (15)[4-5]: colorless oil; ^{1}H NMR (500 MHz, $CDCl_3$) δ 6.90 (dt, *J* = 3.8, 1.2 Hz, 1H), 6.55 (dt, *J* = 10.0, 1.1 Hz, 1H), 6.08 (dd, *J* = 10.0, 3.9 Hz, 1H), 4.83 (dd, *J* = 8.8, 3.6 Hz, 1H), 4.66 (dd, *J* = 8.8, 4.0 Hz, 1H), 3.82 (s, 3H), 1.76 – 1.27 (m, 10H).

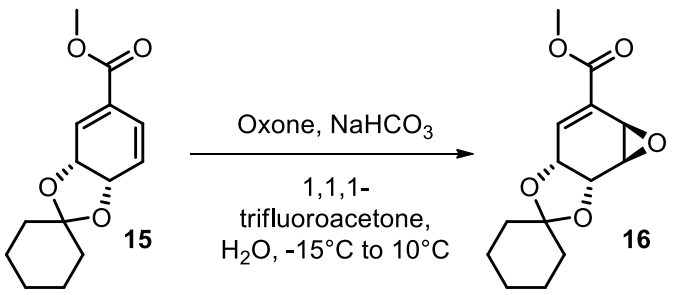

To a solution of **15** (3.86 mmol, 967 mg) and $NaHCO_3$ (10 equiv, 38.6 mmol, 3.24 g) in H_2O (16 mL) and 1,1,1-trifluoroacetone (16 mL), oxone was added in 4 portions every 15 min (2 equiv, 7.73 mmol, 1.18 g x 4) at -15°C. After complete addition, the reactant mixture was a stirred at -15°C for 3 h and then warm naturally to 10°C. After stirring for an additional hour at 10°C, the reaction was completed as judged by TLC (1% acetone/DCM). The reactant mixture was diluted with MTBE and treated with $NaHCO_3$. The aqueous layer was partitioned 3x with MTBE. The organic layers were combined and dried over sodium sulfate and concentrated under reduced pressure. Purification was performed using a silica gel column, eluting with 100% DCM to 2.5% acetone/ DCM to yield compound **16** (609 mg, 60 % yield, containing 6.5 wt % DCM).

(3a'*R*,5a'*R*,6a'*R*,6b'*R*)-methyl 3a',5a',6a',6b'-tetrahydrospiro[cyclohexane-1,2'-oxireno[2',3':3,4]benzo[1,2-*d*][1,3]dioxole]-5'-carboxylate (16)[4]: colorless oil; ^{1}H NMR (500 MHz, $CDCl_3$) δ 6.85 (t, *J* = 2.0 Hz, 1H), 4.82 (dd, *J* = 6.8, 2.0 Hz, 1H), 4.60 (dd, *J* = 6.7, 2.2 Hz, 1H), 4.01 (dd, *J* = 3.9, 1.8 Hz, 1H), 3.86 (s, 3H), 3.70 (br dd, *J* = 3.7, 1.7 Hz, 1H), 1.70 – 1.35 (m, 10H).

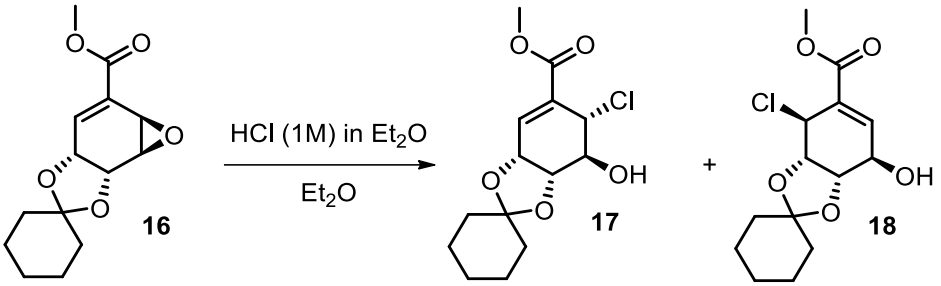

To a nitrogen sparged flask was added a solution of **16** (2.0 mmol, 534 mg) in Et_2O (9.5 mL) at 0°C followed by HCl (1M) in Et_2O (1.5 equiv, 3.0 mmol, 3.0 mL). The reactant mixture was warmed to room temperature and stirred overnight. The reactant mixture was concentrated under reduced pressure. Purification was performed using a silica gel column, eluting with 2% MeOH/DCM to yield compounds **17** (386.6 mg, 64 % yield, containing 2.6 wt% DCM and 3.3 wt% acetone) and **18** (148.4 mg, 25 % yield, contains 3.9 wt % DCM).

(3a*S*,4*S*,5*S*,7a*R*)-methyl 5-chloro-4-hydroxy-3a,4,5,7a-tetrahydrospiro[benzo[*d*][1,3]dioxole-2,1'-cyclohexane]-6-carboxylate (17)[4-5]: colorless oil; ^{1}H NMR (500 MHz, $CDCl_3$) δ 6.91 (d, *J* = 3.7 Hz, 1H), 4.78 (m, *J* = 3.1 Hz, 1H), 4.77 – 4.74 (m, 1H), 4.44 (q, *J* = 4.5 Hz, 1H), 4.32 (t, *J* = 5.5 Hz, 1H), 3.85 (s, 3H), 2.33 (d, *J* = 4.2 Hz, 1H), 1.77 – 1.32 (m, 10H).

(3a*S*,4*S*,7*R*,7a*S*)-methyl 4-chloro-7-hydroxy-3a,4,7,7a-tetrahydrospiro[benzo[*d*][1,3]dioxole-2,1'-cyclohexane]-5-carboxylate (18)[4-5]: colorless oil; ^{1}H NMR (500 MHz, $CDCl_3$) δ 7.36 (d, *J* = 6.2 Hz, 1H), 5.10 (d, *J* = 1.7 Hz, 1H), 4.86 (dd, *J* = 6.6, 1.7 Hz, 1H), 4.67 (dt, *J* = 6.6, 1.4 Hz, 1H), 4.43 (ddd, *J* = 10.5, 6.3, 1.8 Hz, 1H), 3.88 (s, 3H), 2.22 (d, *J* = 4.2 Hz, 1H), 1.67 – 1.32 (m, 10H).

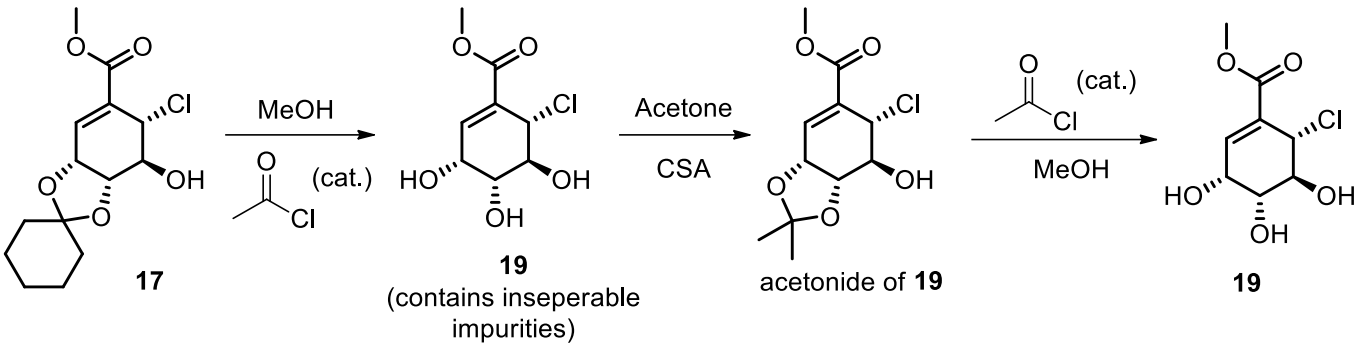

To a solution of **17** (1.16 mmol, 354.1 mg) in MeOH (15 mL), acetyl chloride (3 drops) was added. After completion of the reaction as judged by TLC, the solution was concentrated under reduced pressure. Purification was performed using reverse phase chromatography, eluting with 60% MeOH/H_2O. This yielded an inseparable mixture of product and impurities. Therefore, impure product **19** (166 mg) was placed in a round bottom flask with CSA (10 mol%, 0.074, 17 mg) and acetone (8 mL). The reaction was stirred at room temperature overnight. Upon completion as determined by ^1H NMR, the reactant mixture was concentrated under reduced pressure and purified using a silica gel column, eluting with 5% acetone/DCM, to yield the acetonide derivative **19** (52.3 mg, 27 % yield), which was used directly in the next step. To a solution of the acetonide (0.19 mmol, 52.3 mg) in MeOH (2.5 mL), 3 drops of acetyl chloride were added. The solution was stirred overnight at room temperature and concentrated under reduced pressure. The resultant mixture was placed in a freezer and recrystallized to yield pure compound **19** (42.8 mg, 17 % yield).

(3*R*,4*R*,5*S*,6*S*)-methyl 6-chloro-3,4,5-trihydroxycyclohex-1-enecarboxylate (19)[5a]: white solid; ^1H and ^{13}C NMR data, see Table S3; HRESIMS *m*/*z* 223.0374, $[M+H]^+$ (calcd for $C_8H_{12}ClO_5$, 223.0368).

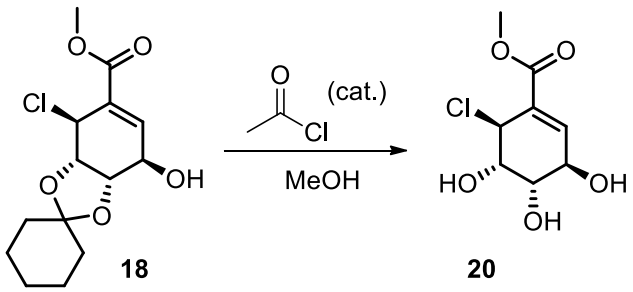

To a solution of **18** (0.49 mmol, 148.9 mg) in MeOH (6.2 mL), 3 drops of acetyl chloride were added. After completion of the reaction as judged by TLC, the solution was concentrated under reduced pressure. Purification was performed using reverse phase chromatography, eluting with 60% MeOH/H_2O, to produce compound **20** (87.6 mg, 80 % yield).

Pericosine D$_O$ **(20)**[6]: white solid; ^1H and ^{13}C NMR data, see Table S3; HRESIMS *m*/*z* 223.0373, $[M+H]^+$ (calcd for $C_8H_{12}ClO_5$, 223.0368).

Table S1. Crystal data and structure refinement for compound **3**

Empirical formula	$C_{22}\ H_{24}\ N_2\ O_4\ S_3$
Formula weight	476.61
Crystal system	monoclinic
Space group	$P2_1/n$
Unit cell dimensions	a = 12.2411(8) Å α= 90°
	b = 8.5886(6) Å β= 94.469(3)°
	c = 22.1443(15) Å γ= 90°
Volume	2321.0(3) $Å^3$
Z, Z'	4, 1
Density (calculated)	1.364 Mg/m^3
Wavelength	0.71073 Å
Temperature	100(2) K
F(000)	1000
Absorption coefficient	0.350 mm^{-1}
Absorption correction	semi-empirical from equivalents
Max. and min. transmission	0.7471 and 0.7049
Theta range for data collection	2.545 to 36.349°
Reflections collected	105369
Independent reflections	11275 [R(int) = 0.0493]
Data / restraints / parameters	11275 / 0 / 283
***wR*(F^2 all data)**	$wR2$ = 0.1063
***R*(*F* obsd data)**	$R1$ = 0.0338
Goodness-of-fit on F^2	1.000
Observed data [I > 2σ(I)]	9370
Largest and mean shift / s.u.	0.003 and 0.000
Largest diff. peak and hole	0.655 and -0.438 e/$Å^3$

Table S2. Calculated carbon chemical shifts of selected carbon atoms for the C-6 epimers of **7**, **8**, and **12**.

Carbon	**7a**[a]	**7b**[a]	**8a**[a]	**8b**[a]	**12a**[b]	**12b**[b]
1	139.2	136.8	139.6	138.3	131.7	132.5
2	143.2	148.3	144.6	148.7	132.5	131.5
3	70.9	72.7	71.5	72.2	65.2	69.3
4	70.1	77.1	71.6	76.4	66.6	68.6
5	80.9	73.2	80.2	72.5	76.0	70.6
6	52.7	53.1	49.3	52.5	48.9	48.7
7	173.2	172.7	174.4	173.6	159.0	159.6
8	53.7	53.6	53.8	53.6	51.3	51.2

[a] Calculated using B3LYP/6-311+G(2d,p) in gas phase; [b] Calculated using B3LYP/6-31G(d,p) in gas phase.

Table S3. The results of the AMES II™ assay[a] of **4**.

Compound	Precipiate (μg/mL)	TA98[b]		TA_{Mix}[b]	
		-S9[c]	+S9	-S9	+S9
4	≥1000	Negetive[d]	Negetive	Negetive	Negetive

[a]From the service provider – BioReliance. The assay was performed following the standard protocol as described in *Proc. Natl. Acad. Sci. USA*, **1994**, *91*, 11606-11610. The purpose of this study is to evaluate the mutagenic potential of the test article by measuring its ability to induce reverse mutations at selected loci of the tester strains in the presense and absence of S9 activation. [b] *Salmonella* tester strains. The TA98 strain is used for the detection of frameshift mutations. TA_{Mix} is a mixture of six tester strains which are designed to revert by one specific base-pair substitution out of all possible changes. [c] Exogenous metabolic activation system containing majorly S9 liver homogenate (30%) and other reagents. [d] One or more test article concentrations had at least a two-fold increase in the number of positive wells. However, the average number of positive wells was within the historical vehicle control range and this increase was not dose dependent. Therefore the conclusion was negative.

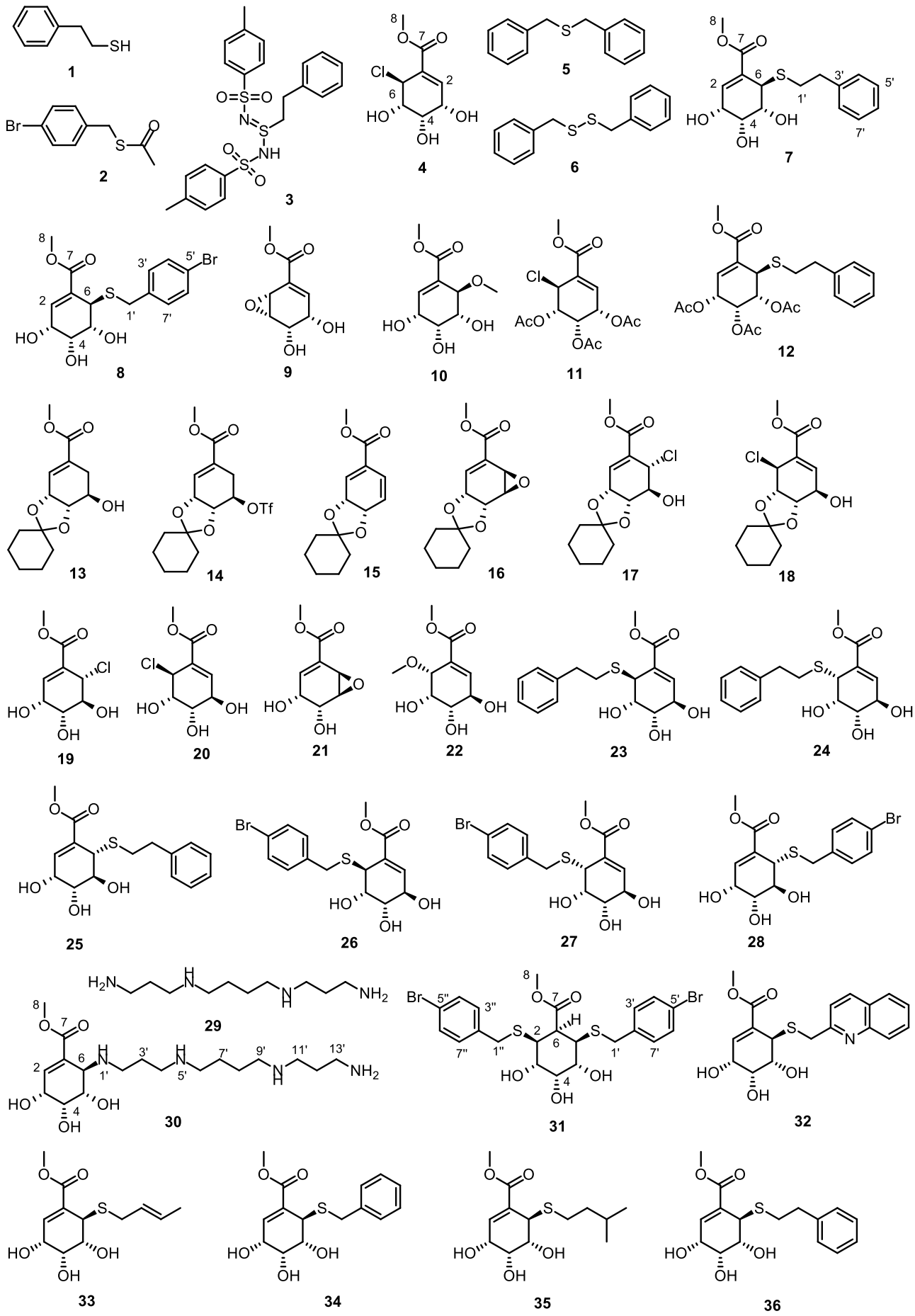

Figure S1. Structures of compounds **1-36**.

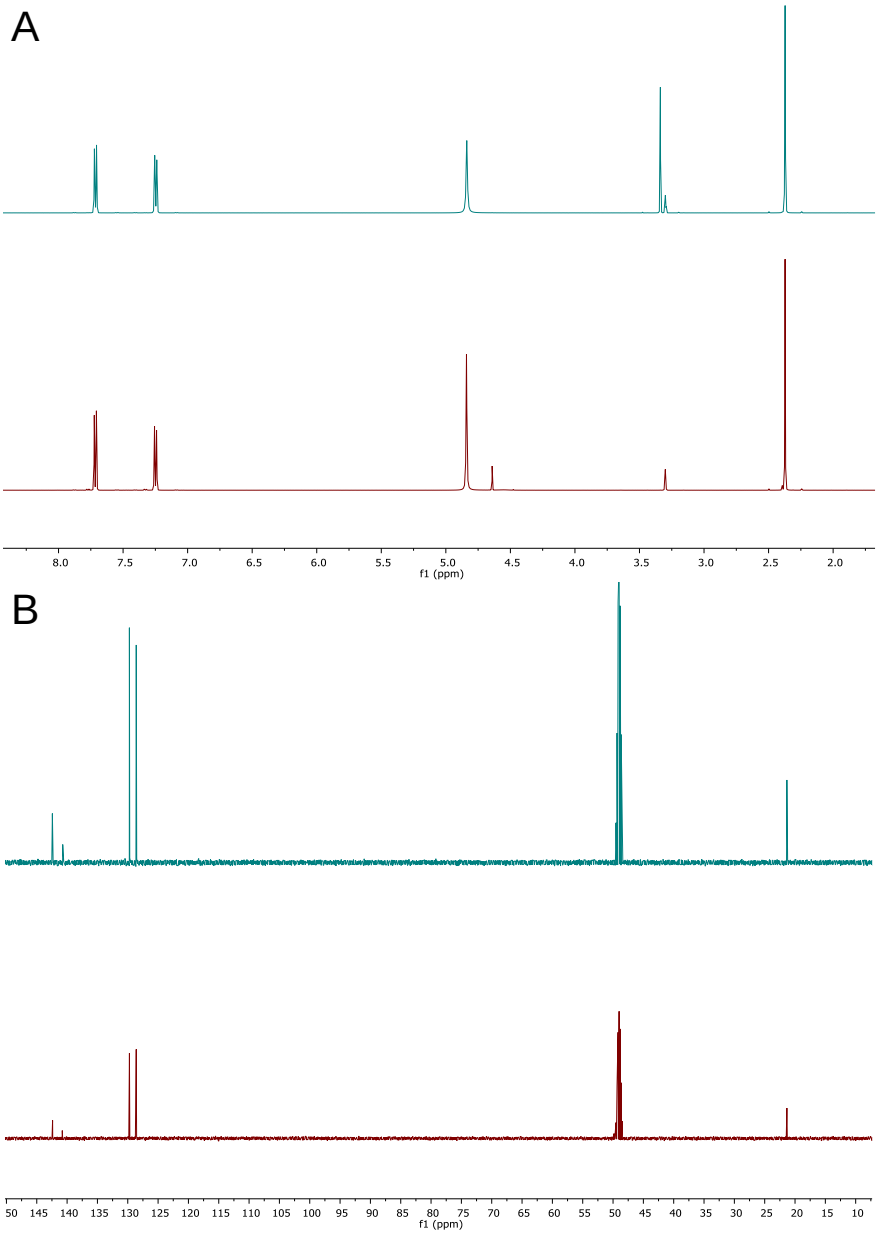

Figure S2. Comparison of the ^{1}H (A) and ^{13}C (B) NMR spectra of chloramine-T (blue) and Product A (red, residue after evaporation of solvent). All spectra were measured in methanol-d_4.

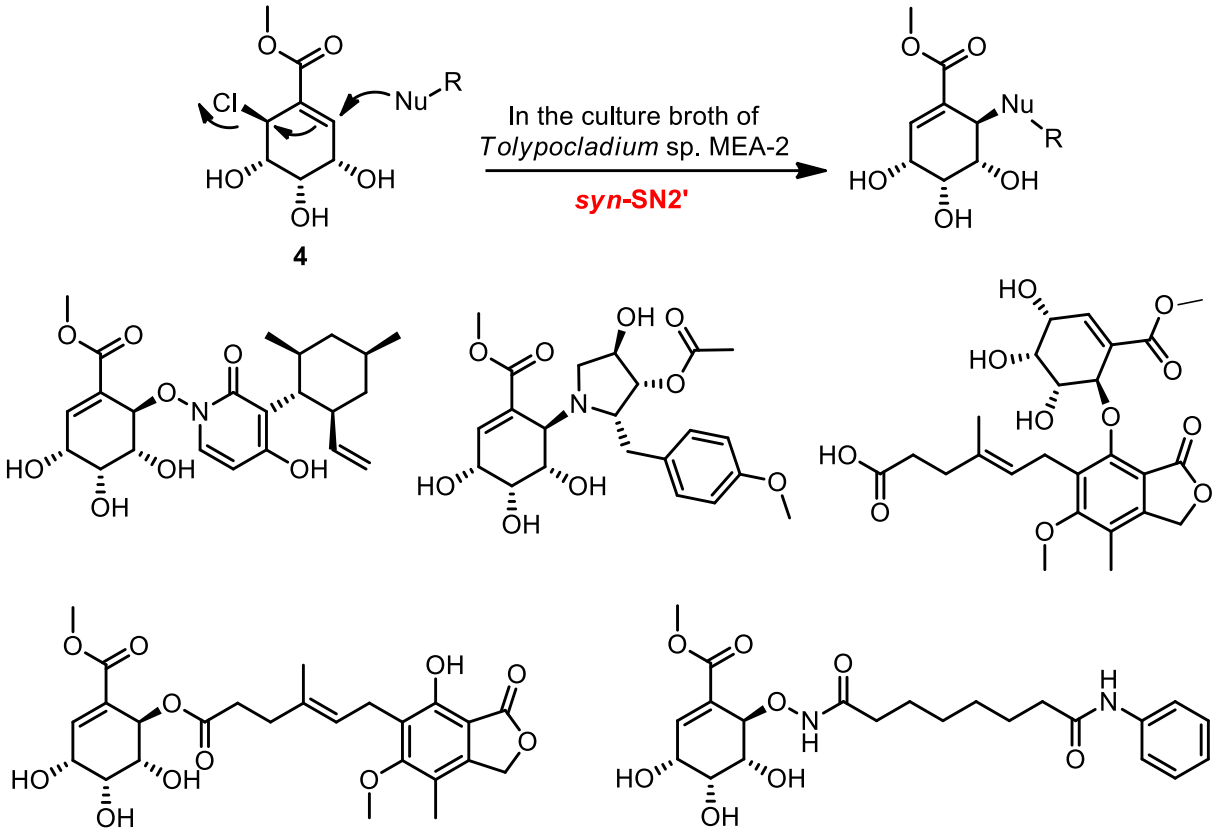

Figure S3. The fungal metabolite pericosine A (**4**) reacts with natural and synthetic nucleophiles to form pericosine-nucleophile adducts. All the pericosine-nucleophile conjugated products were generated by providing the nucleophilic compounds directly to the culture broth of *Tolypocladium* sp. MEA-2.

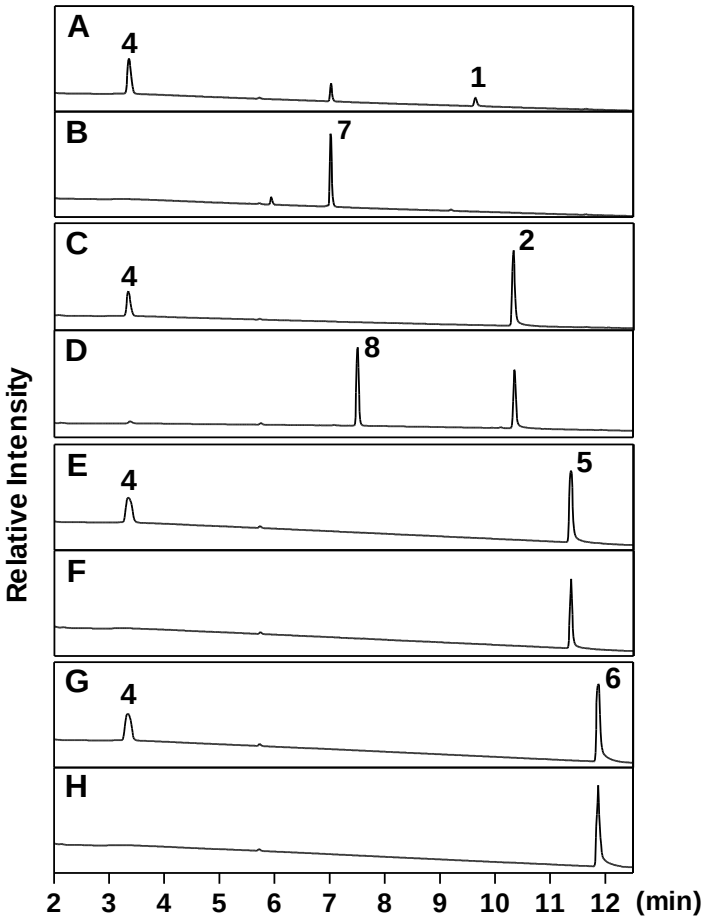

Figure S4. LCMS analysis for the reactions of pericosine A (**4**) with selected sulfur-containing compounds (**1**, **2**, **5**, and **6**). Compound **4** (1 equiv) was mixed with **1** [1 equiv, (A) and (B)], **2** [1 equiv, (C) and (D)], **5** [1 equiv, (E) and (F)], or **6** ([1 equiv, (G) and (H)], respectively, in 50% MeOH with [(A), (C), (E), and (G)] / without [(B), (D), (F), and (H)] the presence of Et_3N (2 equiv). The reaction mixtures were kept static overnight at room temperature prior to LCMS analysis (210 nm UV traces were shown).

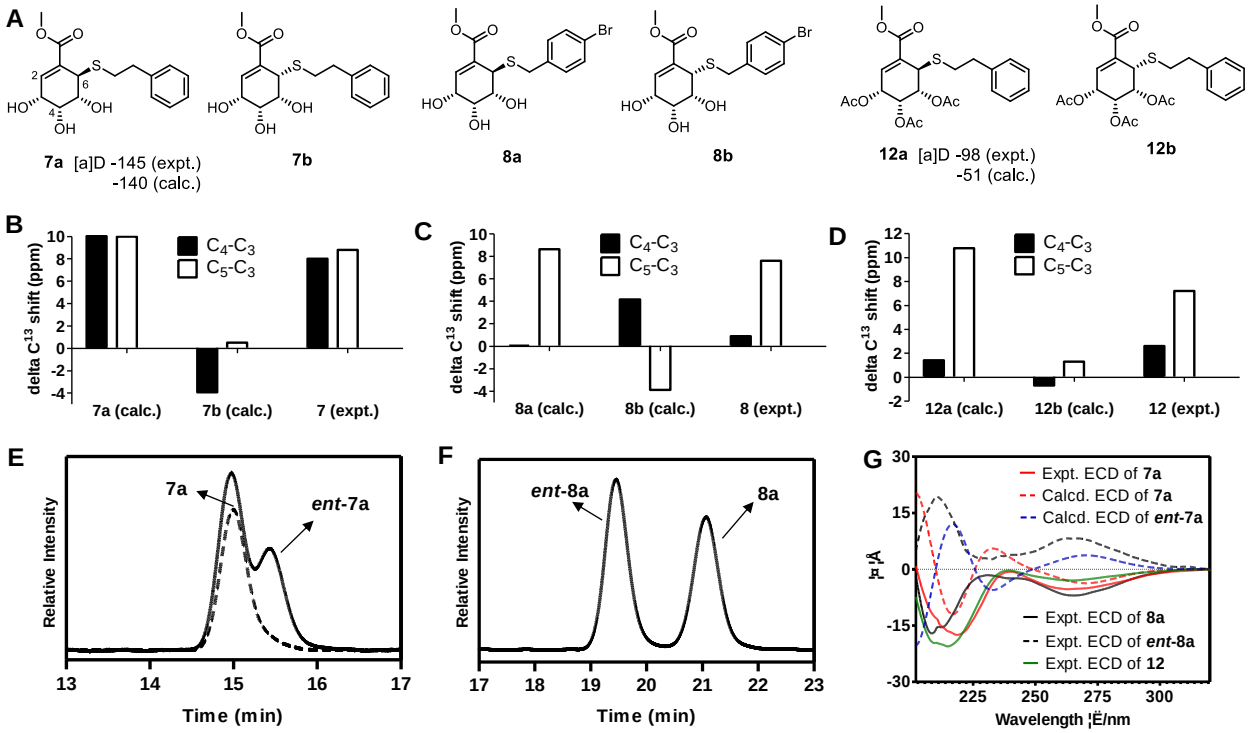

Figure S5. The absolute configurations of **7**, **8**, and **12**. (A) Structures of **7a**, **7b**, **8a**, **8b, 12a**, and **12b**. B3LYP/6-311+G(2d,p) was used to calculate the specific rotation value and ECD spectrum of **7a** and B3LYP/6-31+G(d,p) was used to calculate the specific rotation value of **12a**. (B)–(D) Comparison of the experimental (**7**, **8**, and **12**) and calculated (**7a**, **7b**, **8a**, **8b**, **12a**, and **12b**) differences of carbon chemical shifts between C_4 and C_3 and between C_5 and C_3. B3LYP/6-311+G(2d,p) was used to calculate the ^{13}C chemical shifts of **7a**, **7b**, **8a**, and **8b**, and B3LYP/6-31+G(d,p) was used to calculate the ^{13}C chemical shifts of **12a** and **12b**. (E) and (F) Chiral HPLC analysis of **7** [(E), solid line, **7** obtained from the reaction conditions: **4** : **1** : Et_3N = 1 : 1.5 : 2; dashed line, **7** obtained from the reaction conditions: **4** : **1** : Et_3N = 1 : 1 : 0] and **8** [(F), obtained from the reaction conditions: **4** : **2** : Et_3N = 1 : 1.5 : 10]. HPLC conditions: (E) Lux cellulose-2 analytical column, 30% MeCN elution, 200 nm; (F) Lux cellulose-3 analytical column, 25% MeCN elution, 200 nm. (G) Comparison of the experimental and calculated ECD spectra of **7a**, ***ent*-7a**, **8a**, ***ent*-8a**, and **12**. B3LYP/6-311+G(2d,p) was used to calculate the ECD spectra of **7a** and ***ent*-7a**.

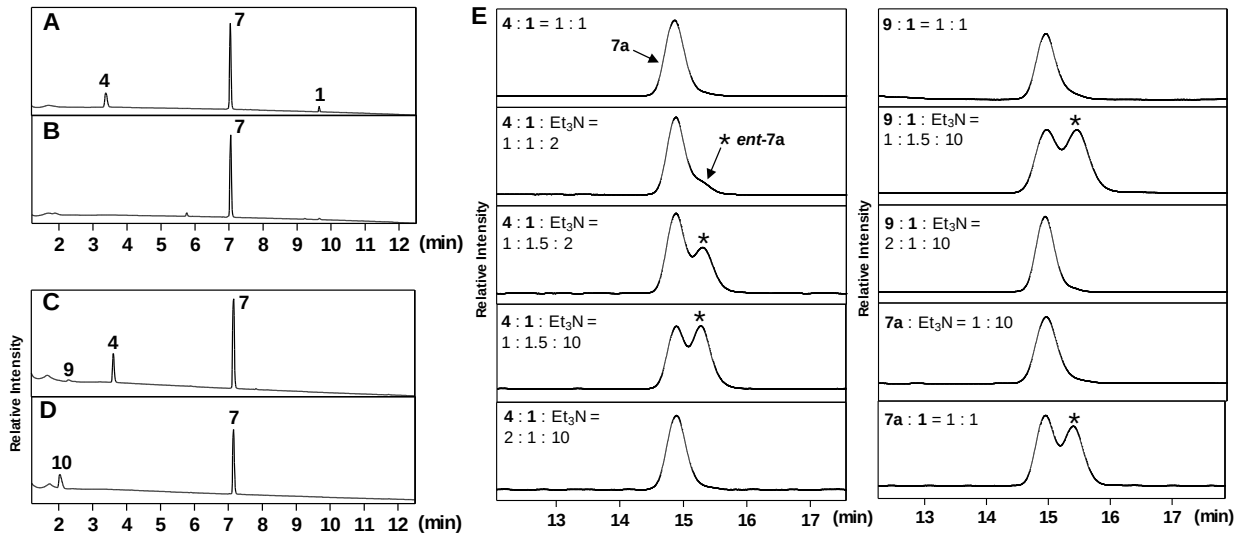

Figure S6. Investigating the mechanism of the formation of **7**. **4** (1 equiv) was mixed with **1** [1 equiv for (A) and (B); 0.5 equiv for (C) and (D)] in 50% MeOH containing Et_3N [2 equiv for (A) and (B); 10 equiv for (C) and (D)]. The reactant mixtures were analyzed by LCMS at different time points [(A) and (C) 1 min; (B) and (D) 120 min]. (E) Chiral-HPLC analysis of **7** derived from different conditions. The reactants/reagents were incubated in 50% MeOH overnight prior to HPLC analysis. The initial ratios of reactants/reagents were shown on the chromatograms. HPLC conditions: Lux cellulose-2 analytical column, 30% MeCN elution, 200 nm.

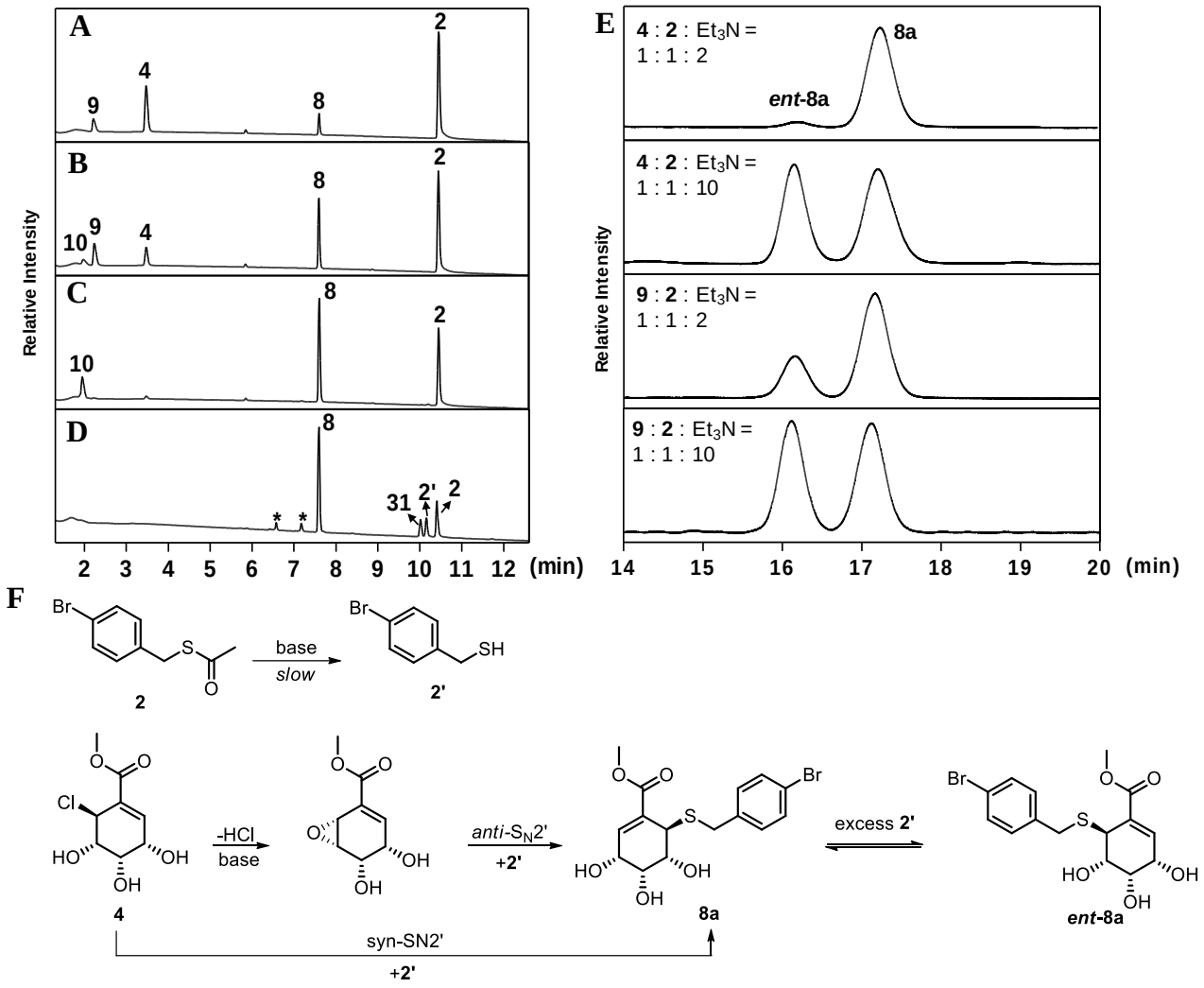

Figure S7. The mechanism of Et_3N-catalyzed formation of **8** by the reaction between pericosine A (**4**) and 4-bromo-alpha-toluene thioacetate (**2**). (A)-(C) **4** (1 equiv) was mixed with **2** (1 equiv) in 50% MeOH containing Et_3N (2 equiv). The reactant mixtures were injected into LCMS at different time [(A) 1 min; (B) 30 min; (C) overnight] after the mixing. d) **4** (1 equiv) was mixed with **2** (1.5 equiv) in 50% MeOH containing Et_3N (10 equiv). The reactant mixtures were analyzed by LCMS after the overnight reaction. *Unidentified minor products. The structure of minor product **31** was identified in following experiments. (E) Chiral HPLC analysis of **8** that was produced in 50% MeOH under different reaction conditions. The ratio of reactants/reagents in each reaction was shown on the chromatograms. HPLC conditions Lux cellulose-3 analytical column, 25% MeCN elution, 200 nm. (F) The proposed mechanism of the reaction between **4** and **2**.

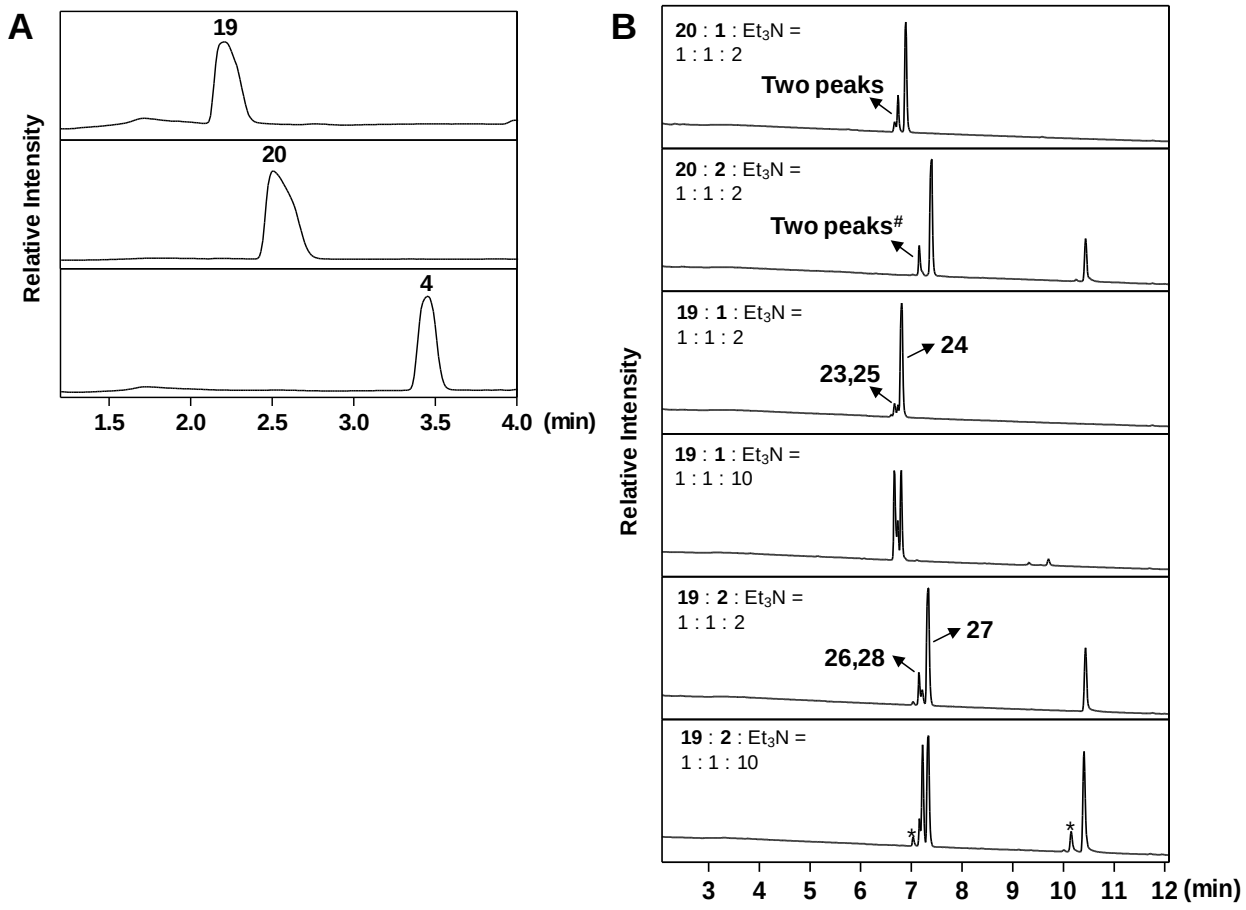

Figure S8. LCMS analysis of the pericosine analogs **4**, **19** and **20** (A) and the reactions of **19** and **20** with sulfur-containing compounds **1** and **2** in 50% MeOH with the presence of Et_3N (B). The reaction mixtures were kept static overnight at room temperature prior to LCMS analysis (210 nm UV traces were shown). The ratio of reactants/reagents in each reaction was shown on the chromatograms. #The separation of the two peaks were resolved by HPLC using a longer C18 column (Gemini 5 μm C18, 110 Å, 250 × 4.6 mm). *Unidentified minor products.

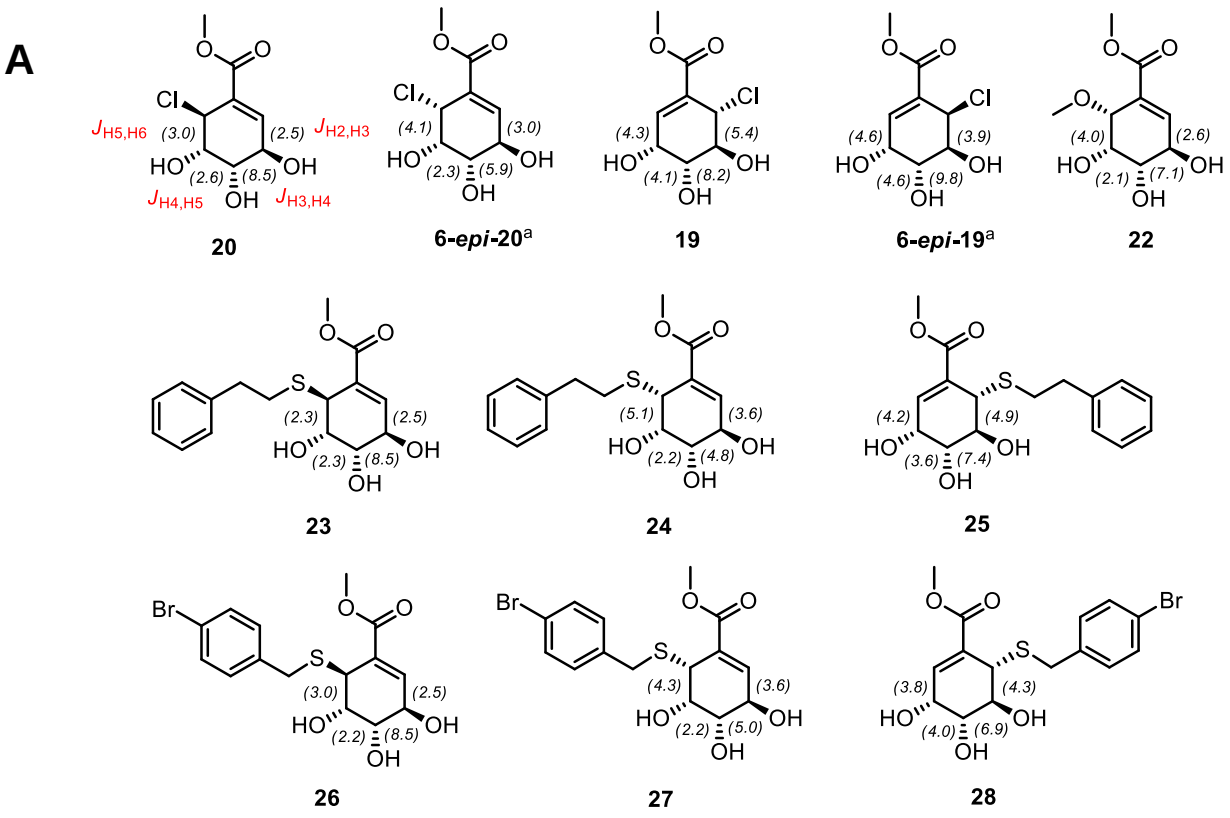

Figure S9. Comparison (A) and principle components analysis (PCA) (B) of the $^{3}J_{H,H}$ coupling constants of **19**, **20**, **6-*epi*-19**, **6-*epi*-20**, and **22-28**. The PCA was performed using the CAMO Unscrambler® X 10.3 software.

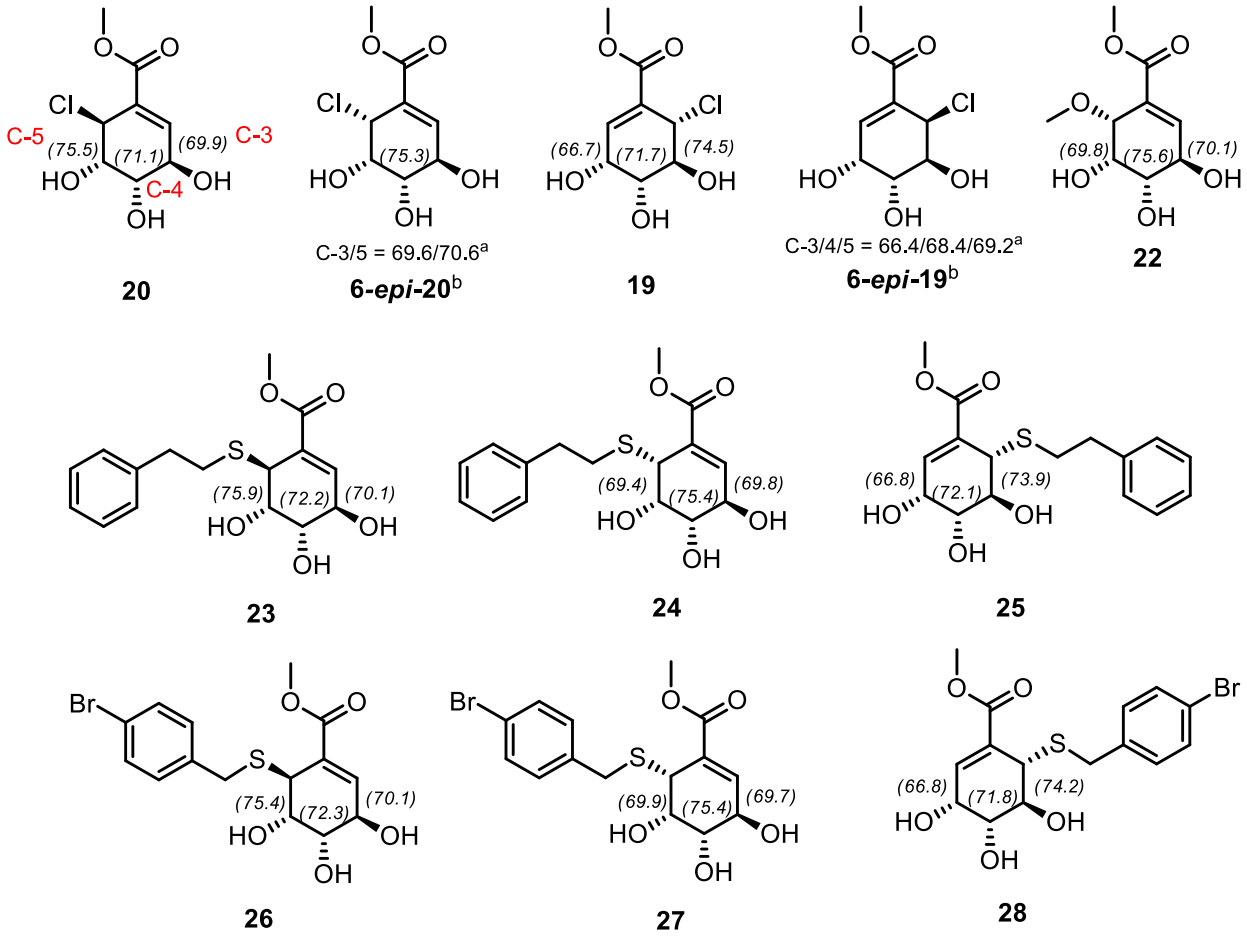

a. ^{13}C chemical shifts were not assigned for indicated positions. b. Spectra were measured in acetone-d_6. All other spectra were measured in methanol-d_4.

Figure S10. Comparison of the ^{13}C NMR-derived chemical shifts (δ) of **19**, **20**, **6-*epi*-19**, **6-*epi*-20**, and **22-28.**

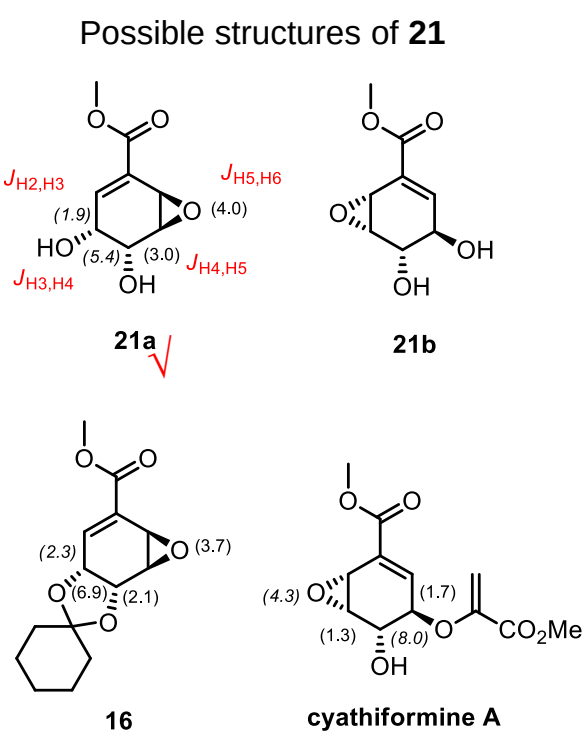

Figure S11. Comparing the $^{3}J_{H,H}$ coupling constants of **21** with selected model compounds.

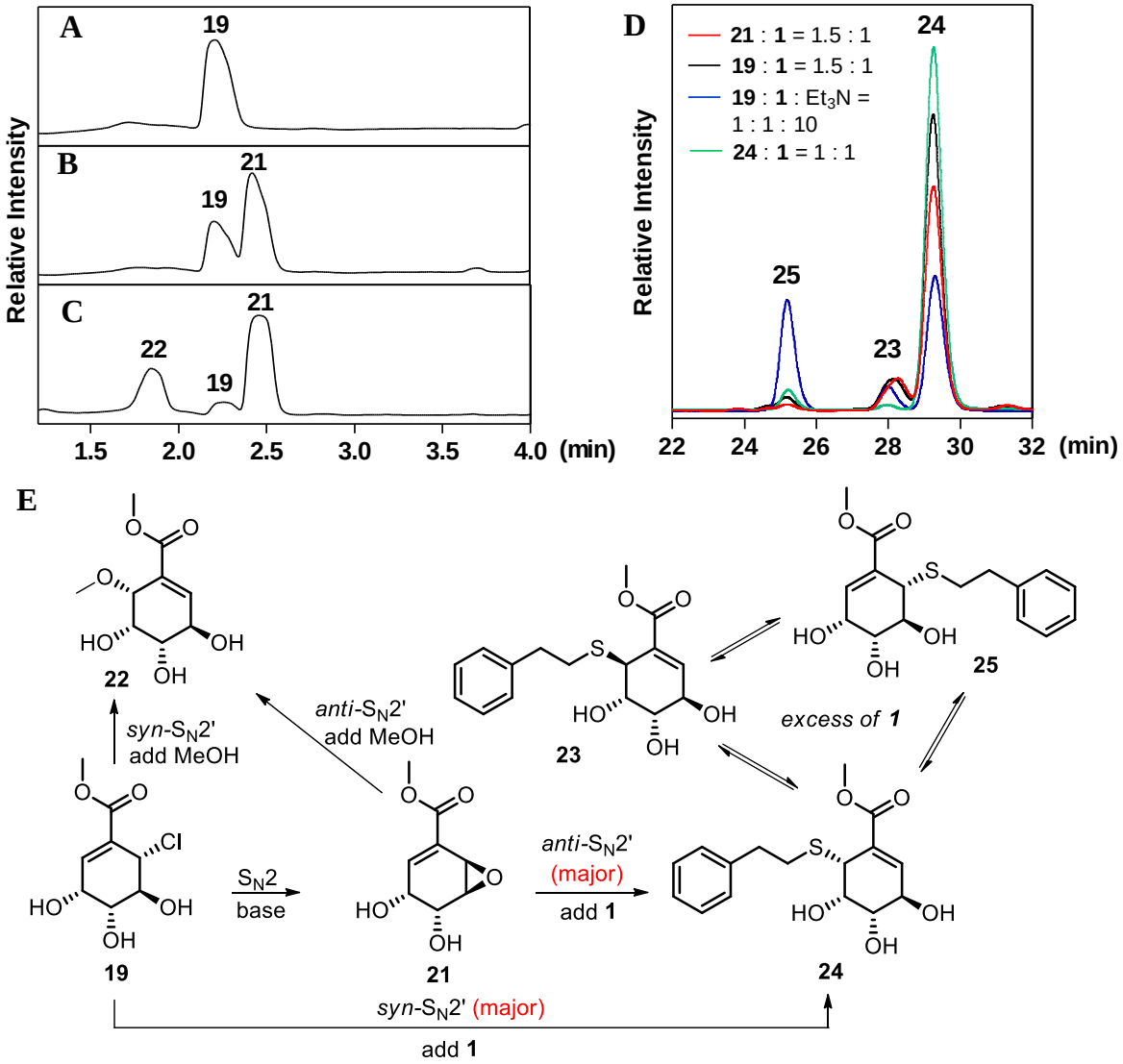

Figure S12. Investigating the mechanism of Et_3N-catalyzed formation of **23**-**25** from the reactions between **19** and **1**. **19** (1 equiv) was mixed with Et_3N (2 equiv) in 50% MeOH and the reactant mixture was analyzed by LCMS at different times [(A) 1 min; (B) 15 min; (C) 60 min] after the mixing. (D) The overlaid LCMS chromatograms (UV 210 nm) showing comparative production of **23**-**25** in 50% MeOH under different reaction conditions. The ratio of reactants/reagents in each reaction is shown on the chromatograms. The LCMS runs were extended to 40 min to generate better separation of the target analytes. (E) The proposed mechanisms of Et_3N-catalyzed Nu-substitution of **19** by MeOH and **1** in 50% MeOH.

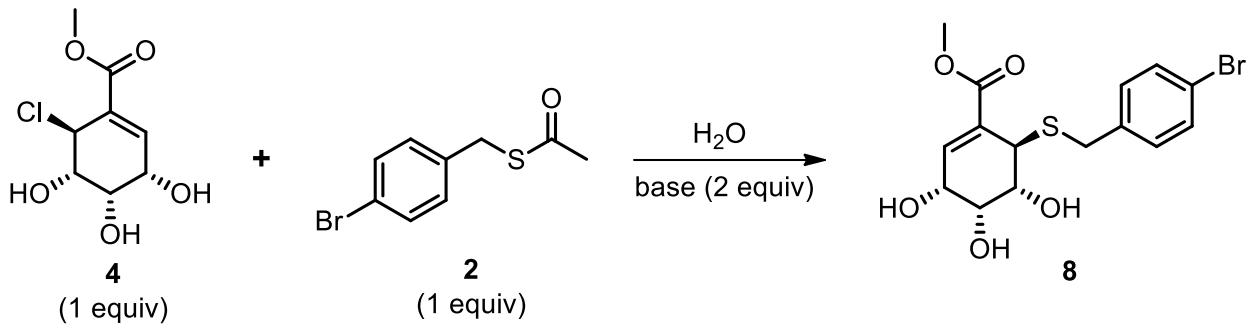

base	Production of **8** (Y/N)	base	Production of **8** (Y/N)	base	Production of **8** (Y/N)
$Ca(OH)_2$	N	triethylenetetramine	Y	quaternium-15	N
K_2CO_3	Y	diethylenetriamine	Y	polyquaternium-2	N
$NaHCO_3$	N	ethylenediamine	Y	ectoine	N
NaI	N	spermine	Y	aminoguanidine	N
triethanolamine	N	L-arginine	N	protoporphyrin IX	N
linear PEI	N	L-histidine	N	Tris base	N
cyclam	Y	ethanolamine	N	urea	N

Figure S13. Catalytic effects of selected basic compounds in the reactions between **4** and **2**.

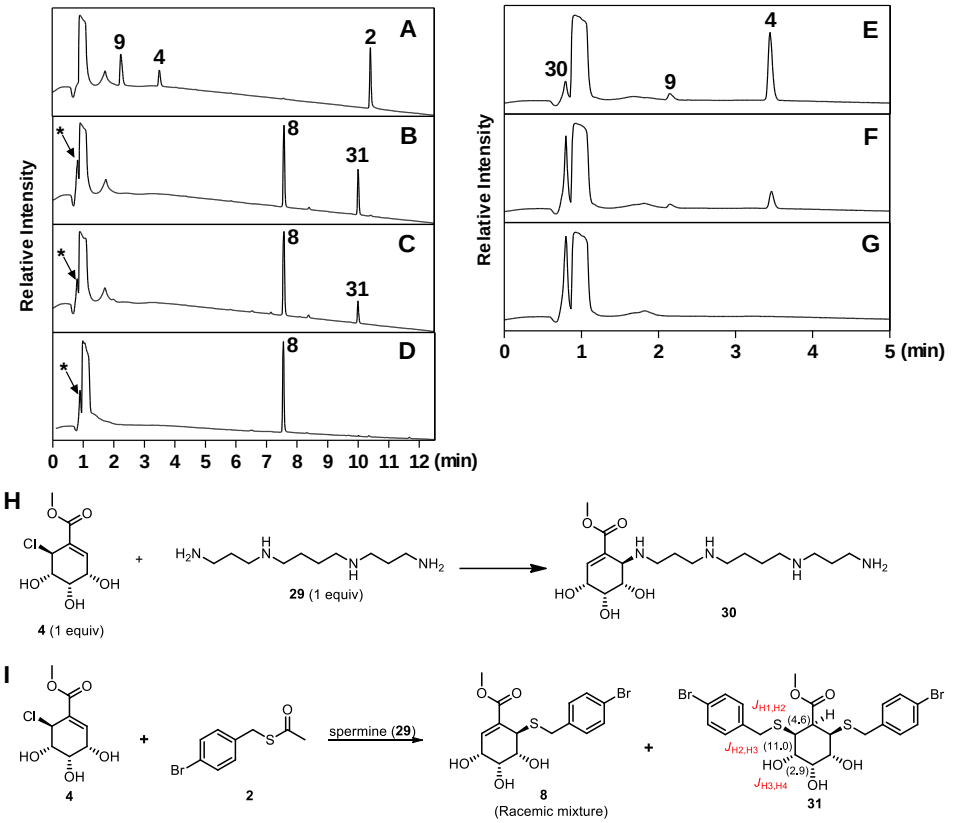

Figure S14. Spermine (**29**) catalyzed reactions of pericosine A (**4**). (A)-(D) Comparison of the catalytic abilities of Et_3N [2 equiv, (A)] and **30** [2 equiv, (B)-(D)] for the reactions between **4** [1 equiv for (A)-(C) and 2 equiv for (D)] and **2** (1 equiv) in H_2O [(A) and (B)] and 50% propylene glycol [PG, (C) and (D)]. All the reactant mixtures were kept static overnight prior to LCMS analysis. *The peak may be a racemic or a scalemic mixture of **30** and ***ent*-30,** which could not be resolved by chiral HPLC analysis using Lux cellulose-2 or cellulose-3 column. (E)-(G) Time-dependent formation of **31** by the reaction between **4** and **29** in 50% PG. **4** (1 equiv) was mixed with **29** (2 equiv) in 50% PG and the reactant mixture was analyzed by LCMS at different times [(E) 1 min; (F) 15 min; (G) 60 min] after mixing. The UV chromatograms (monitored at 210 nm) are displayed for (A)-(G). h) Synthesis of the addition product (**30**) of periecosine A and spermine. i) Synthesis of **8** and **31** via the reaction between **2** and **4** catalyzed by **29**.

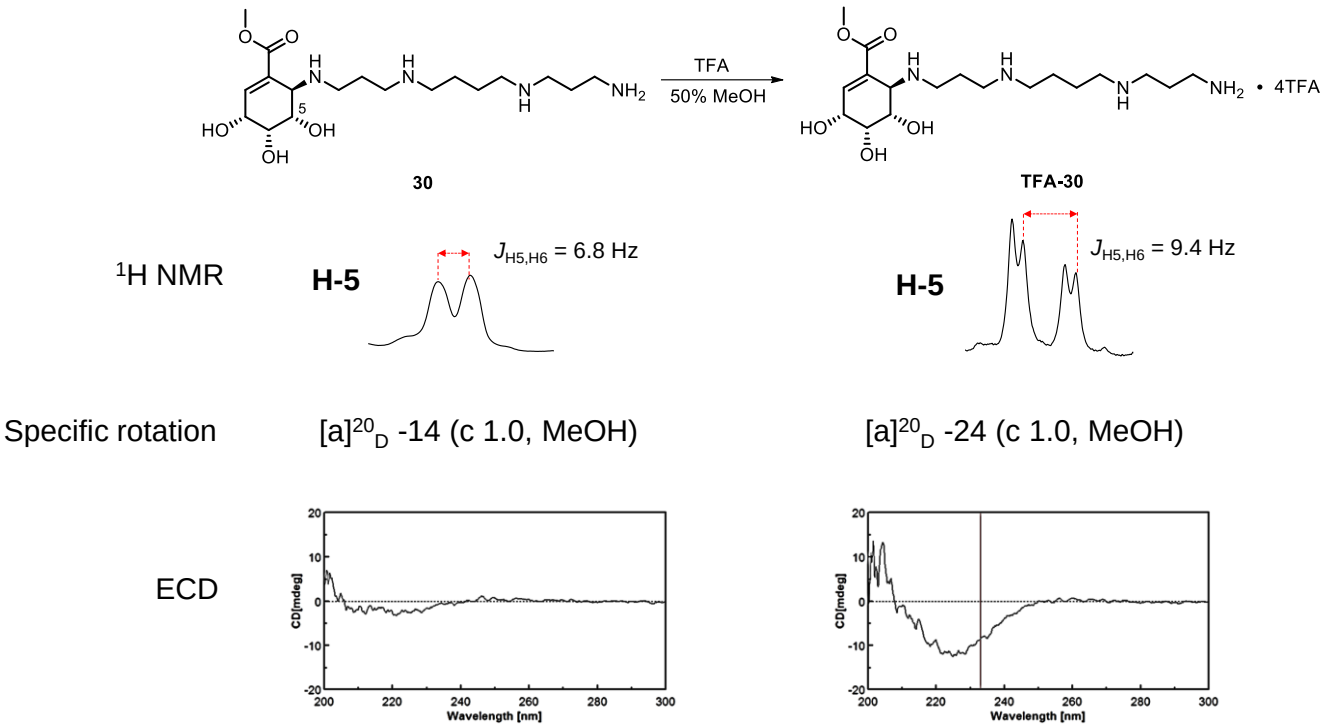

Figure S15. Generating the TFA salt of **30** (**TFA-30**). The selected ^{1}H NMR resonances, specific rotations, and ECD spectral data were compared between **30** and **TFA-30**.

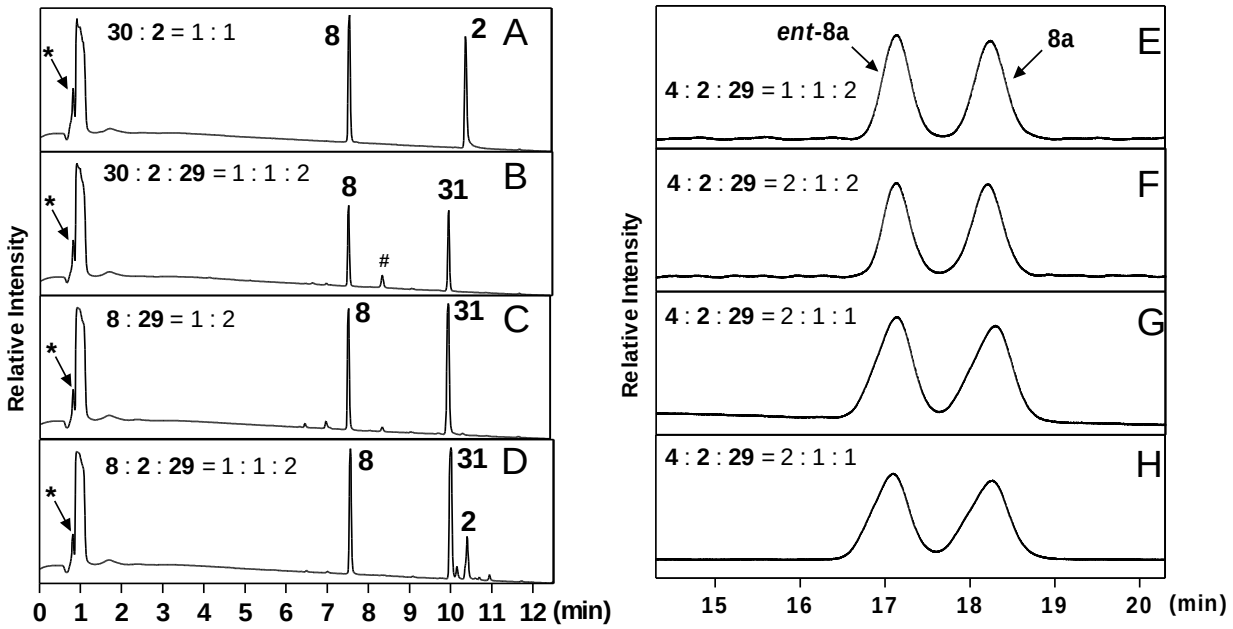

Figure S16. Investigating the mechanism of spermine-catalyzed reaction between **4** and **2** in 50% PG. (A)-(D) LCMS analysis of the reactions between **30** and **2** and between **8** and **29**. The ratio of reactants/reagents in each reaction are shown in the chromatograms. The reactant mixtures were kept static overnight at room temperature prior to LCMS analysis (210 nm UV traces were shown). *The peak may be a racemic or a scalemic mixture of **30** and ***ent*-30**. [#]Unidentified minor products. (E)-(H) Chiral HPLC analysis of **8** that was produced in 50% PG [(E)-(G)] or 50% MeOH (H) under different conditions. The ratio of reactants/reagents in each reaction is shown on the chromatograms. HPLC conditions: Lux cellulose-3 analytical column, 25% MeCN elution, 200 nm.

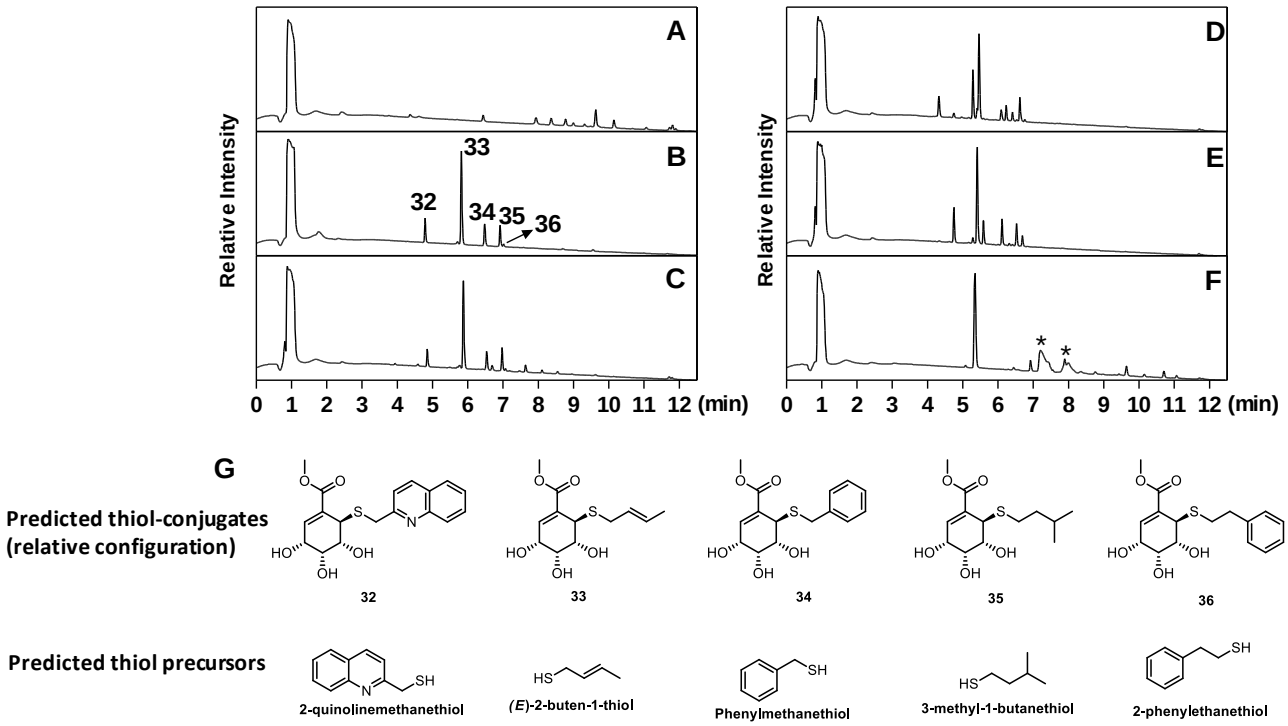

Figure S17. LCMS analysis of the reactions between skunk anal gland secretion (SE) and thiol-reactive compounds (**4**, **19**, **20**, and chloramine-T). The purchased WCS™ skunk essence (SE, 100% pure) was diluted in CH_2Cl_2 as 1 : 100. All other reagents (**4**, **19**, **20**, chloramine-T, **29**, and Et_3N) were dissolved in DMSO to make 100 mM solutions. Reaction conditions: (A) 3 µL SE in 50% PG; (B) 3 µL SE, 3 µL **4**, and 6 µL Et_3N in 50% MeOH; (C) 3 µL SE, 3 µL **4**, and 6 µL **29** in 50% PG; (D) 3 µL SE, 3 µL **19**, and 6 µL **29** in 50% PG; (E) 3 µL SE, 3 µL **20**, and 6 µL **29** in 50% PG; (F) 3 µL SE, 3 µL chloramine-T, and 6 µL **29** in 50% PG. The reactant mixtures were kept static overnight at room temperature prior to LCMS analysis (210 nm UV traces are shown). *Major products of the reaction between chloramine-T and SE. (G) The structures of the major products (**32**-**36**) from the reaction (B) between **4** and SE were predicted by analysis of their MS data. The corresponding thiol precursors were reported[7] from different SE samples.

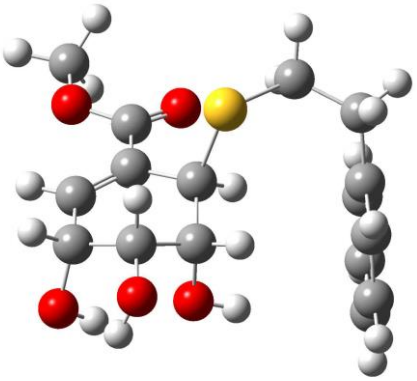

Conformer 1, RE = 0.46 kcal/mol (25.7%)

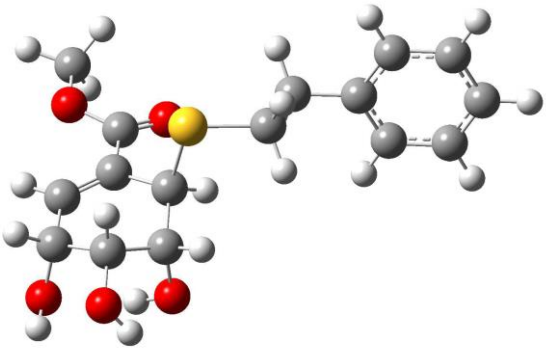

Conformer 2, RE = 0.69 kcal/mol (17.6%)

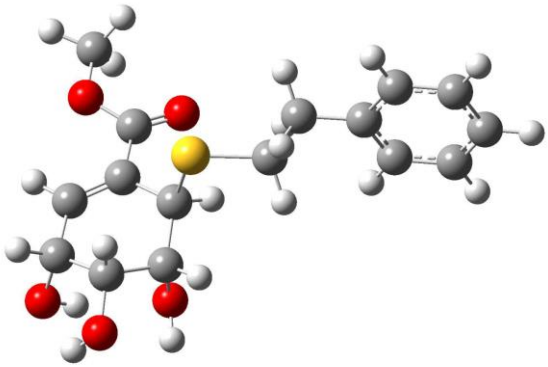

Conformer 3, RE = 0 kcal/mol (36.2%)

Figure S18. Optimized geometries, relative energies, and Boltzmann populations of the calculated lowest-energy conformers of **7a** at the 6-311+G(2d,p) level in the gas phase.

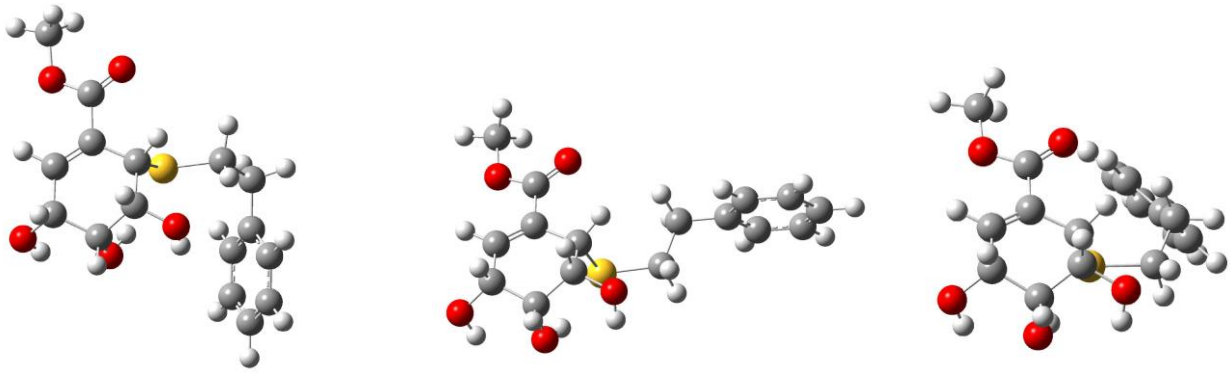

Conformer 1, RE = 1.1 kcal/mol (4.1%) Conformer 2, RE = 0.06 kcal/mol (21.6%) Conformer 3, RE = 0.69 kcal/mol (7.5%)

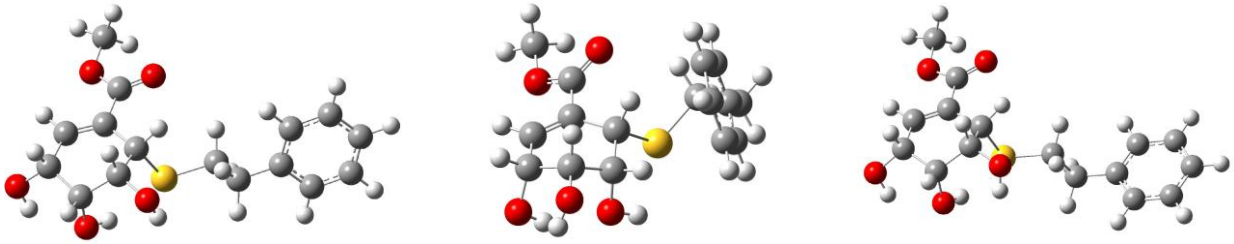

Conformer 4, RE = 1.0 kcal/mol (4.1%) Conformer 5, RE = 1.5 kcal/mol (2.0%) Conformer 6, RE = 0.38 kcal/mol (12.6%)

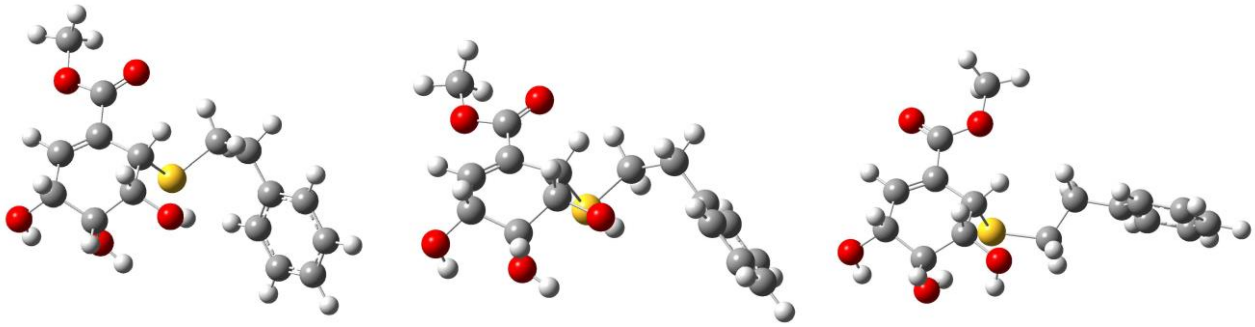

Conformer 7, RE = 0.11 kcal/mol (19.9%) Conformer 8, RE = 0 kcal/mol (24.0%) Conformer 9, RE = 1.0 kcal/mol (4.1%)

Figure S19. Optimized conformers of **7b** at the 6-311+G(2d,p) level in the gas phase.

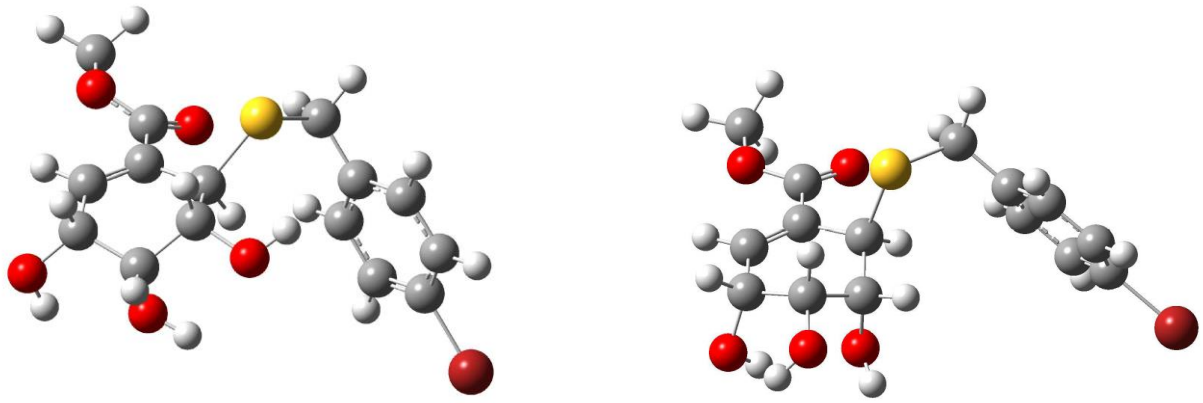

Conformer 1, RE = 0.44 kcal/mol (32.1%) Conformer 2, RE = 0 kcal/mol (67.9%)

Figure S20. Optimized conformers of **8a** at the 6-311+G(2d,p) level in the gas phase.

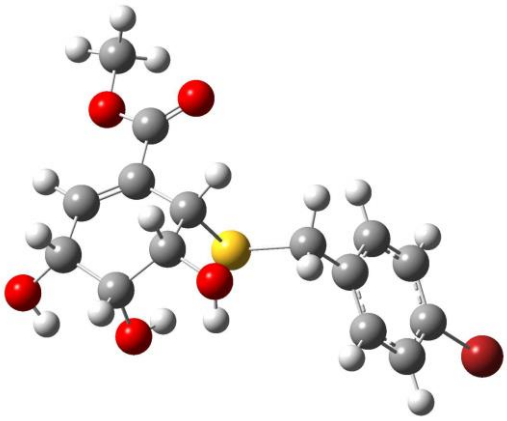

Conformer 1, RE = 1.4 kcal/mol (4.1%)

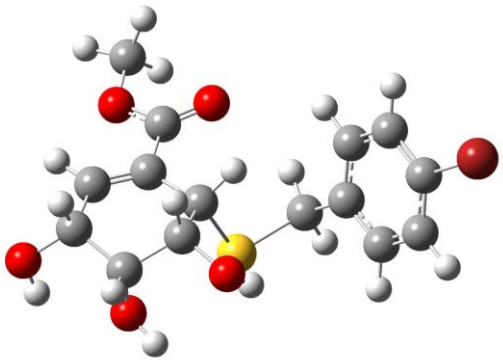

Conformer 2, RE = 0 kcal/mol (46.9%)

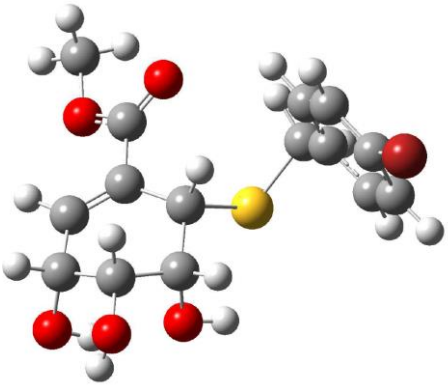

Conformer 3, RE = 1.1 kcal/mol (7.0%)

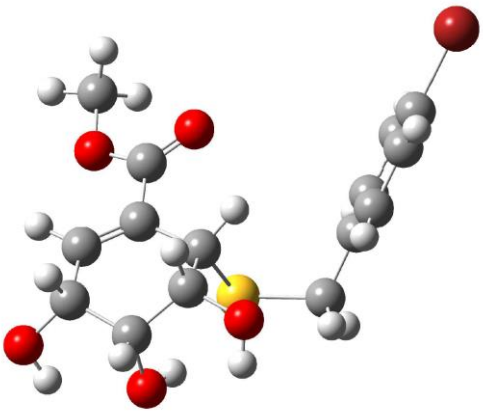

Conformer 4, RE = 1.8 kcal/mol (2.1%)

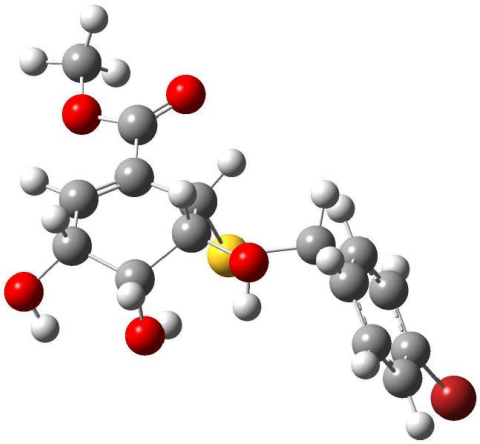

Conformer 5, RE = 1.4 kcal/mol (4.1%)

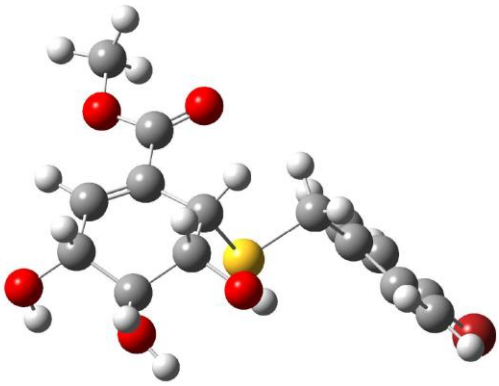

Conformer 6, RE = 0.15 kcal/mol (35.9%)

Figure S21. Optimized conformers of **8b** at the 6-311+G(2d,p) level in the gas phase.

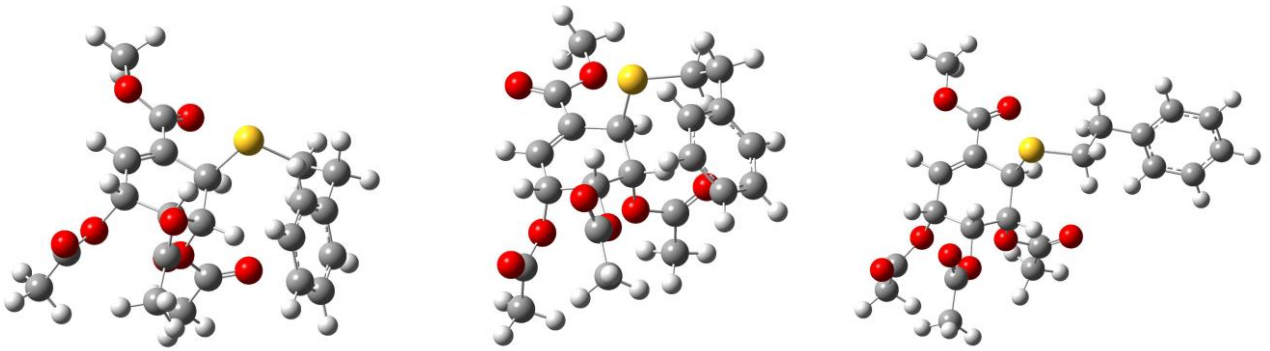

Conformer 1, RE = 1.8 kcal/mol (2.5%) Conformer 2, RE = 1.9 kcal/mol (2.1%) Conformer 3, RE = 0 kcal/mol (51.2%)

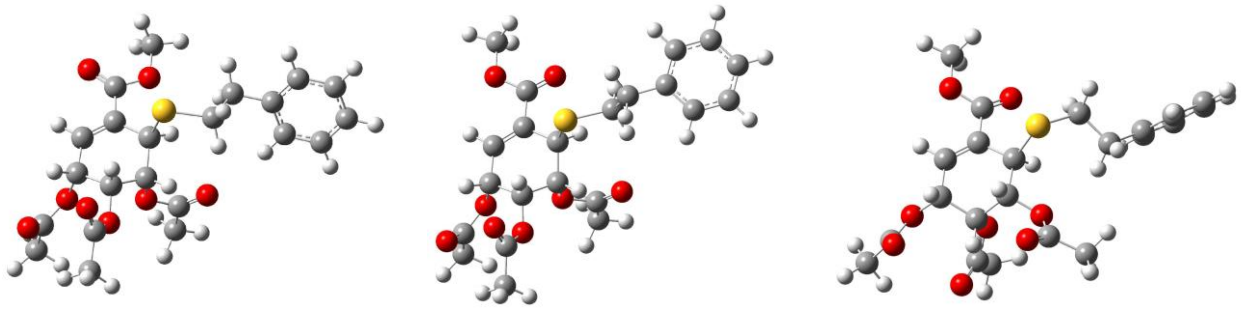

Conformer 4, RE = 0.37 kcal/mol (27.4%) Conformer 5, RE = 1.4 kcal/mol (5.1%) Conformer 6, RE = 1.6 kcal/mol (3.5%)

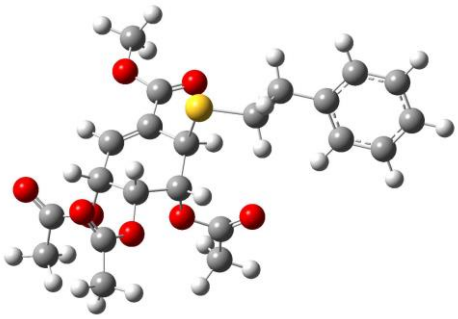

Conformer 7, RE = 1.1 kcal/mol (8.2%)

Figure S22. Optimized conformers of **12a** at the 6-31G(d,p) level in the gas phase.

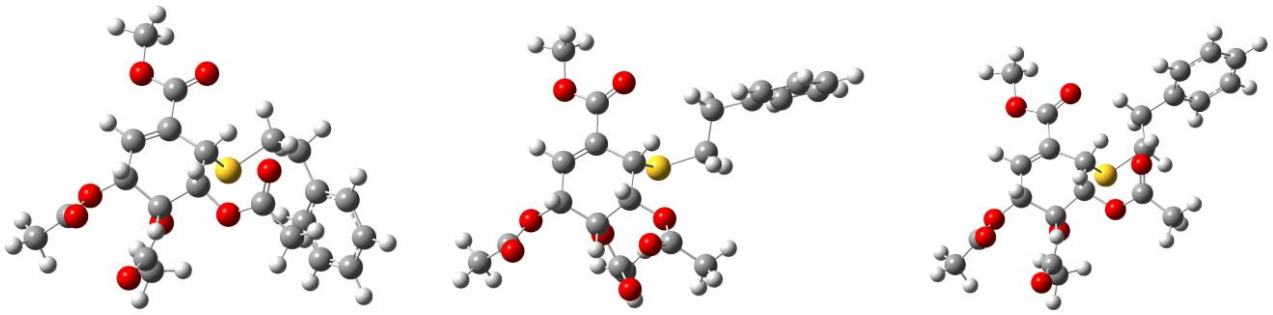

Conformer 1, RE = 0.8 kcal/mol (10.5%) Conformer 2, RE = 1.5 kcal/mol (3.6%) Conformer 3, RE = 1.1 kcal/mol (6.7%)

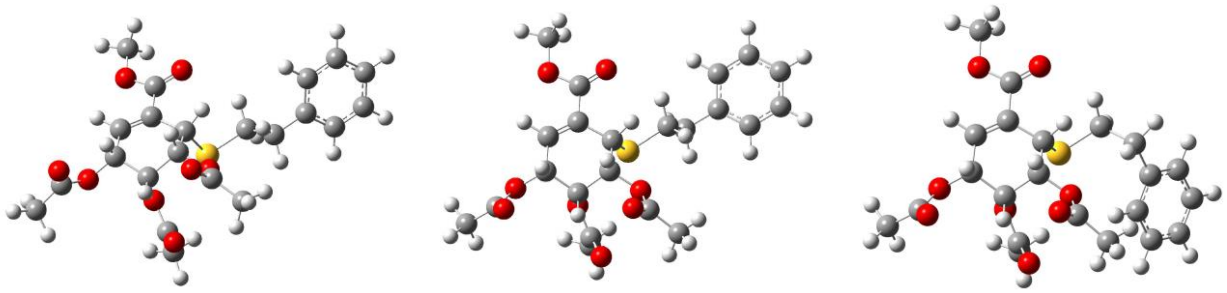

Conformer 4, RE = 0.9 kcal/mol (9.1%) Conformer 5, RE = 1.3 kcal/mol (4.5%) Conformer 6, RE = 1.5 kcal/mol (3.6%)

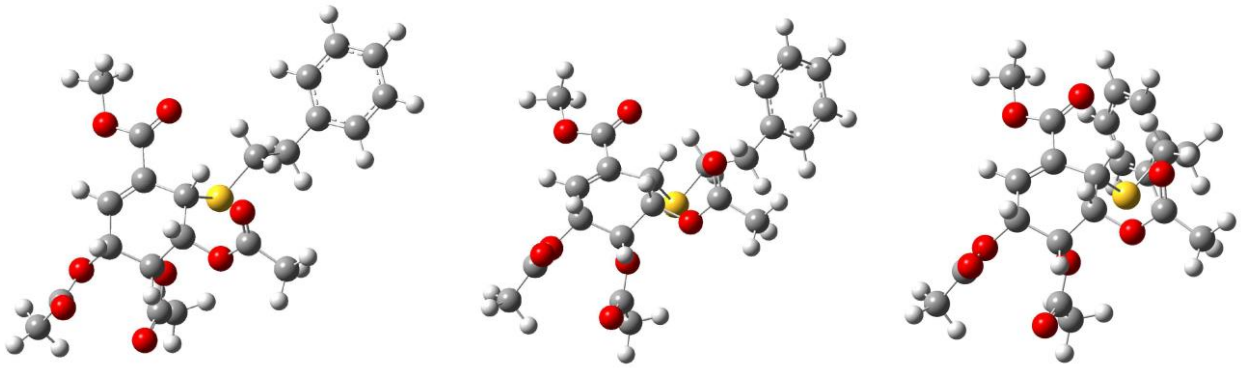

Conformer 7, RE = 0.6 kcal/mol (15.1%) Conformer 8, RE = 0 kcal/mol (44.0%) Conformer 9, RE = 1.6 kcal/mol (2.8%)

Figure S23. Optimized conformers of **12b** at the 6-31G(d,p) level in the gas phase.

Figure S24. ^{1}H NMR (400 MHz, methanol-d_4, 25 ℃) spectrum of compound **3**

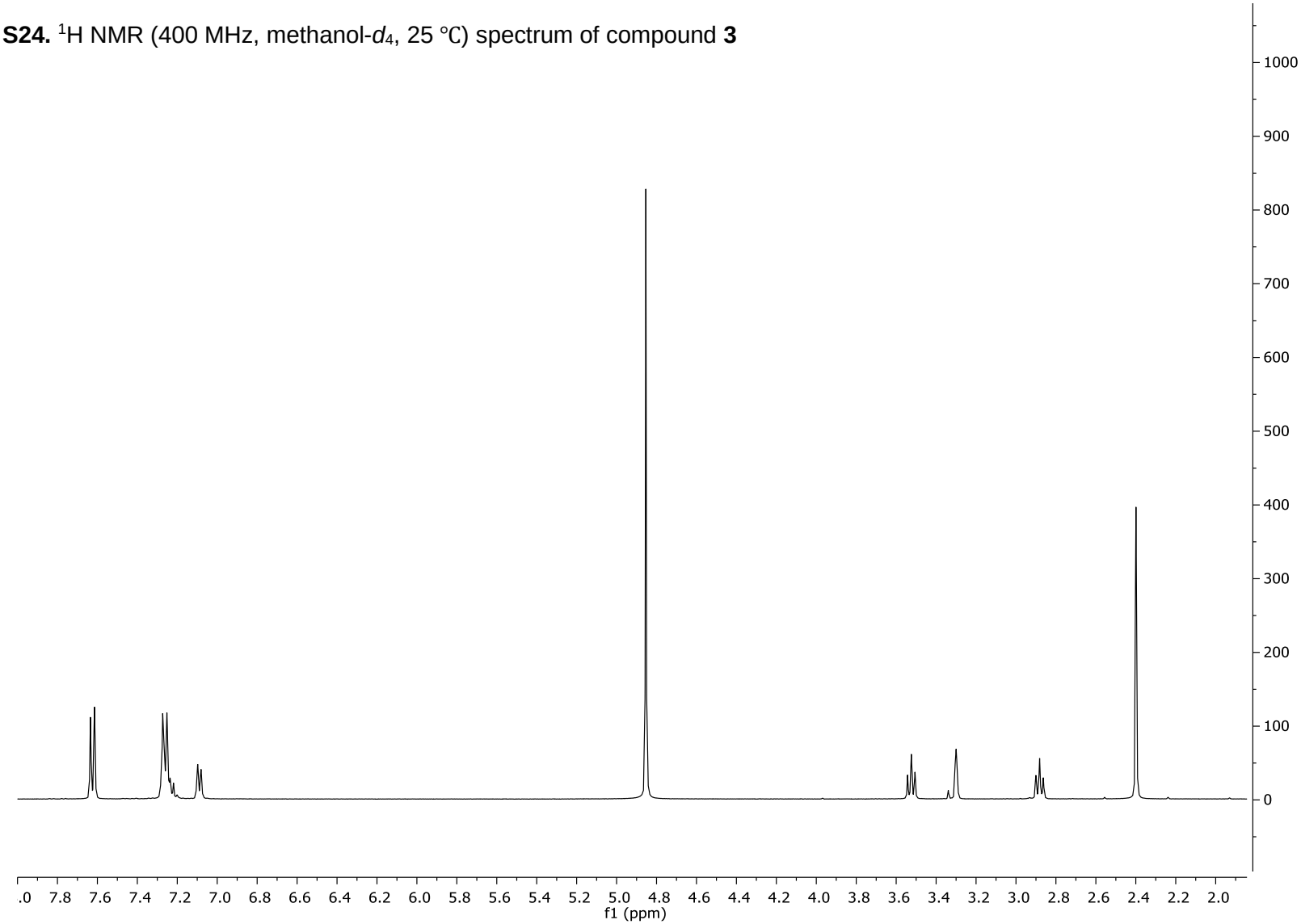

Figure S25. ^{13}C NMR (100 MHz, methanol-d_4, 25 °C) spectrum of compound **3**

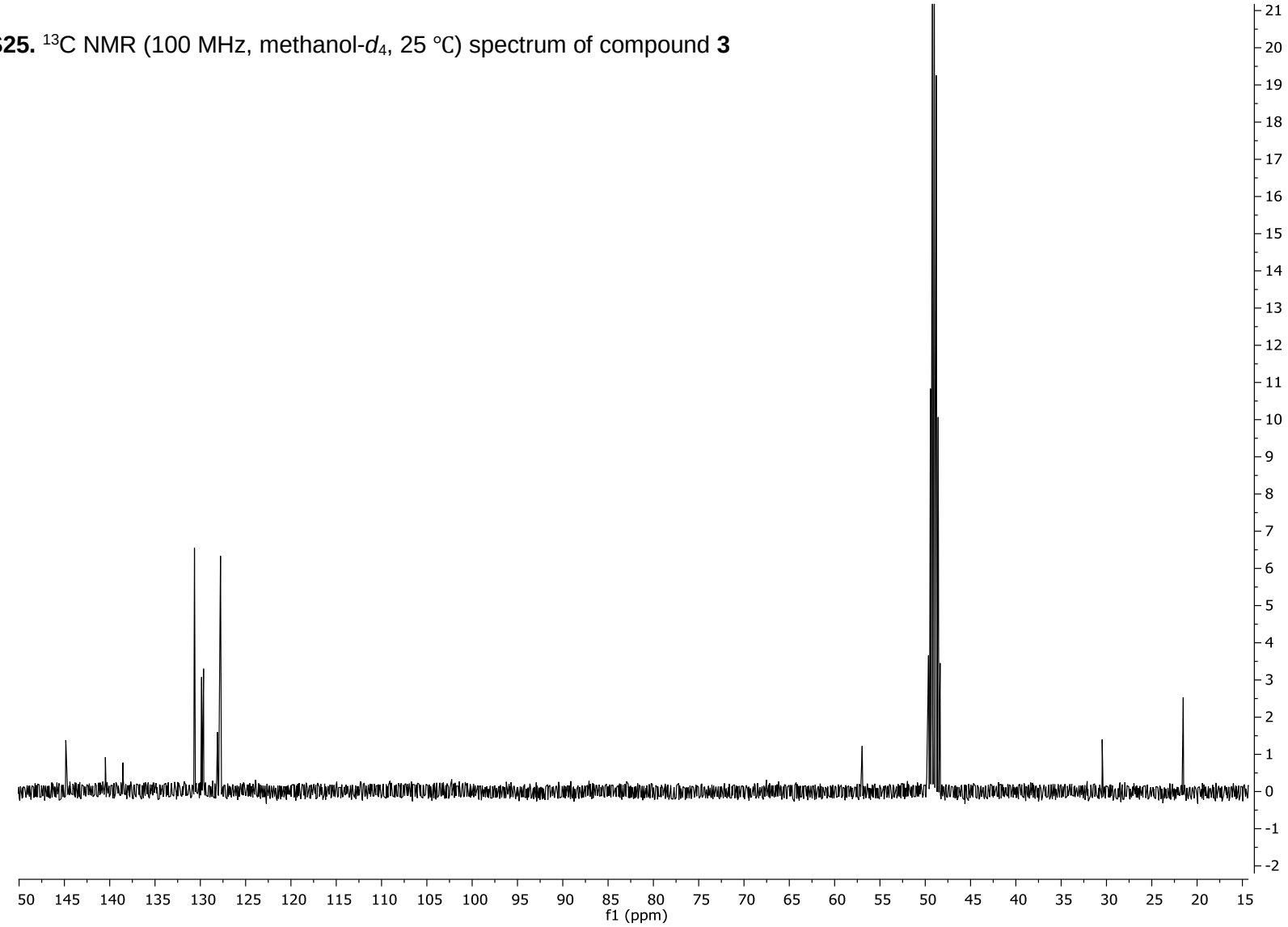

Figure S26. ^{1}H NMR (400 MHz, $CDCl_3$, 25 ℃) spectrum of compound **7**

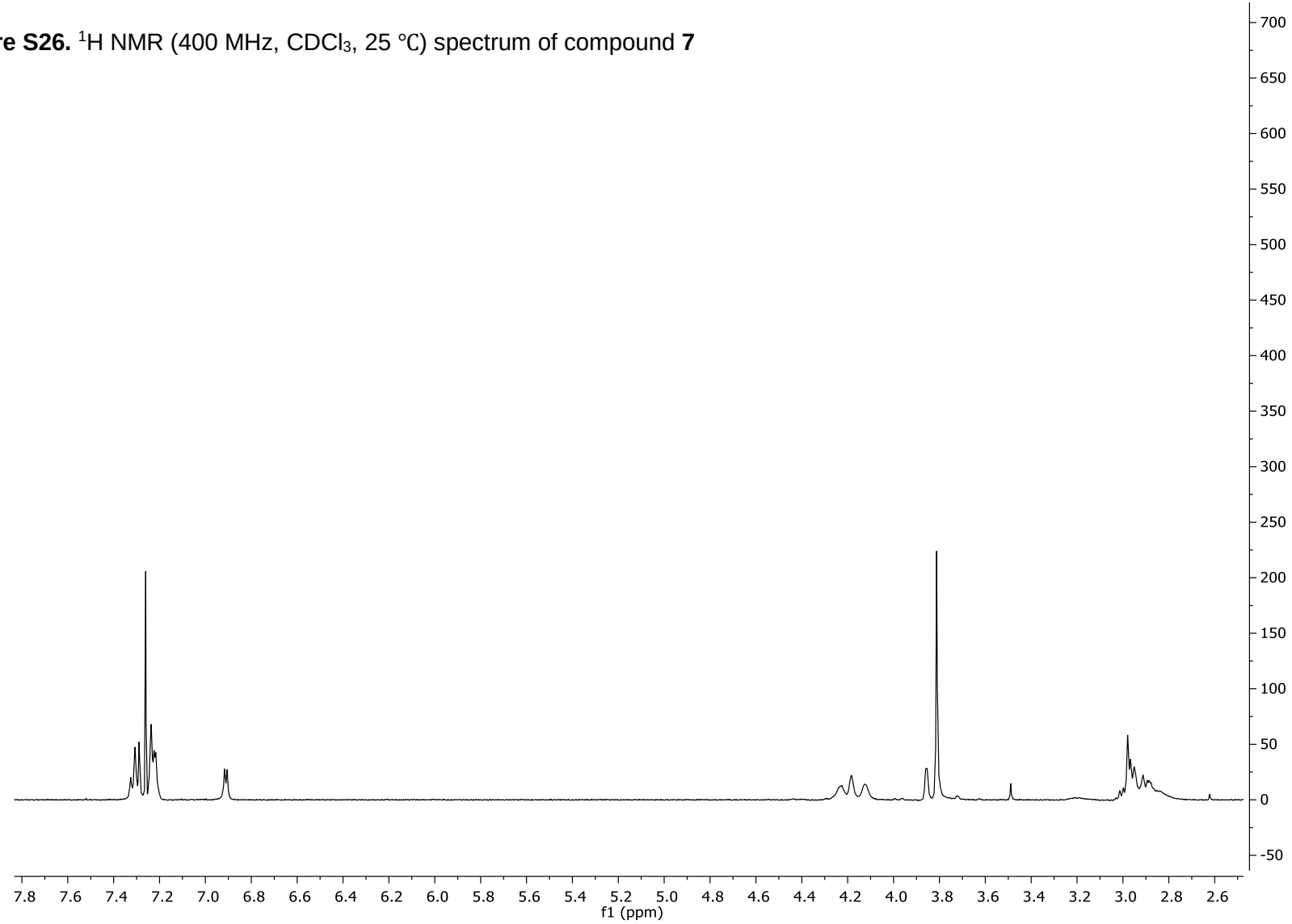

Figure S27. ^{13}C NMR (100 MHz, $CDCl_3$, 25 ℃) spectrum of compound **7**

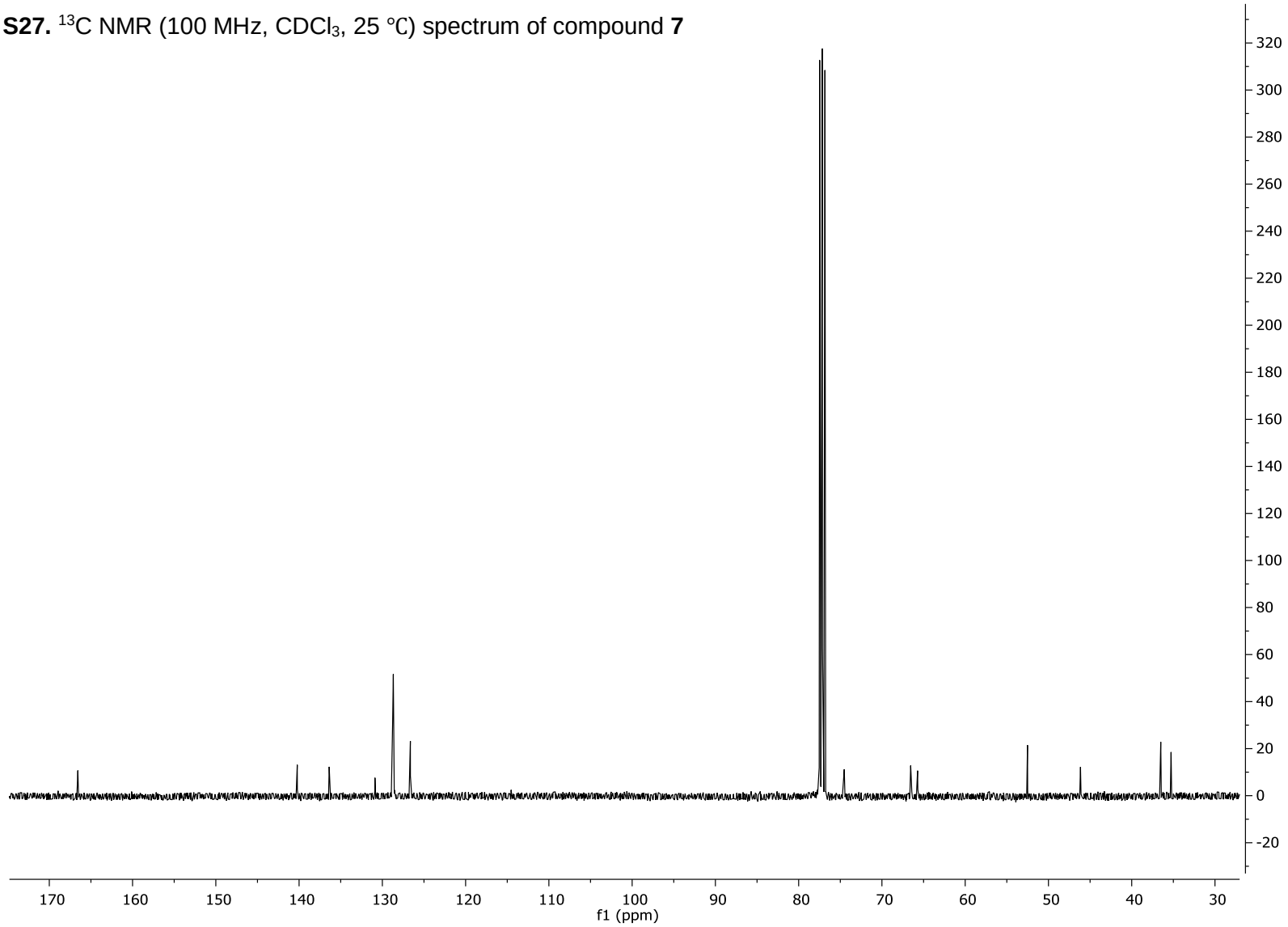

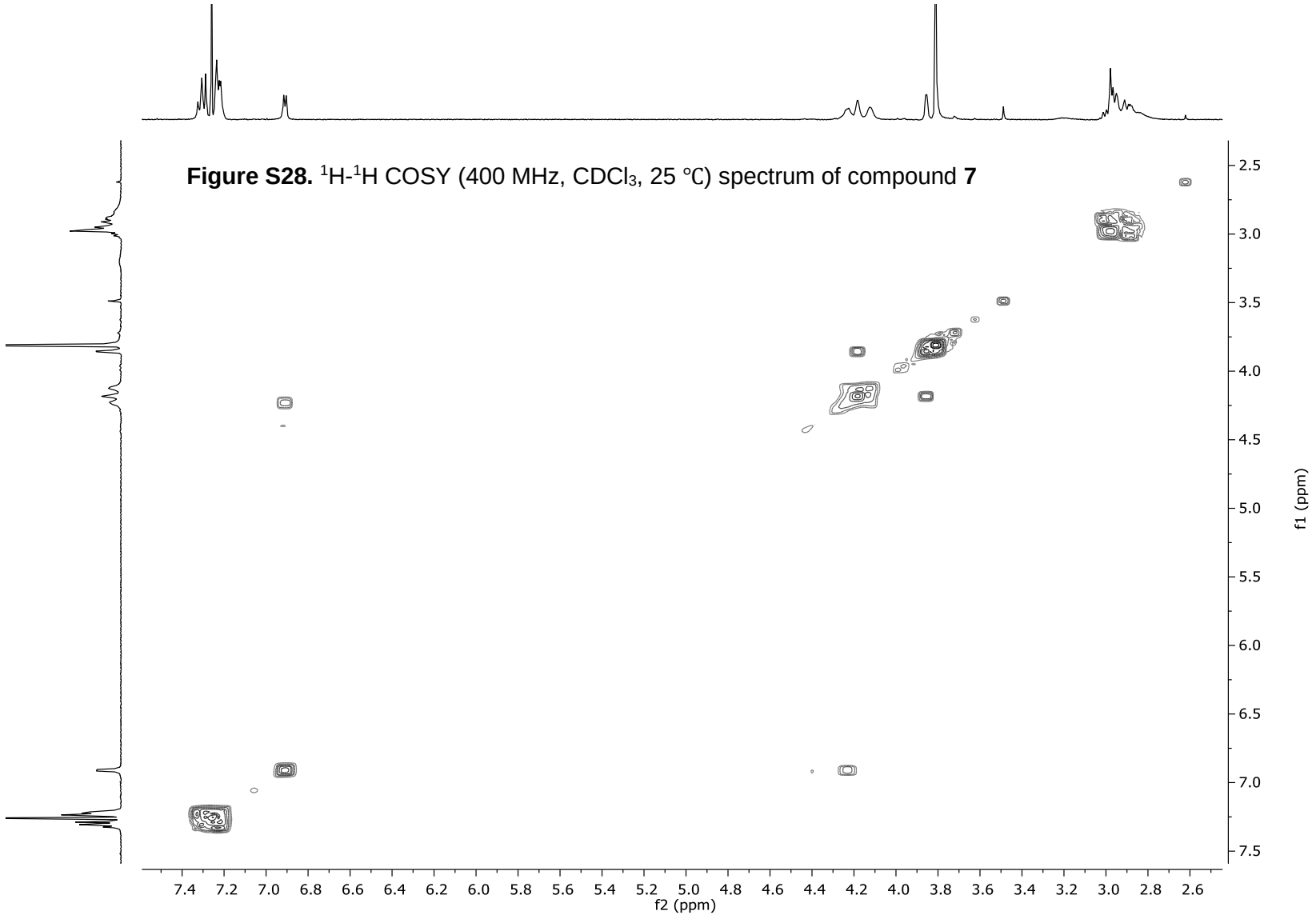

Figure S28. ^{1}H-^{1}H COSY (400 MHz, $CDCl_3$, 25 ℃) spectrum of compound **7**

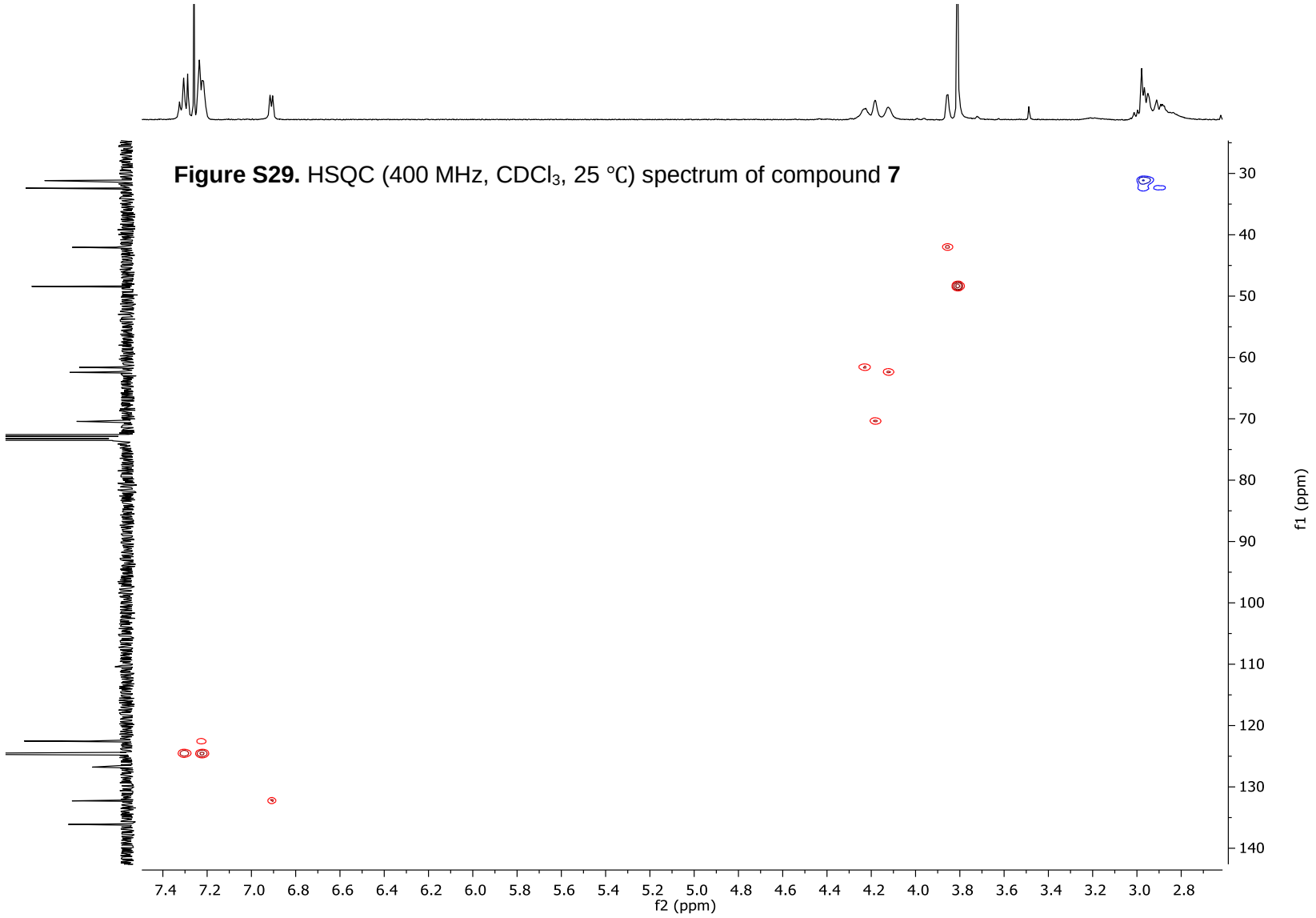

Figure S29. HSQC (400 MHz, $CDCl_3$, 25 ℃) spectrum of compound **7**

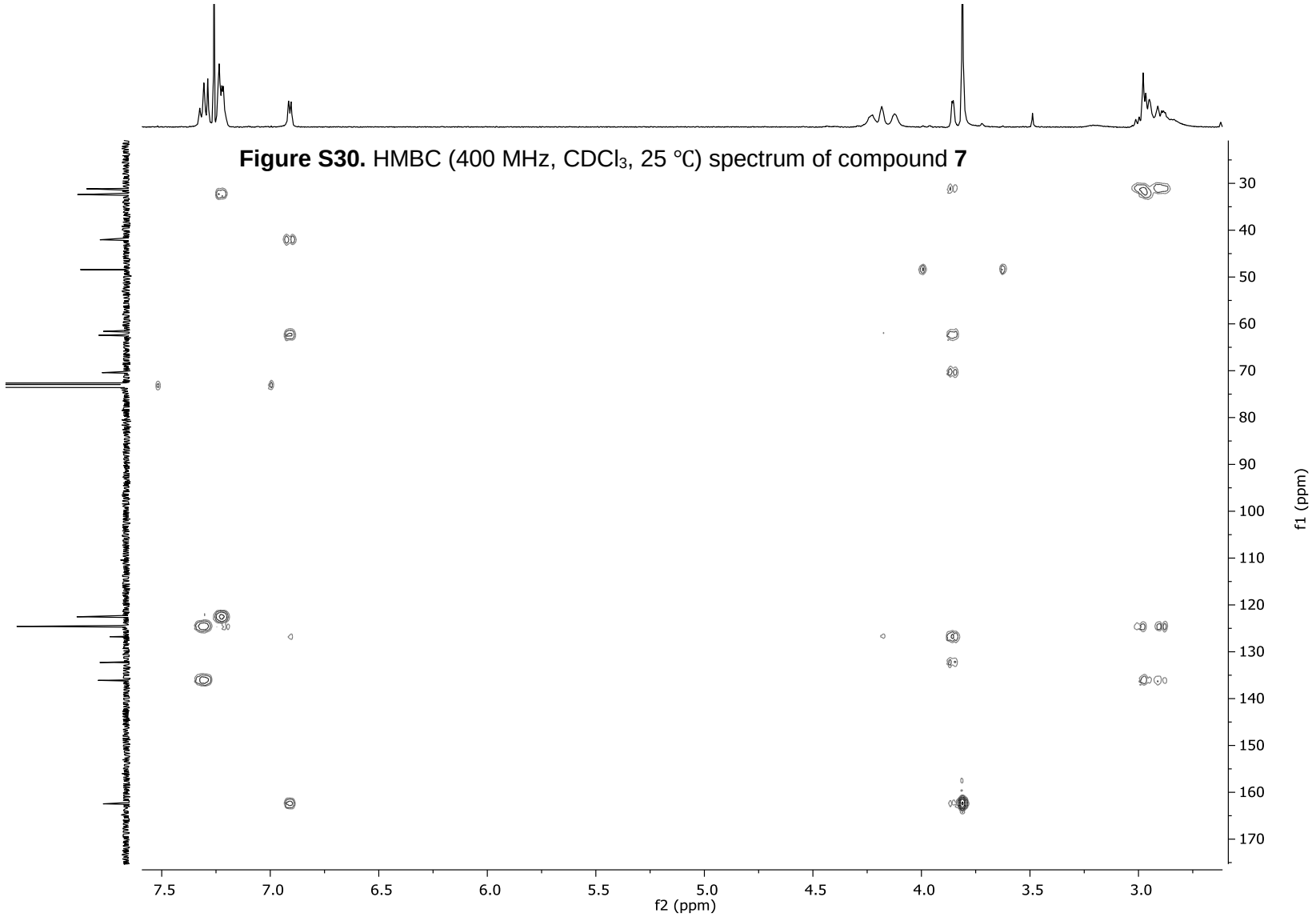

Figure S30. HMBC (400 MHz, $CDCl_3$, 25 ℃) spectrum of compound **7**

Figure S31. ^{1}H NMR (400 MHz, $CDCl_3$, 25 ℃) spectrum of compound **8**

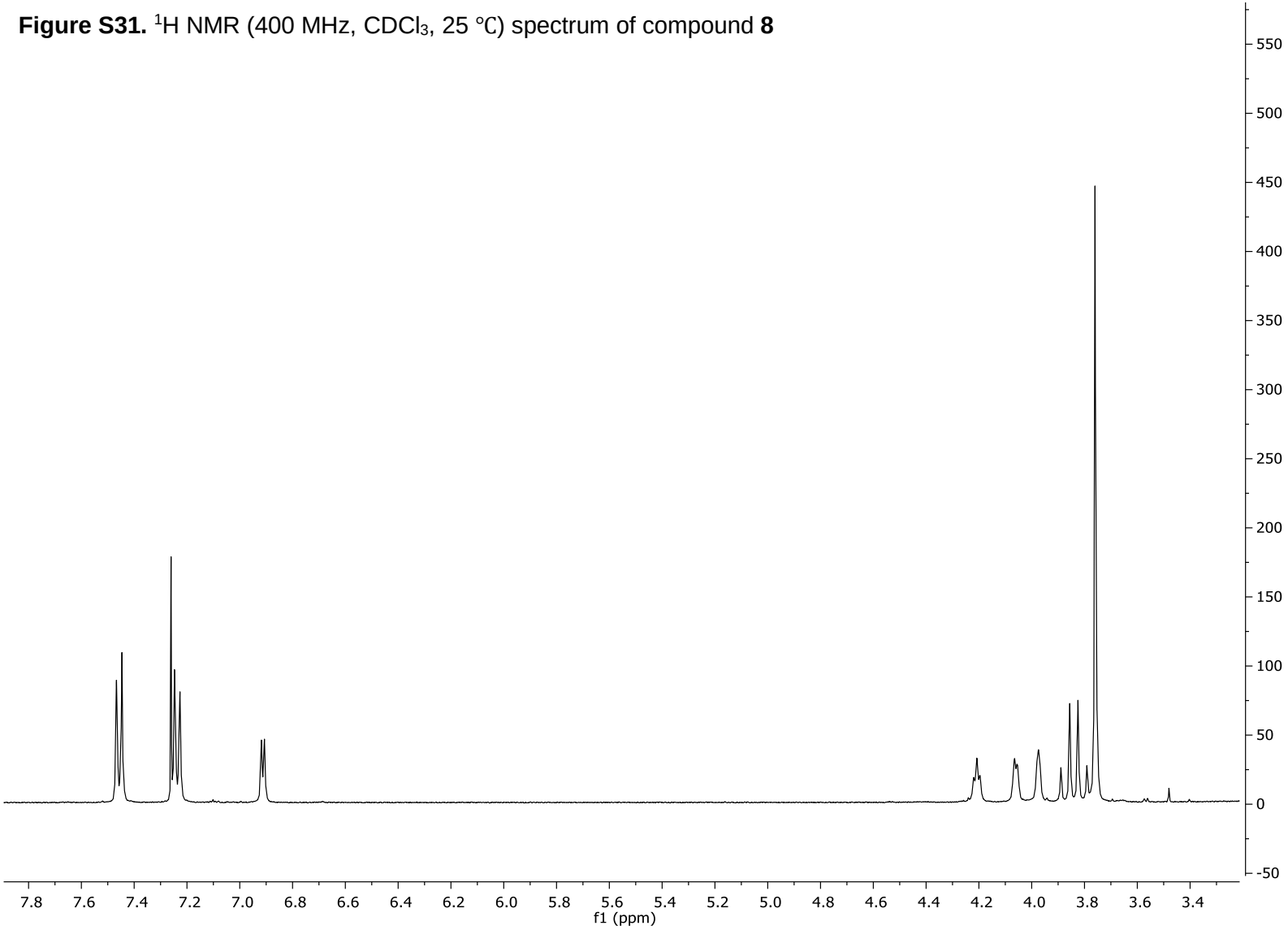

Figure S32. ^{13}C NMR (100 MHz, $CDCl_3$, 25 ℃) spectrum of compound **8**

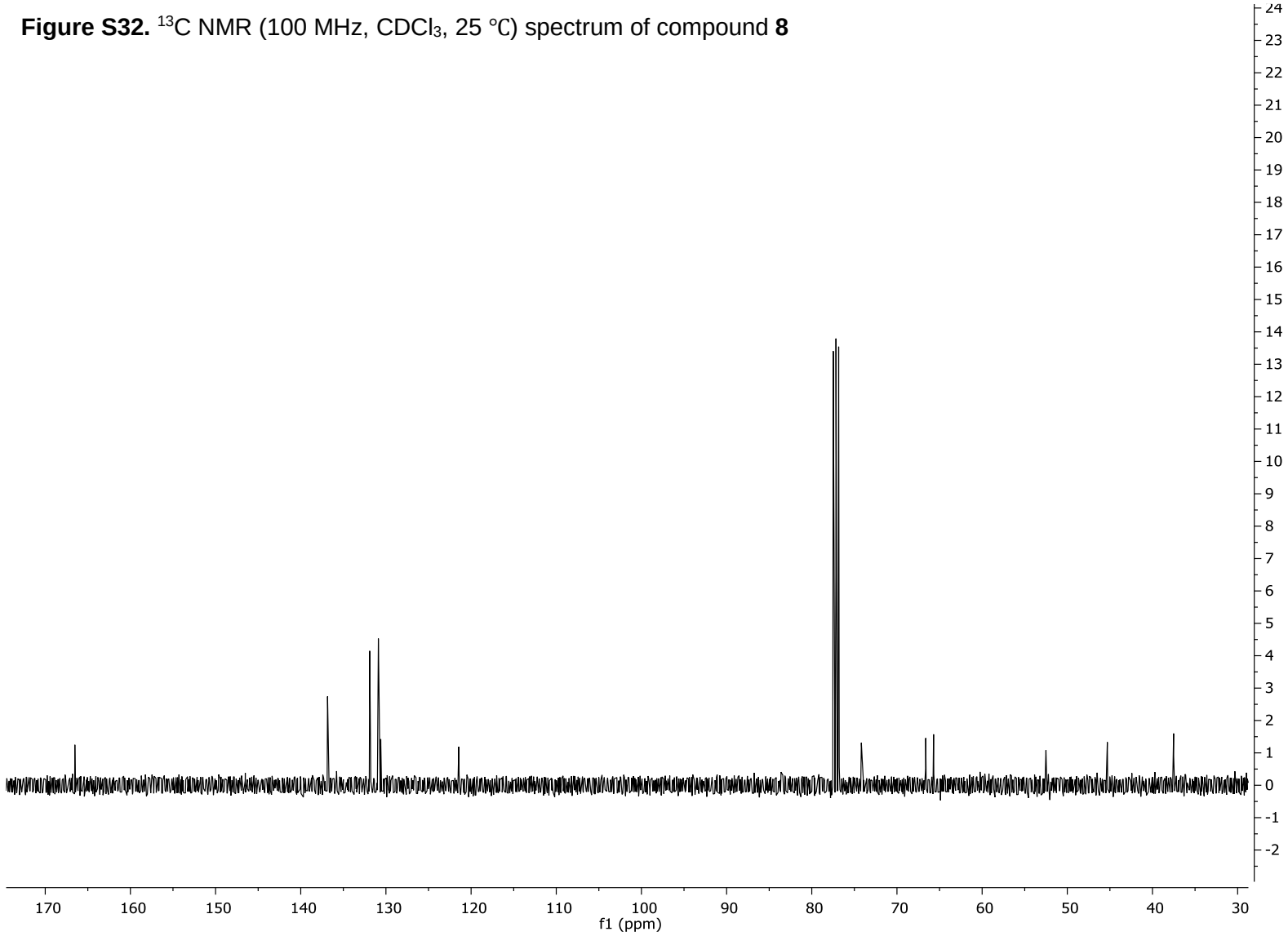

Figure S33. ^{1}H-^{1}H COSY (400 MHz, $CDCl_3$, 25 ℃) spectrum of compound **8**

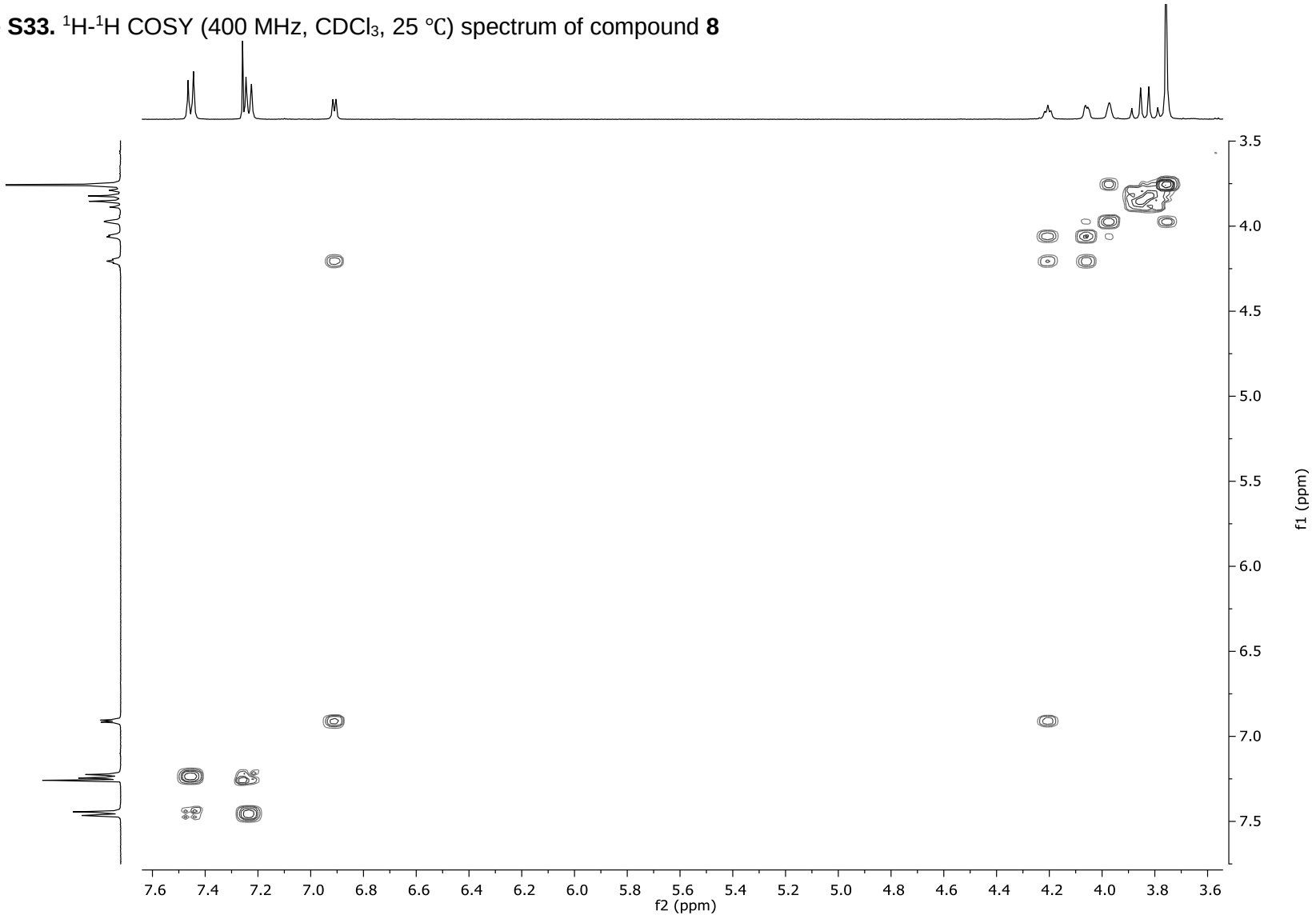

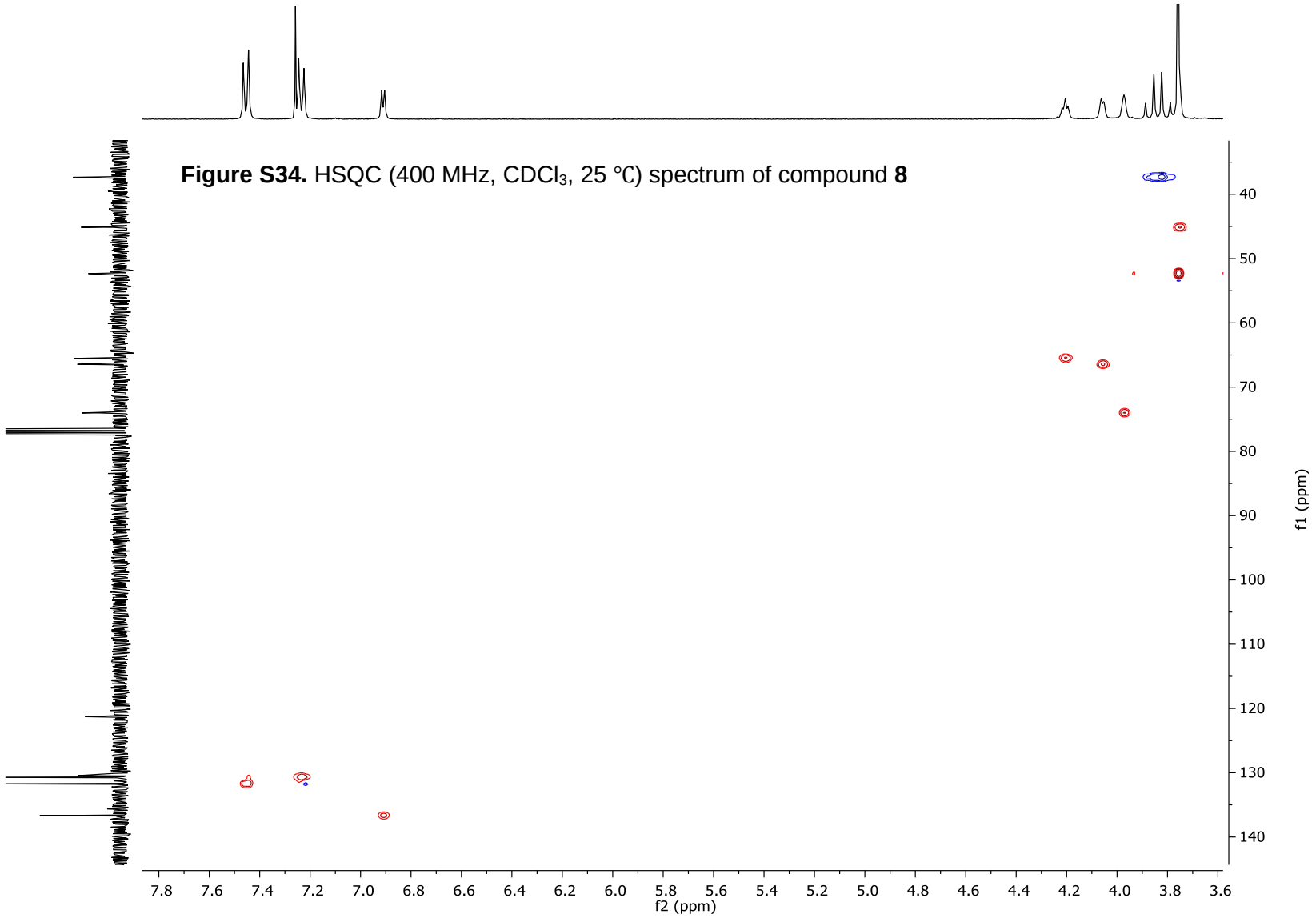

Figure S34. HSQC (400 MHz, $CDCl_3$, 25 ℃) spectrum of compound **8**

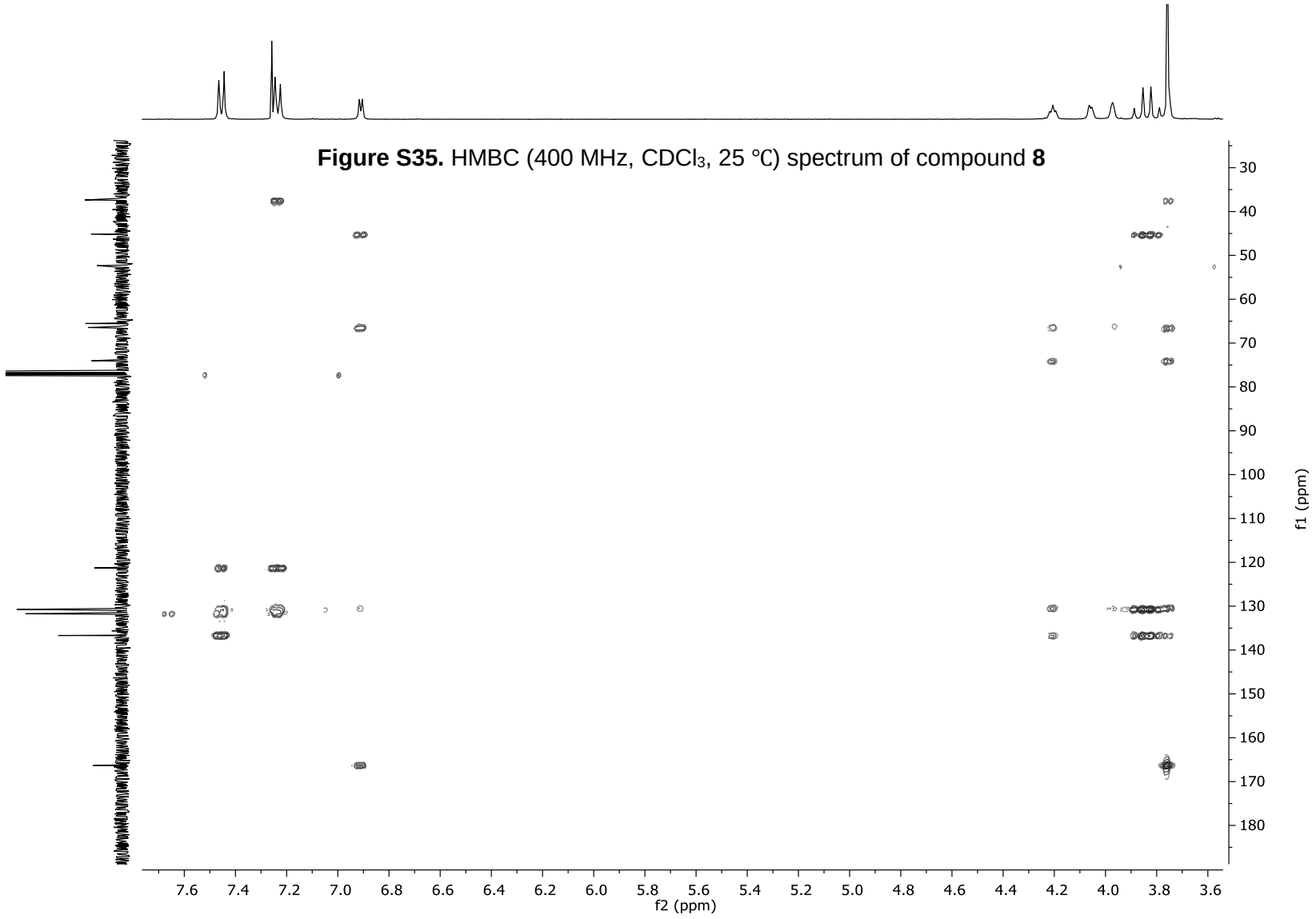

Figure S35. HMBC (400 MHz, $CDCl_3$, 25 ℃) spectrum of compound **8**

Figure S36. ^{1}H NMR (500 MHz, methanol-d_4, 25 °C) spectrum of compound **11**

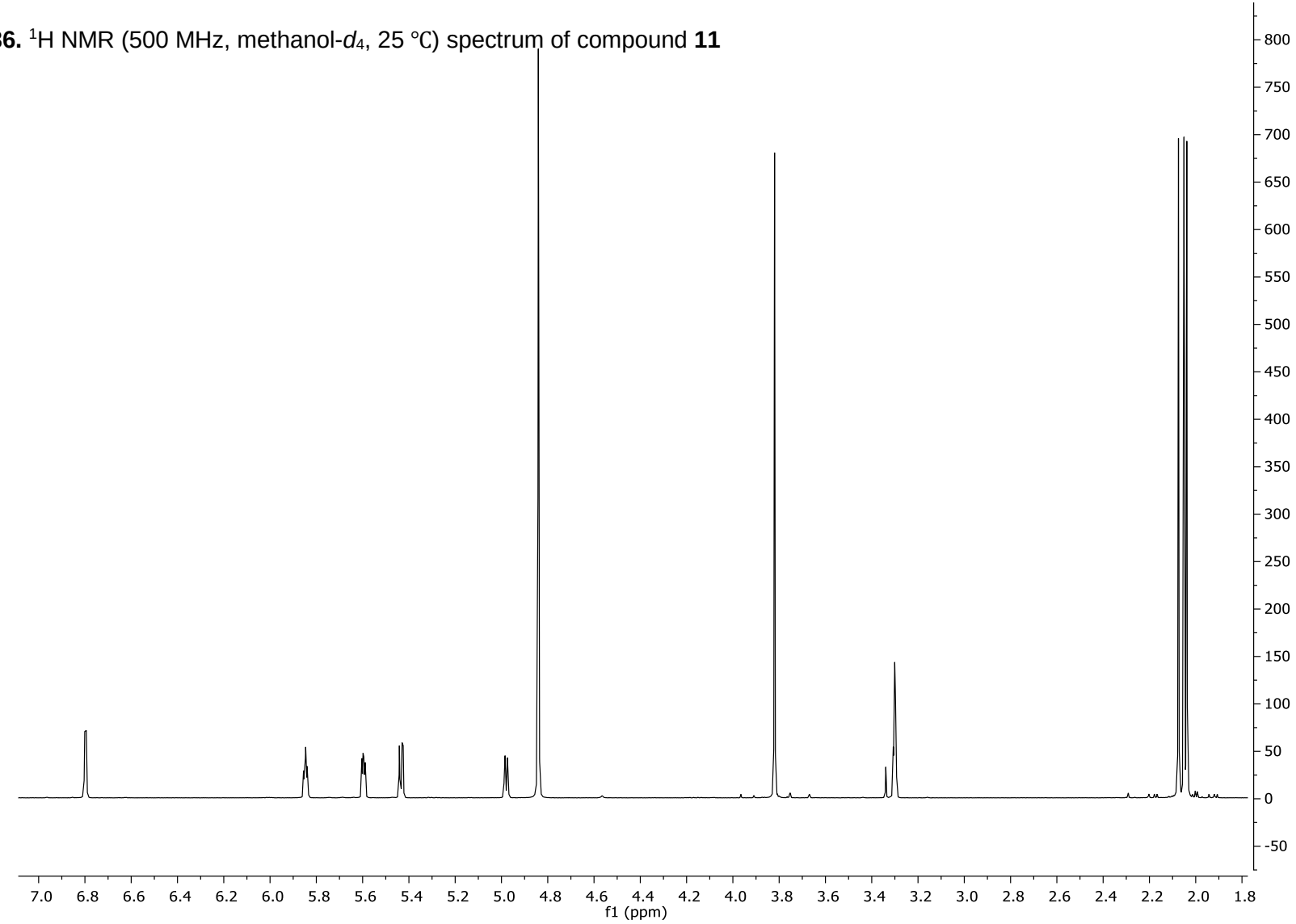

Figure S37. ^{13}C NMR (125 MHz, methanol-d_4, 25 ℃) spectrum of compound **11**

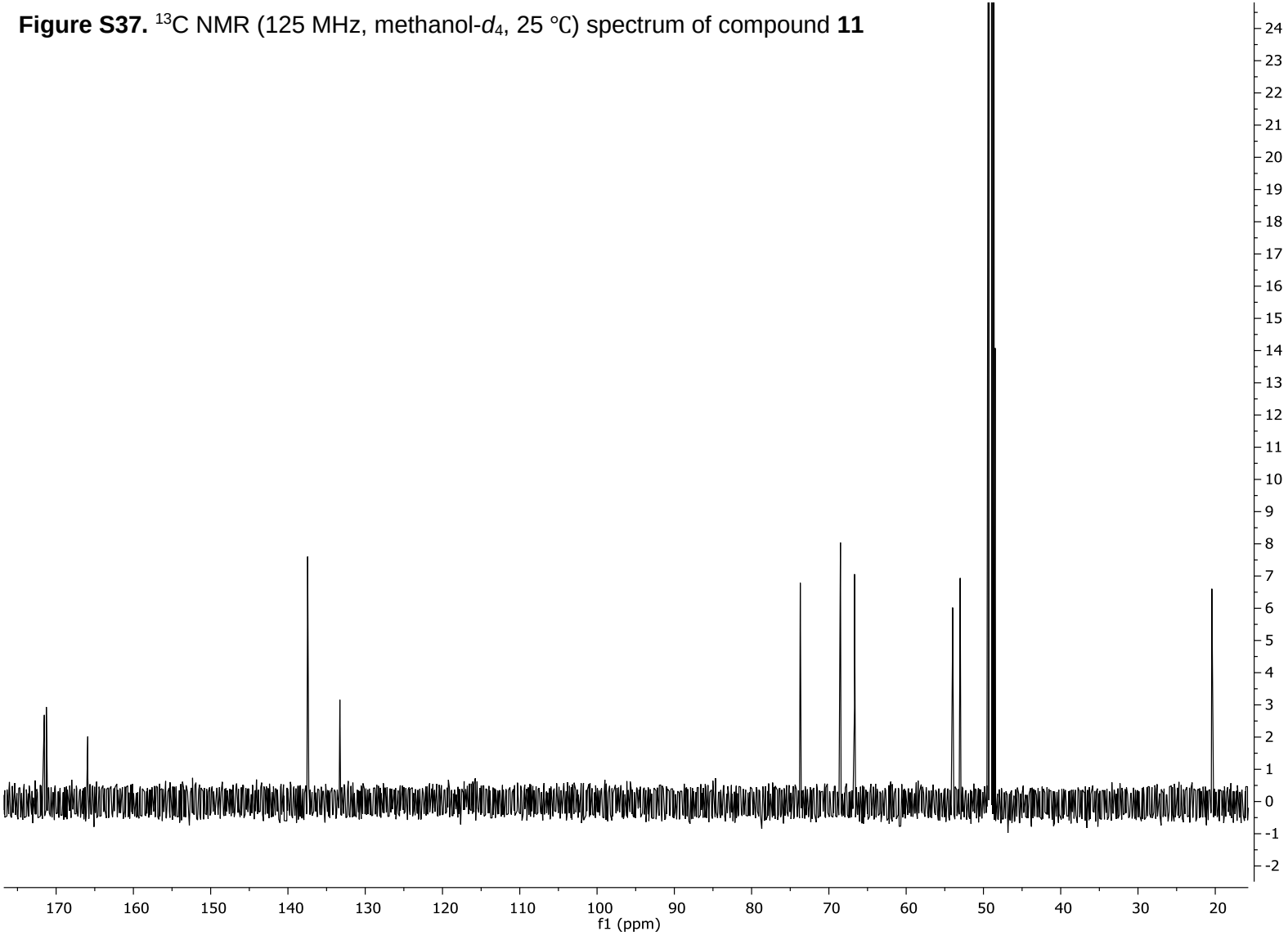

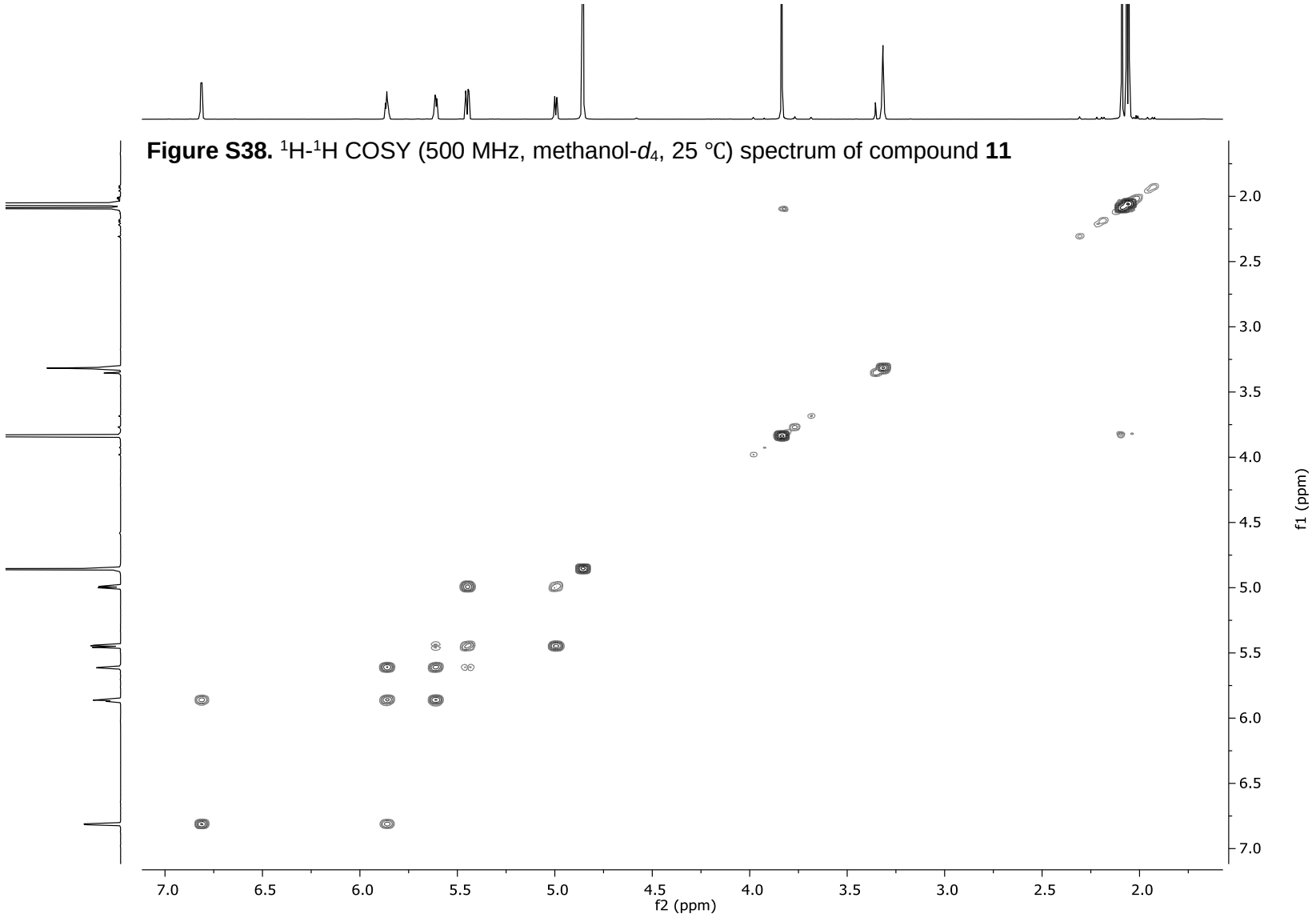

Figure S38. ^{1}H-^{1}H COSY (500 MHz, methanol-d_4, 25 ℃) spectrum of compound **11**

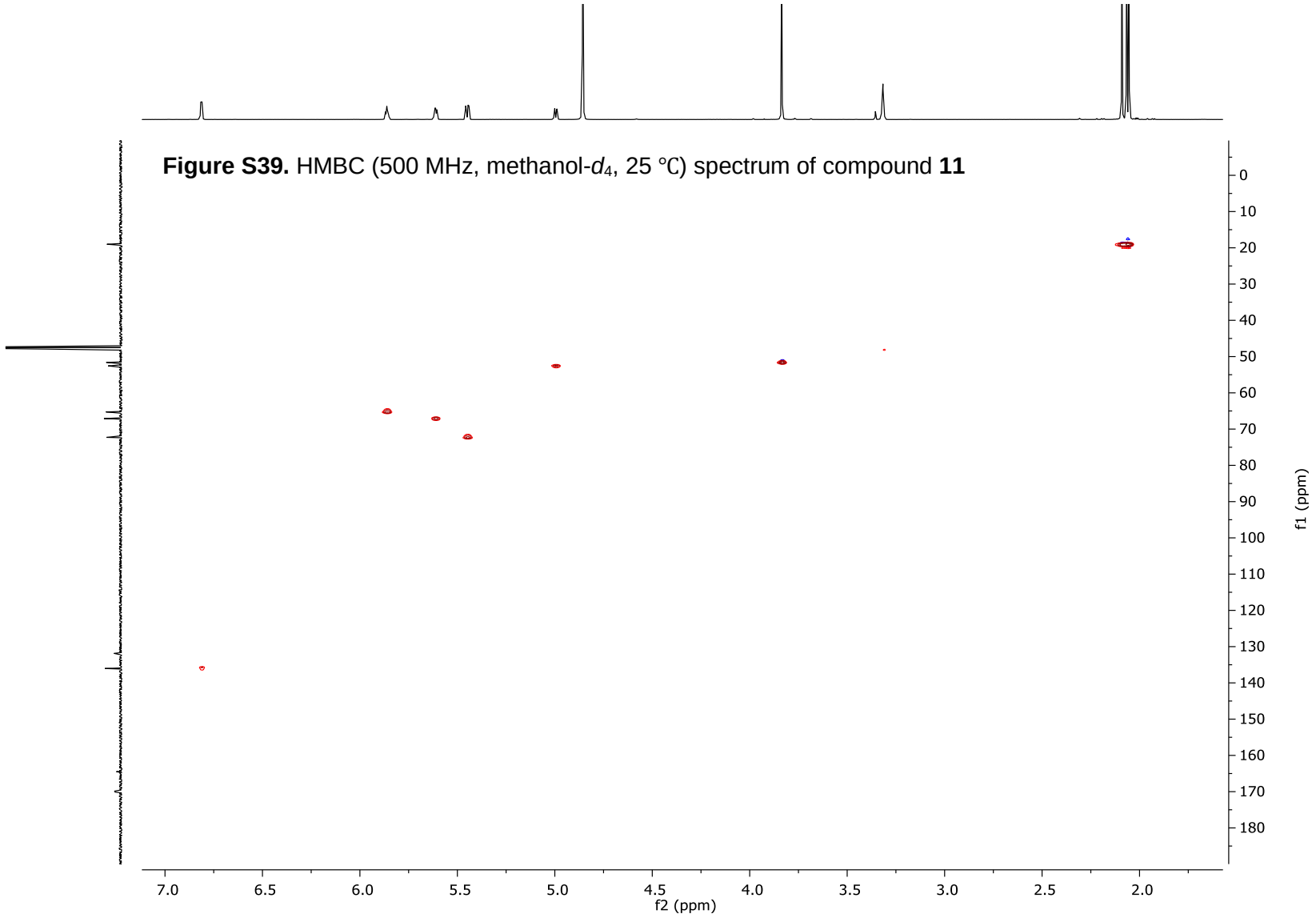

Figure S39. HMBC (500 MHz, methanol-d_4, 25 ℃) spectrum of compound **11**

Figure S40. ^{1}H NMR (500 MHz, methanol-d_4, 25 ℃) spectrum of compound **12**

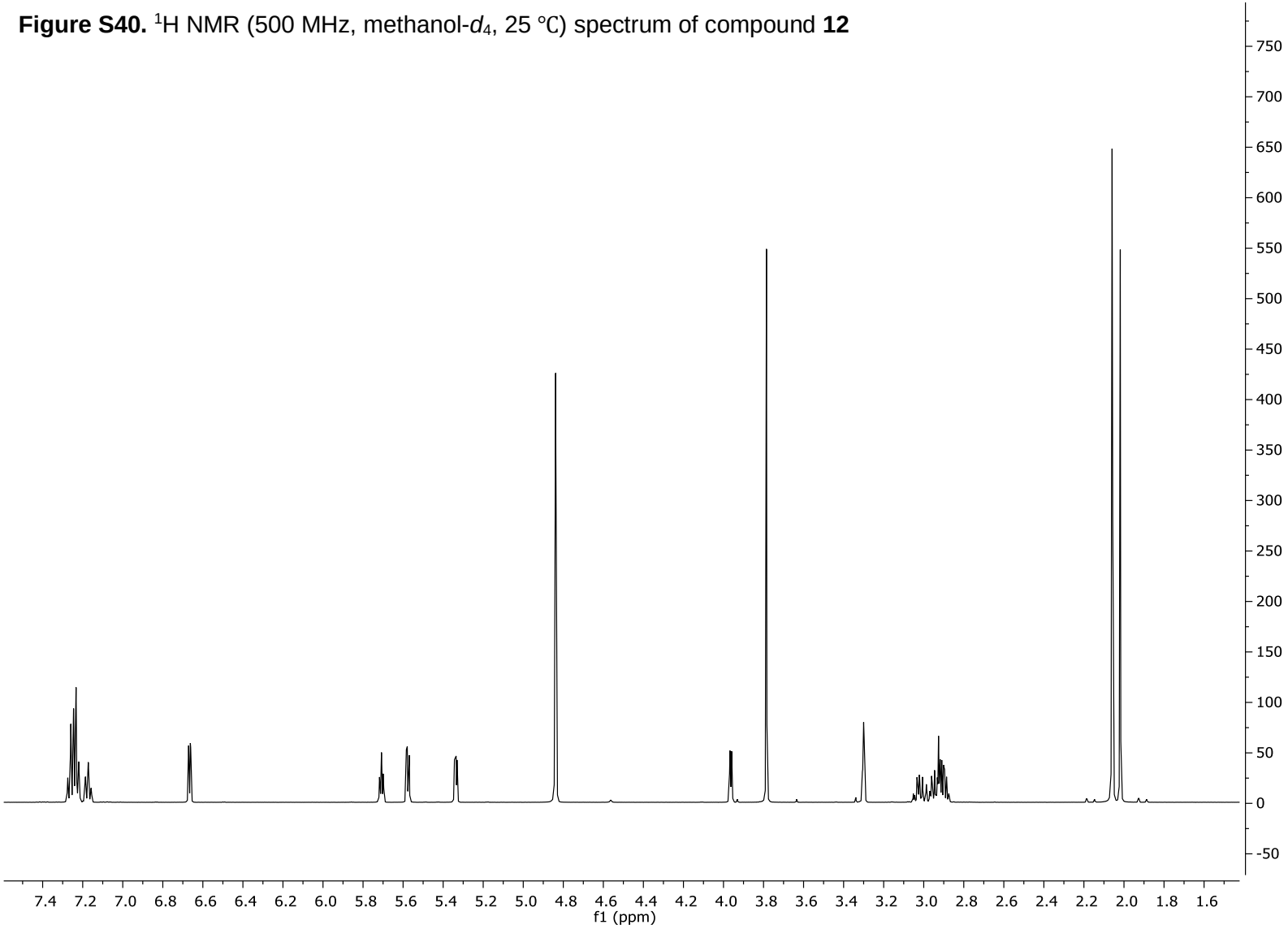

Figure S41. ^{13}C NMR (500 MHz, methanol-d_4, 25 ℃) spectrum of compound **12**

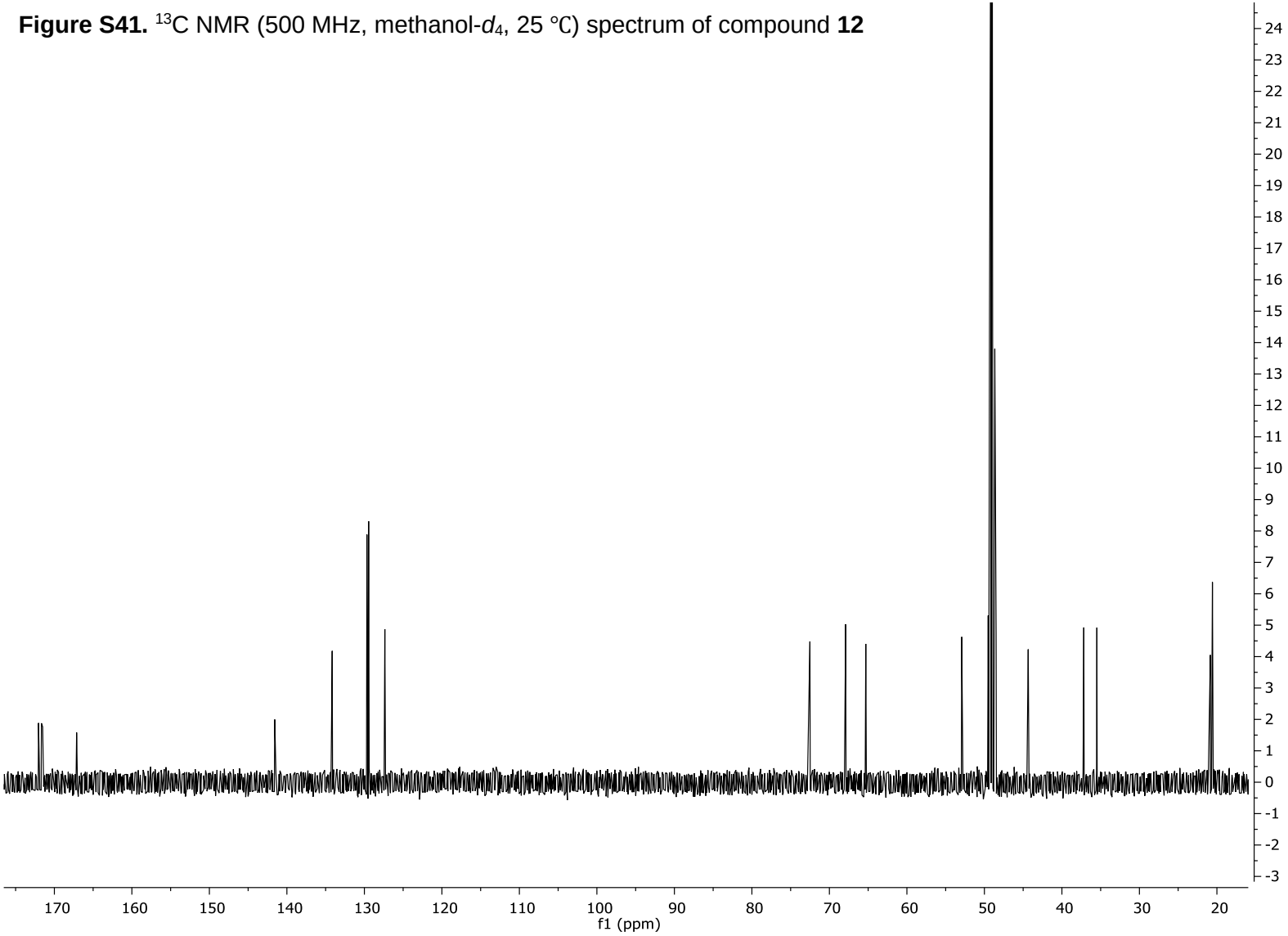

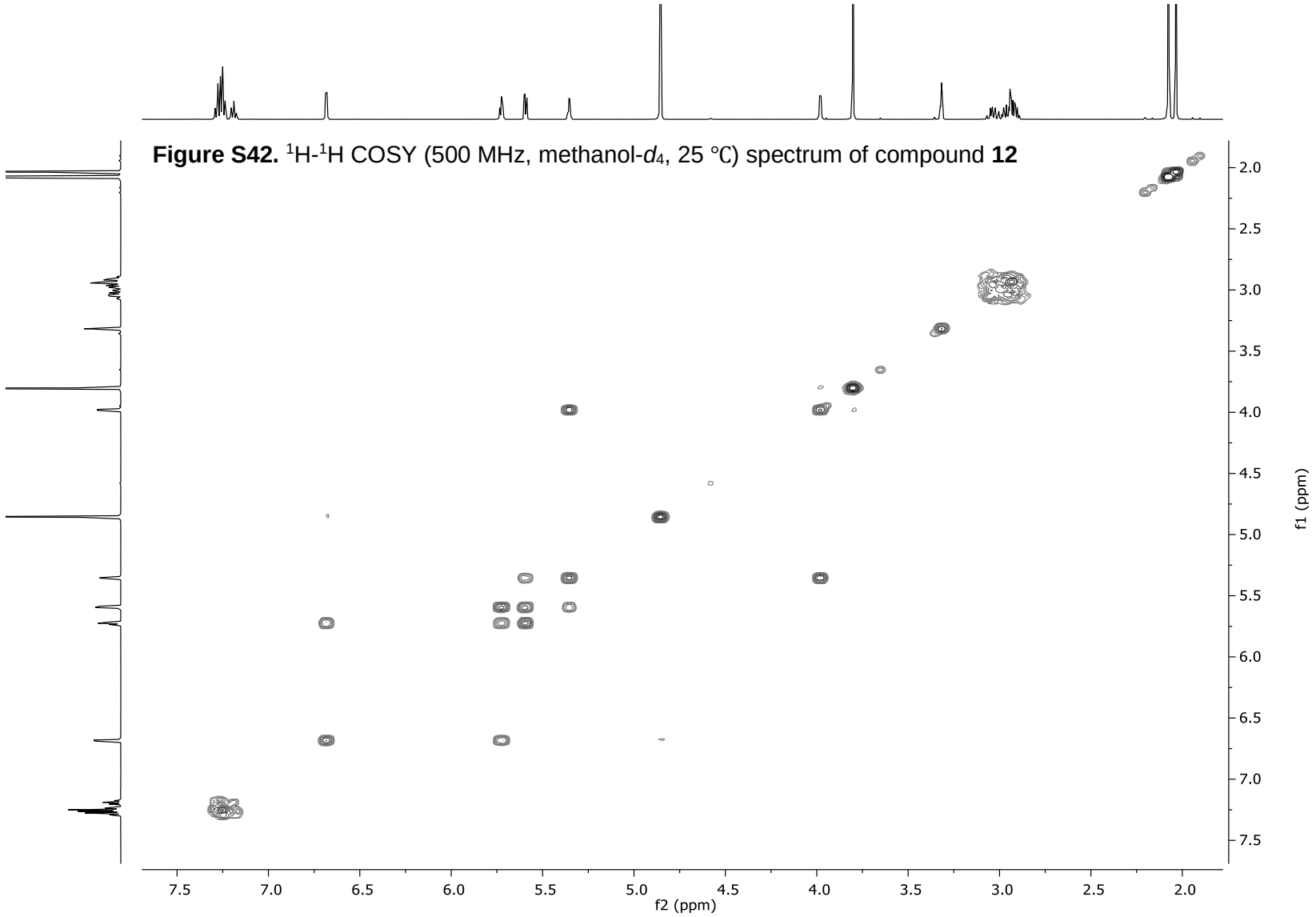

Figure S42. ^{1}H-^{1}H COSY (500 MHz, methanol-d_4, 25 ℃) spectrum of compound **12**

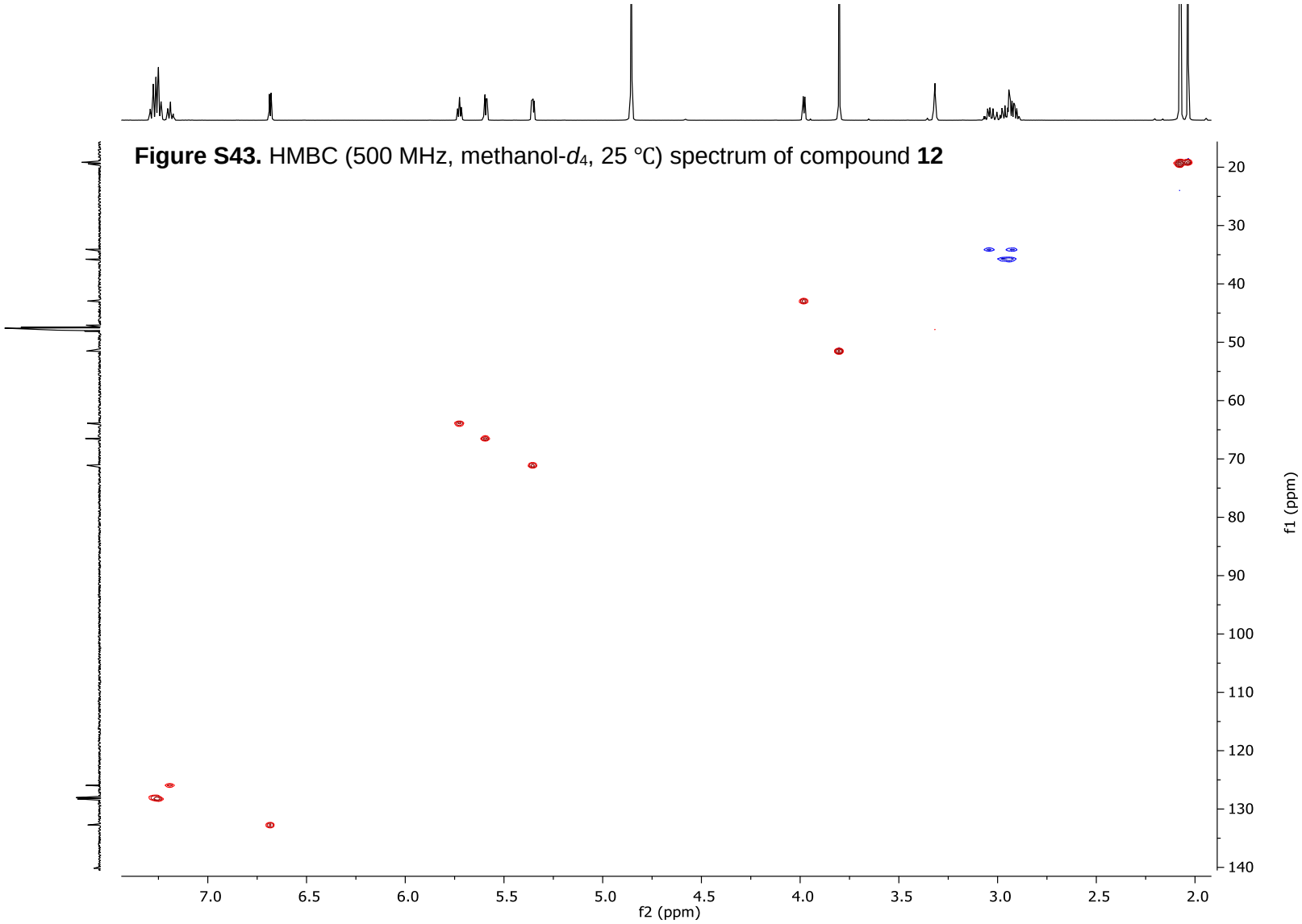

Figure S43. HMBC (500 MHz, methanol-d_4, 25 °C) spectrum of compound **12**

Figure S44. ^{1}H NMR (500 MHz, D_2O, 25 ℃) spectrum of (-)-methylshikimate

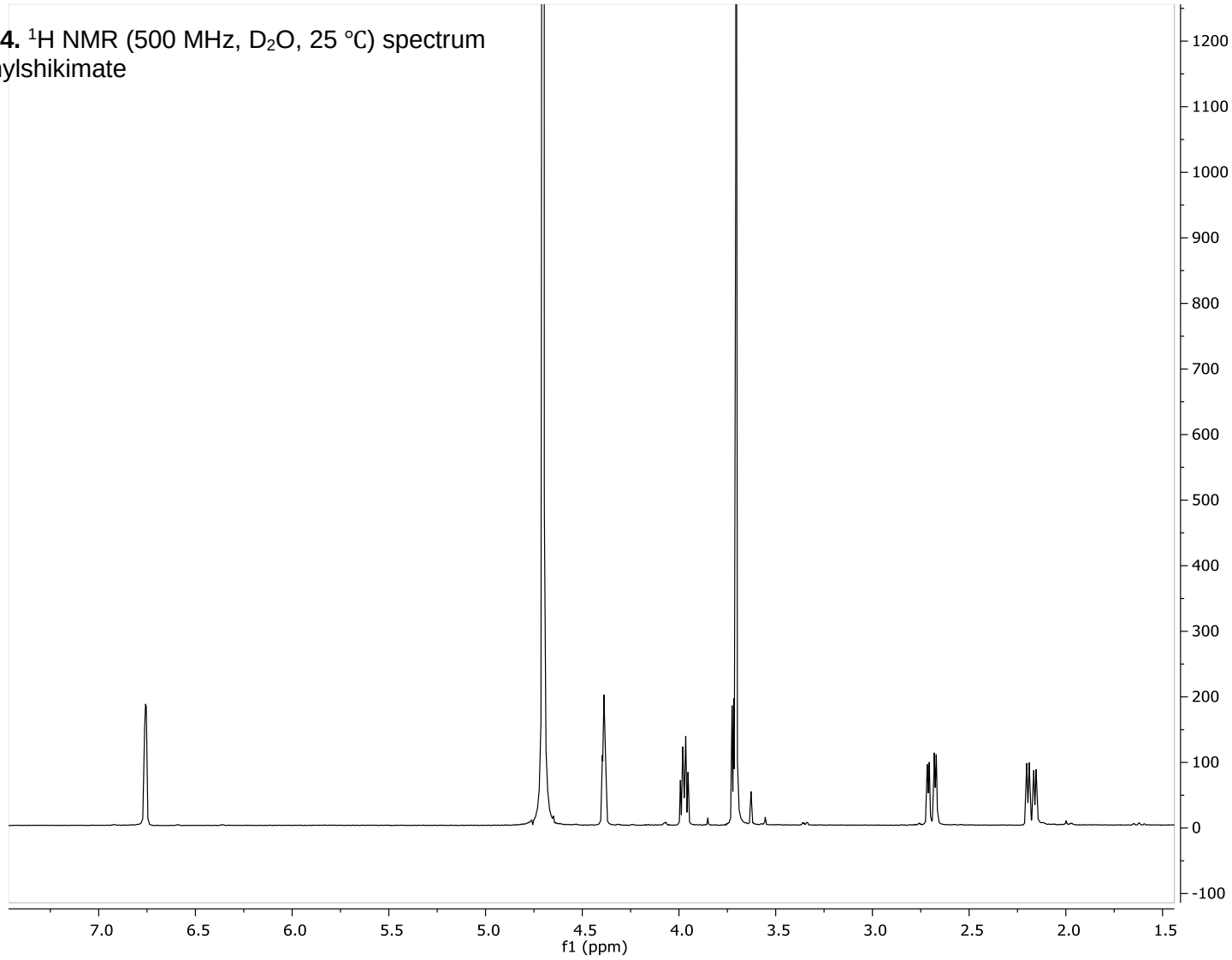

Figure S45. ^{1}H NMR (300 MHz, $CDCl_3$, 25 ℃) spectrum of **13**

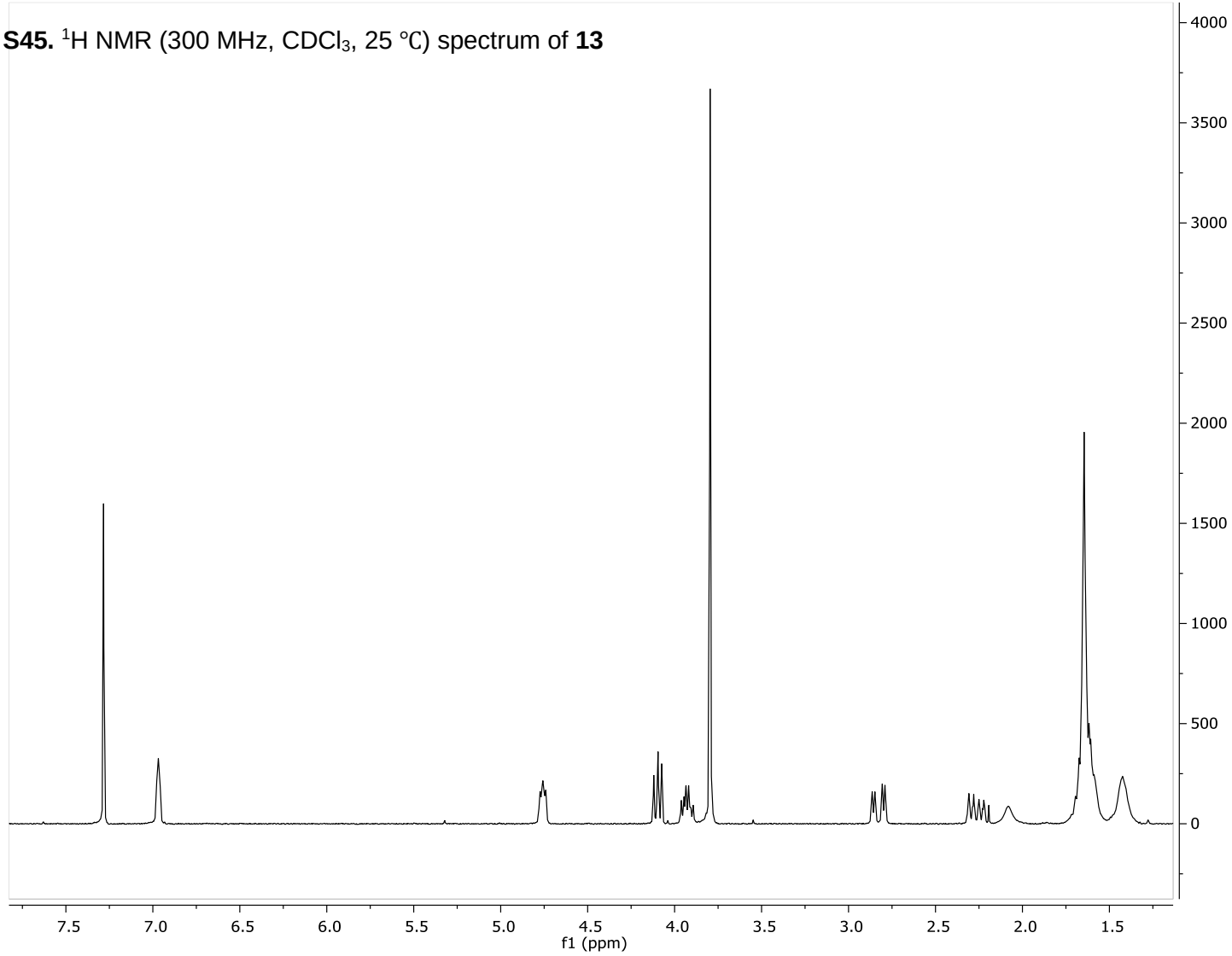

Figure S46. ^{1}H NMR (300 MHz, $CDCl_3$, 25 ℃) spectrum of **14**

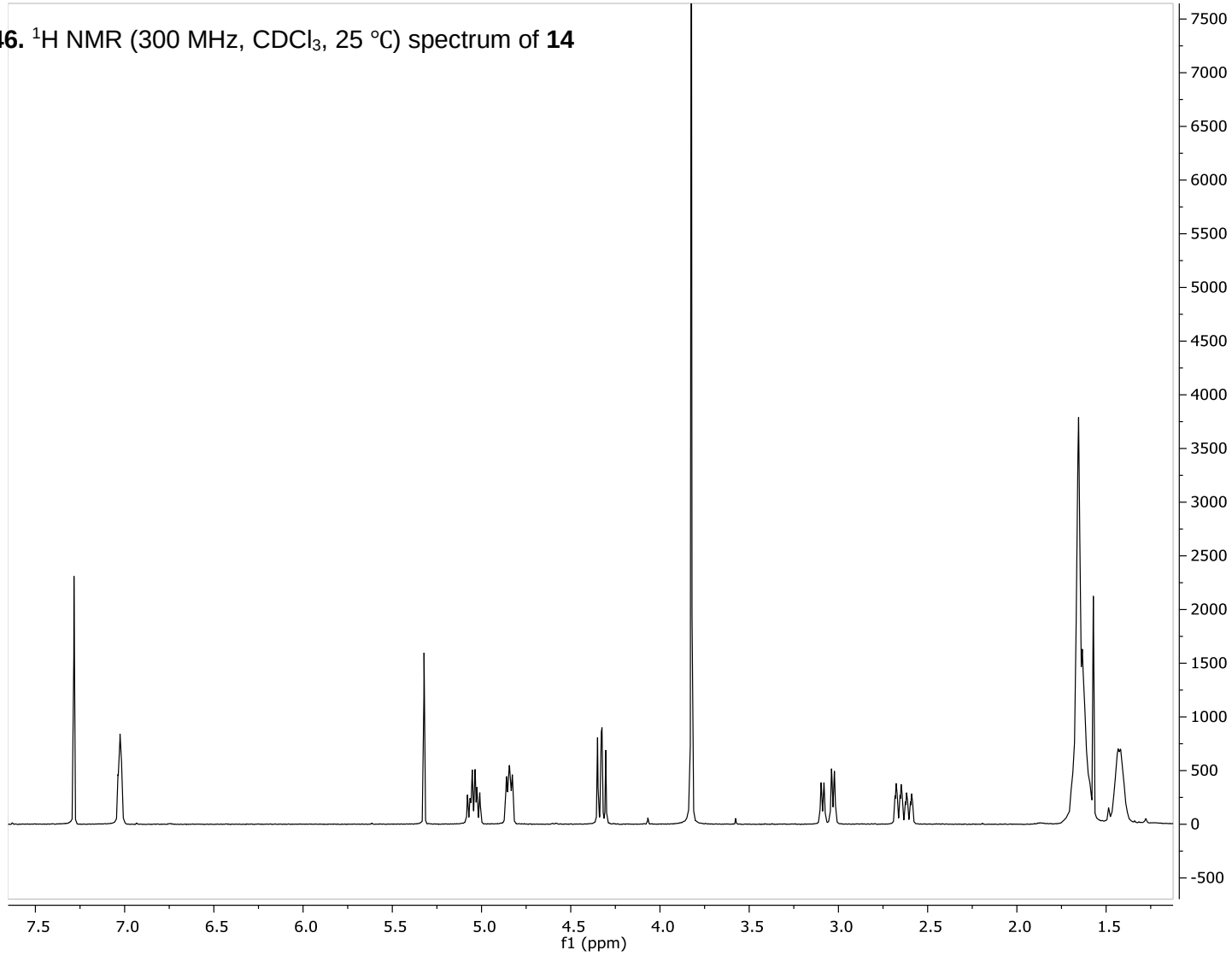

Figure S47. ^{1}H NMR (500 MHz, $CDCl_3$, 25 ℃) spectrum of **15**

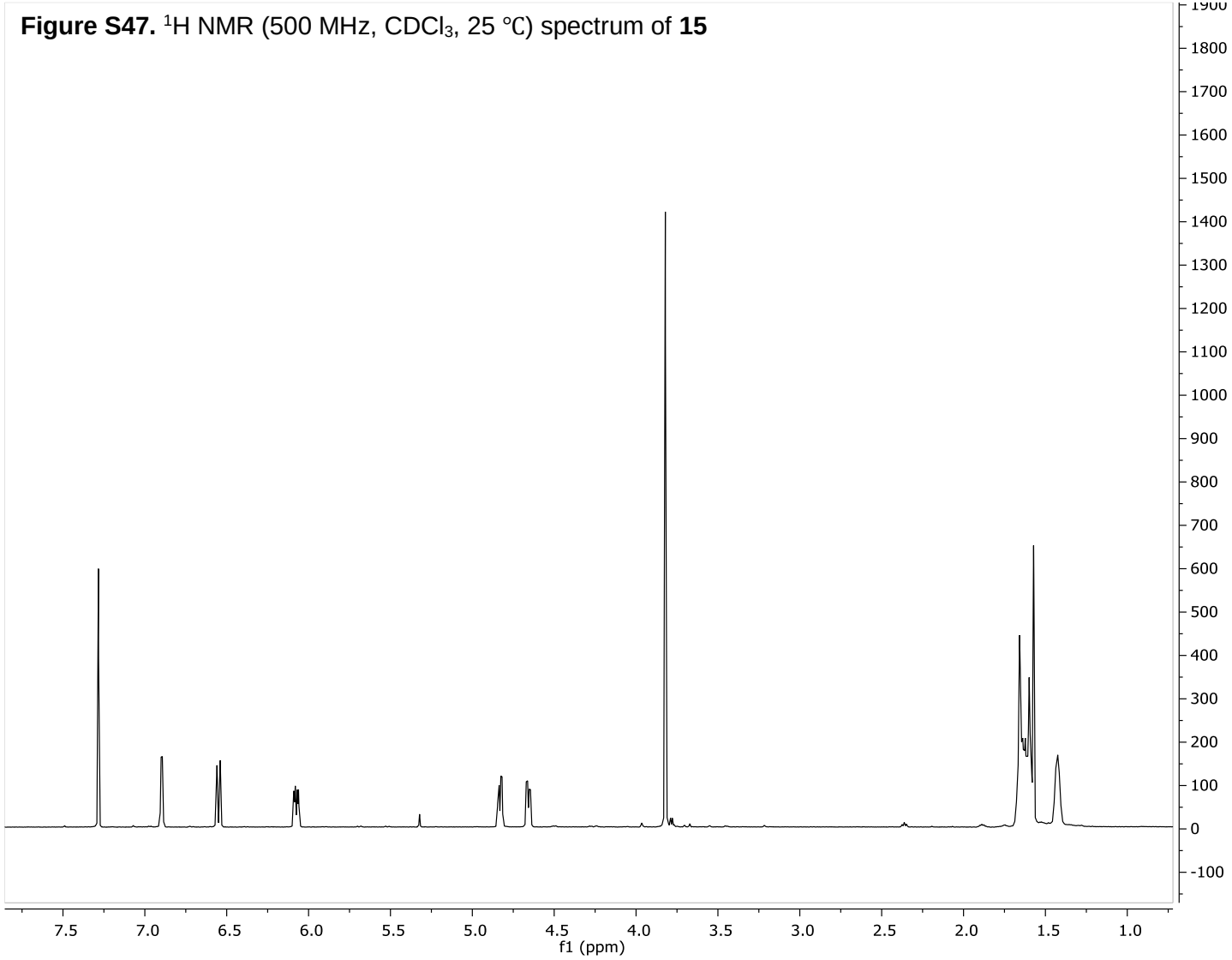

Figure S48. ^{1}H NMR (500 MHz, $CDCl_3$, 25 ℃) spectrum of **16**

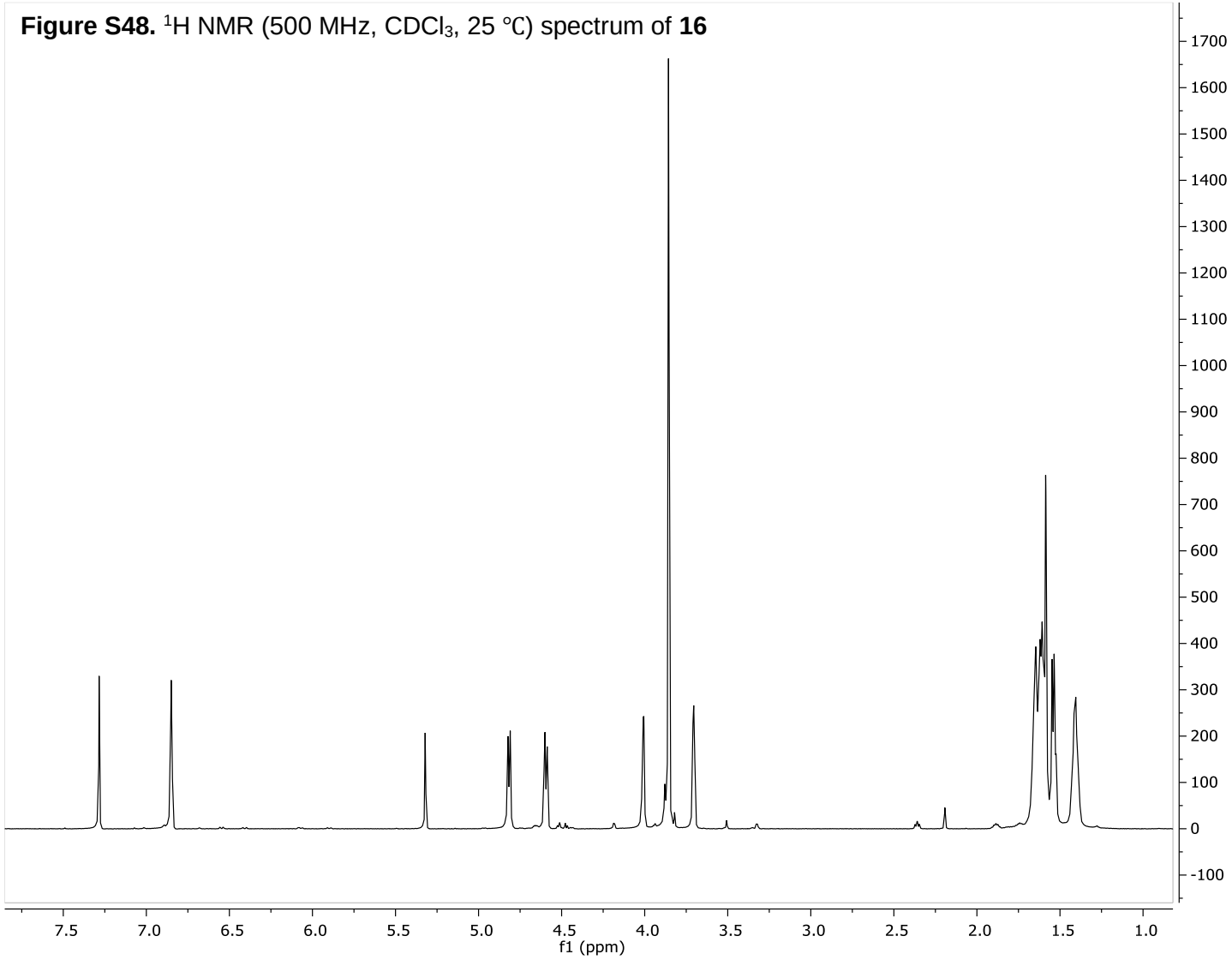

Figure S49. ^{1}H NMR (500 MHz, $CDCl_3$, 25 ℃) spectrum of **17**

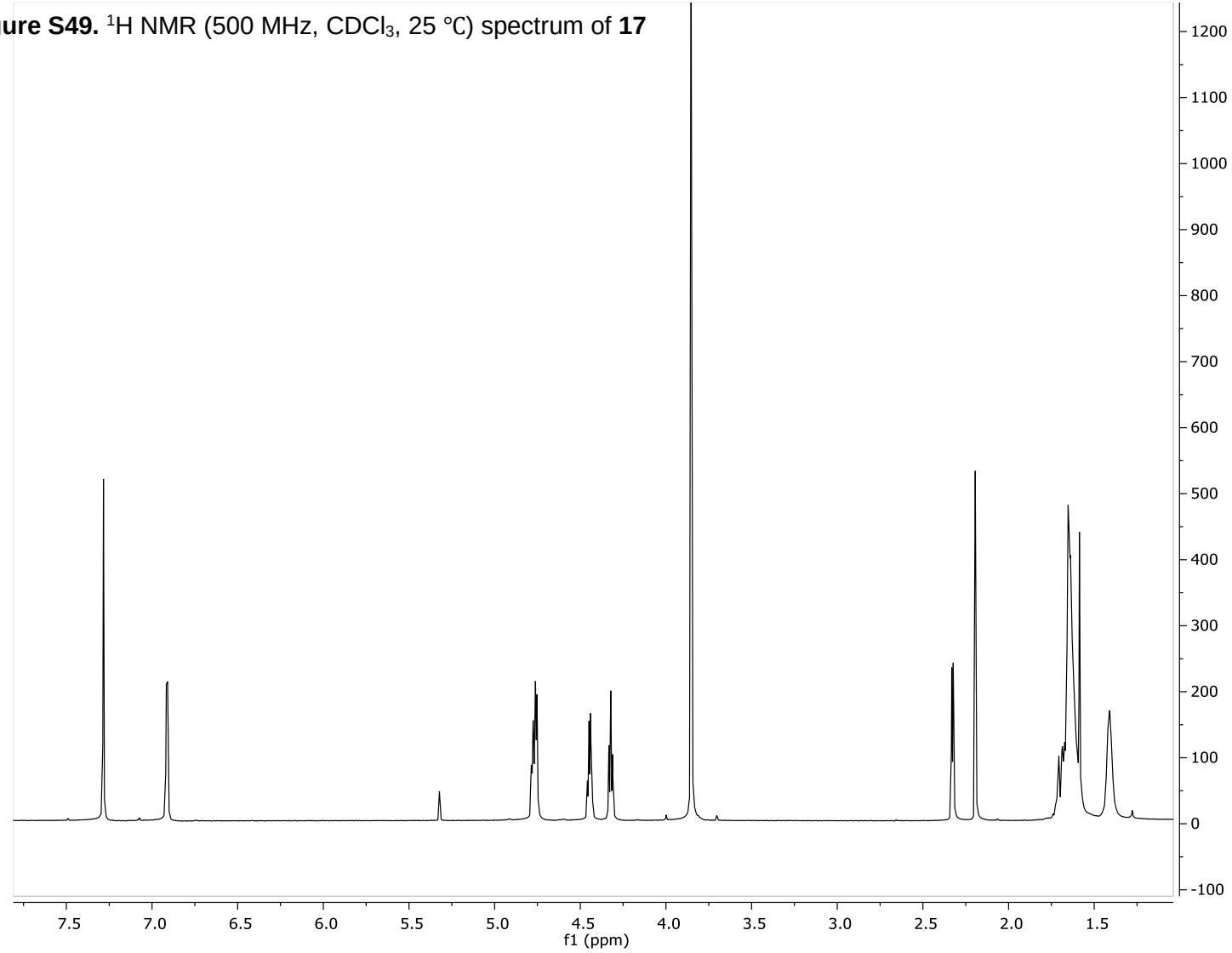

Figure S50. ^{1}H NMR (500 MHz, $CDCl_3$, 25 ℃) spectrum of **18**

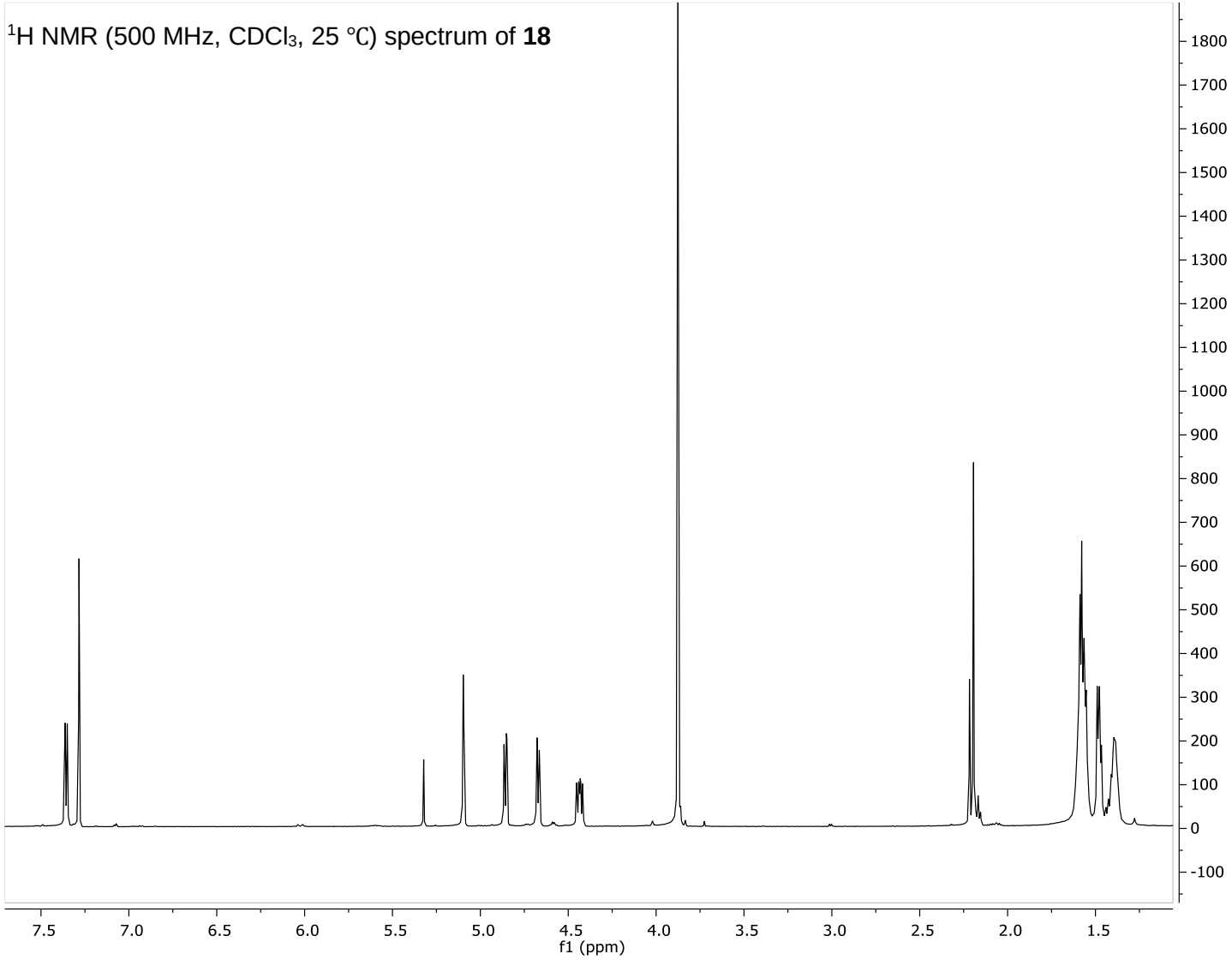

Figure S51. ^{1}H NMR (400 MHz, methanol-d_4, 25 ℃) spectrum of **19**

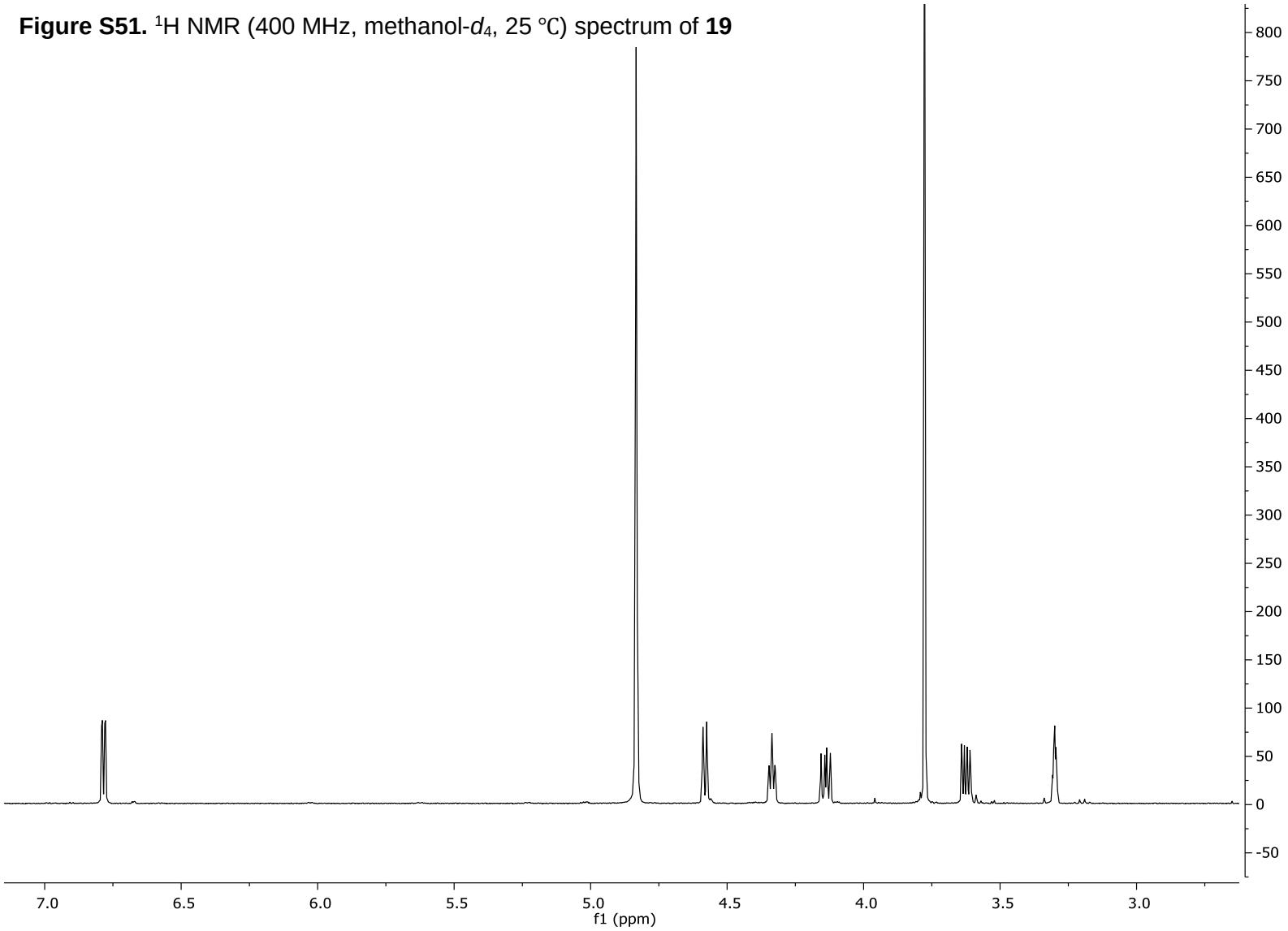

Figure S52. ^{13}C NMR (100 MHz, methanol-d_4, 25 ℃) spectrum of **19**

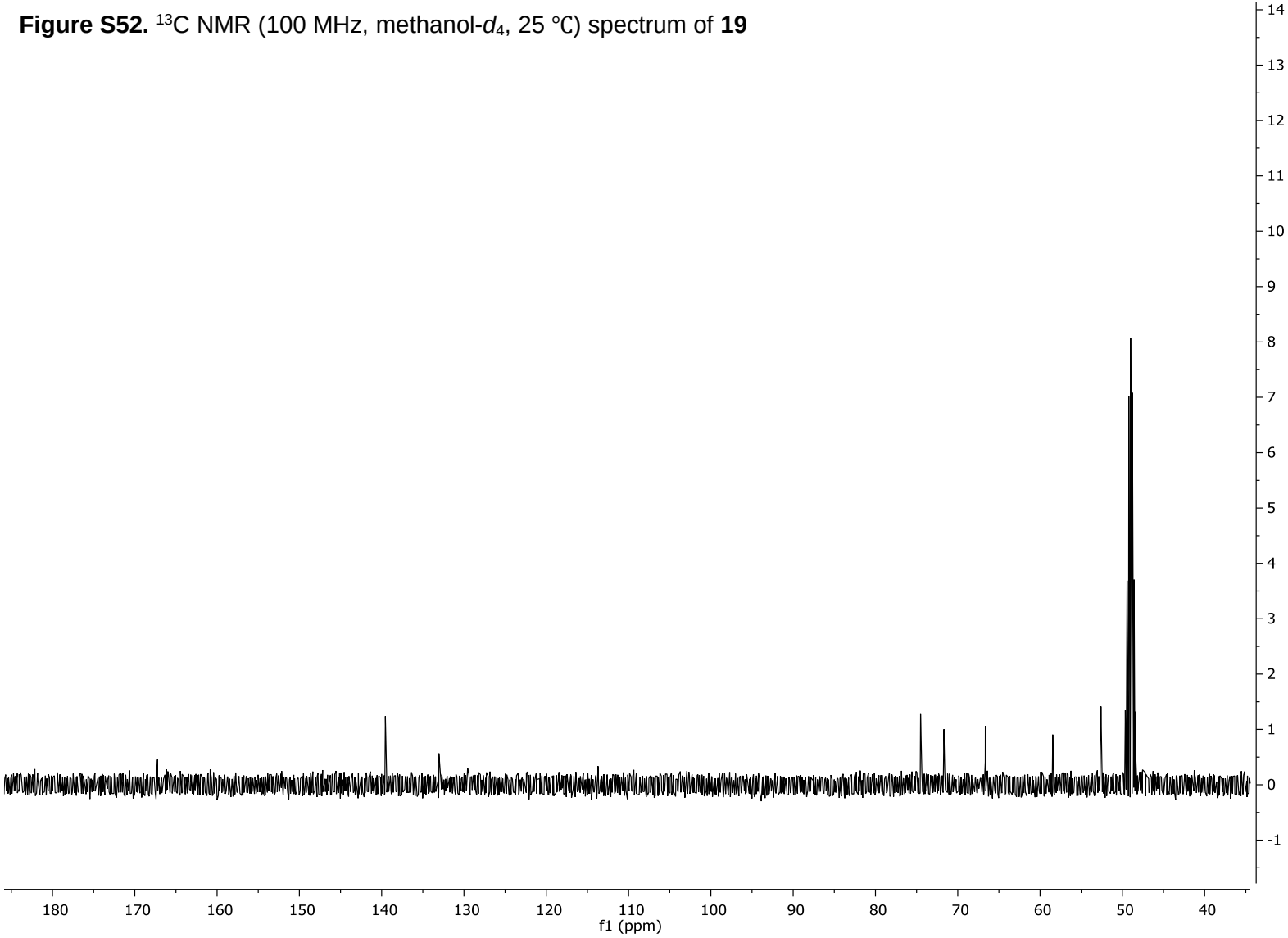

Figure S53. ^{1}H NMR (400 MHz, methanol-d_4, 25 ℃) spectrum of **20**

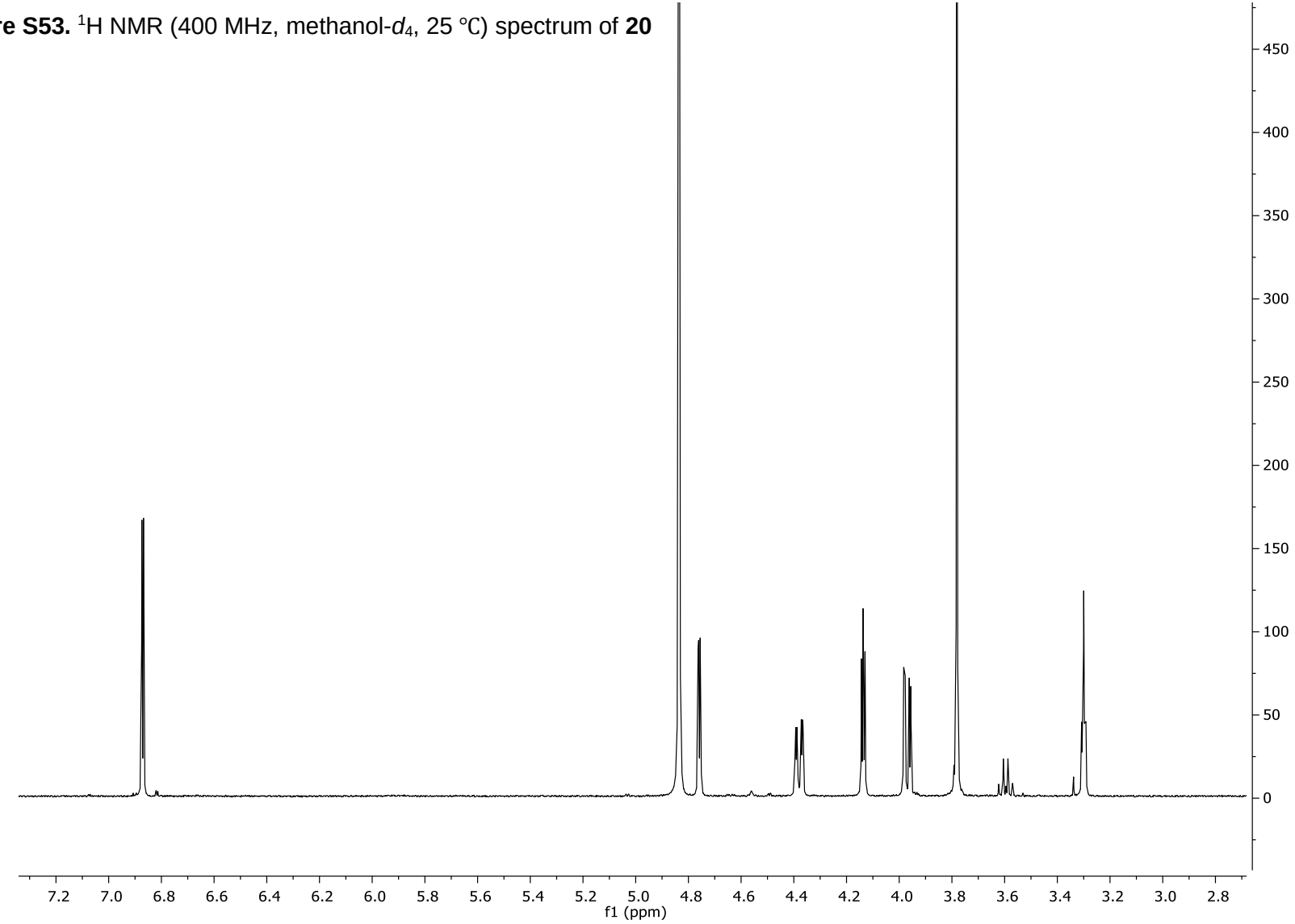

Figure S54. ^{13}C NMR (100 MHz, methanol-d_4, 25 °C) spectrum of **20**

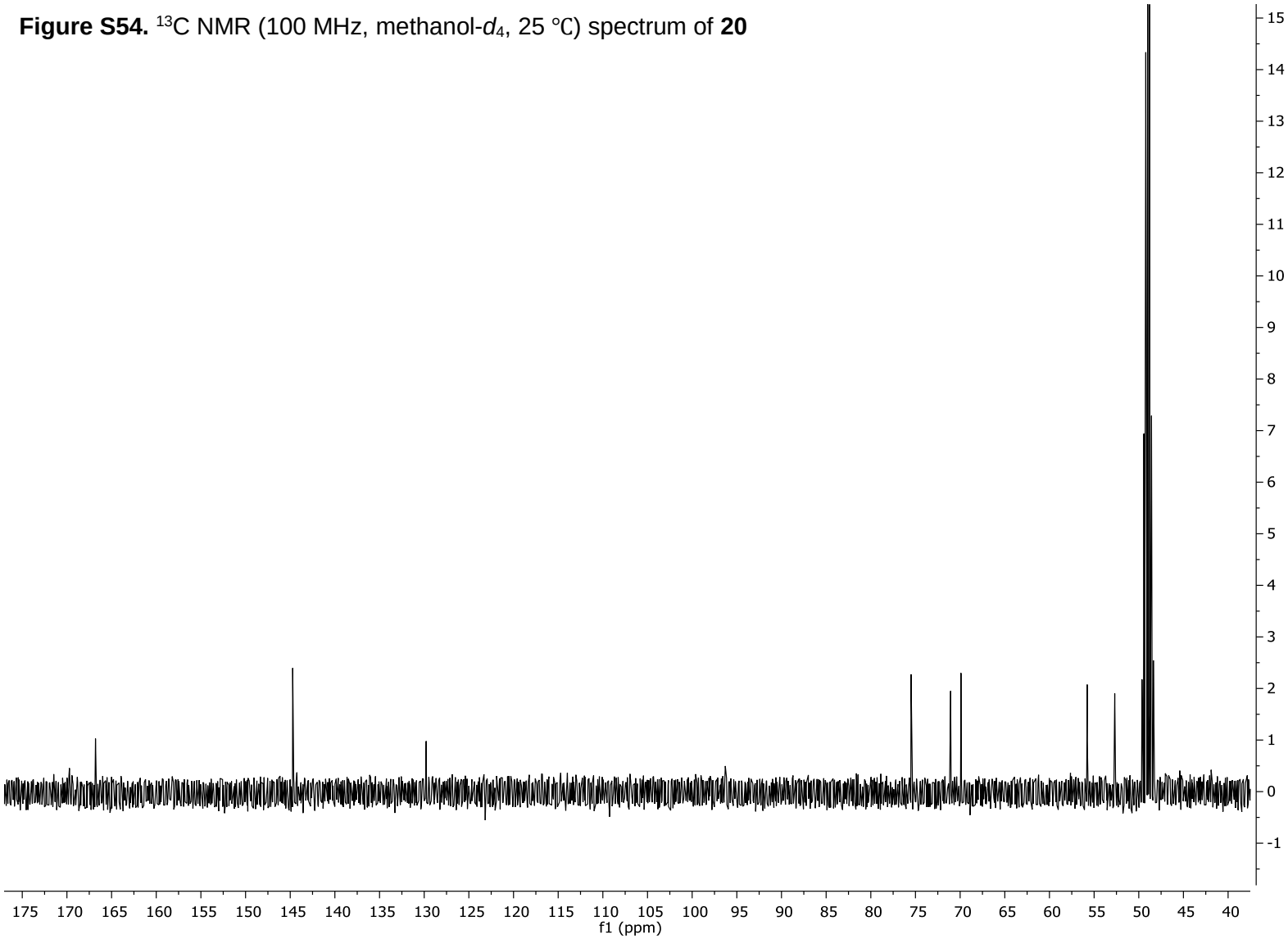

Figure S55. ^{1}H NMR (400 MHz, methanol-d_4, 25 ℃) spectrum of **21**

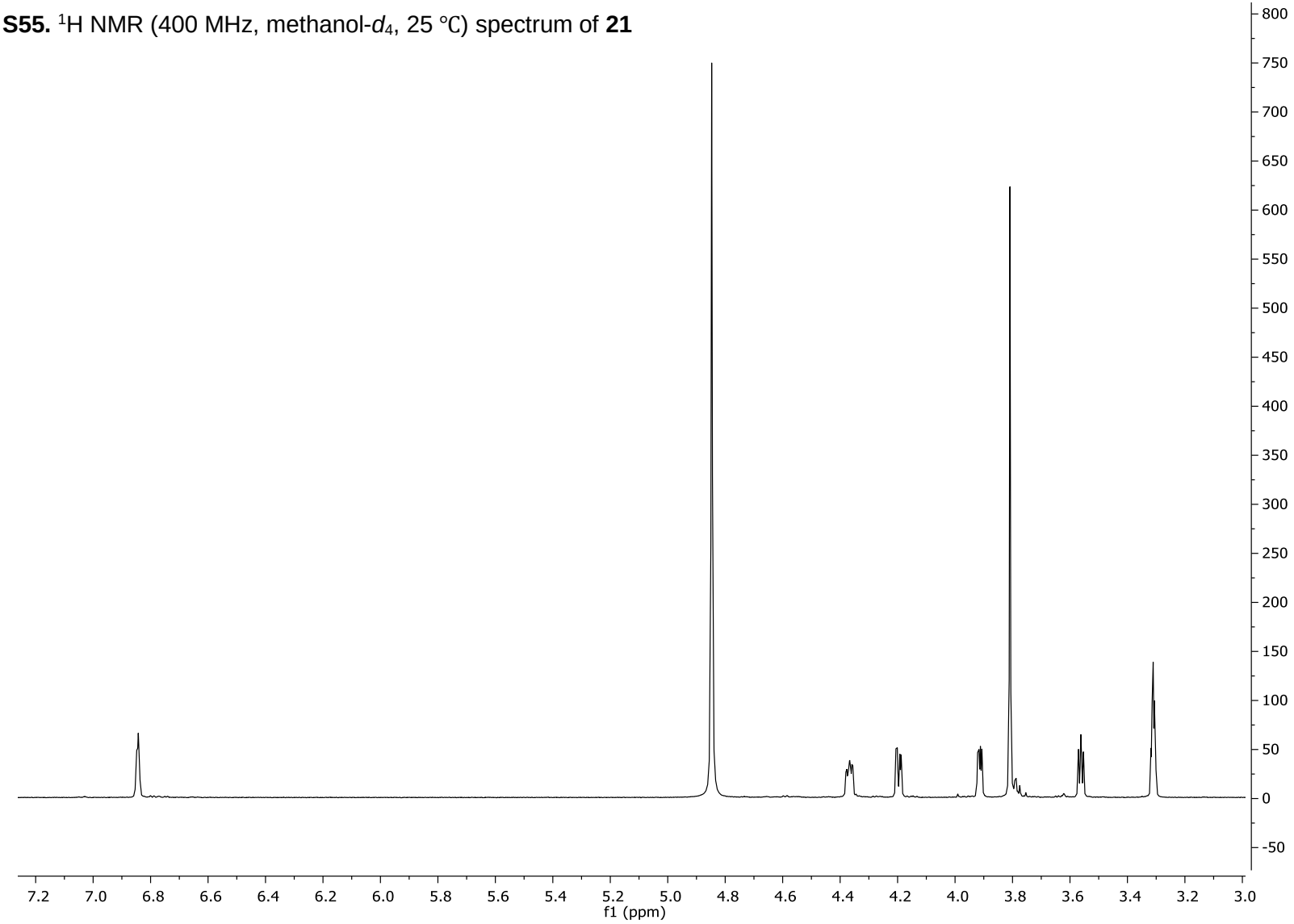

Figure S56. ^{13}C NMR (100 MHz, methanol-d_4, 25 °C) spectrum of **21**

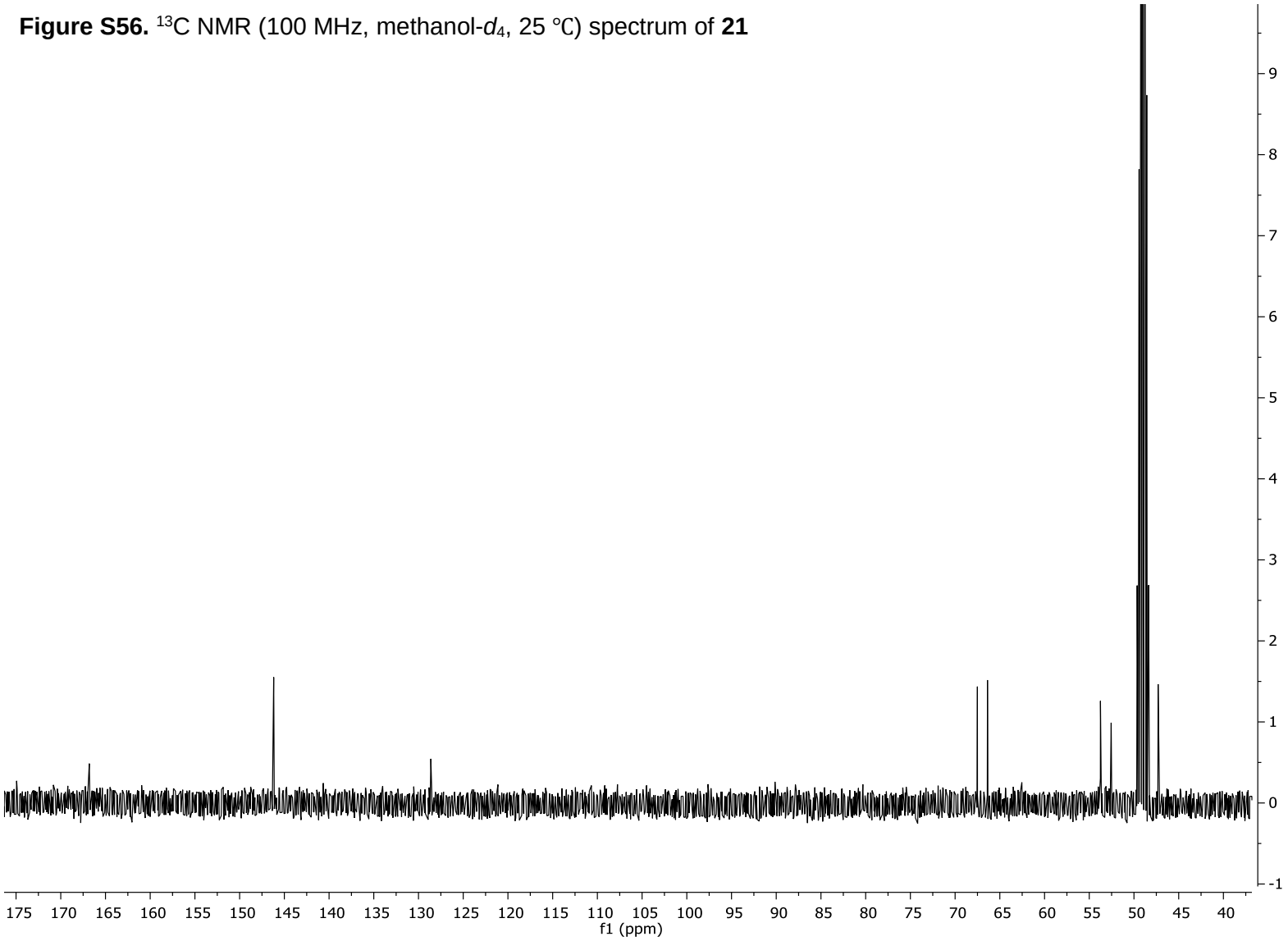

Figure S57. ^{1}H-^{1}H COSY (400 MHz, methanol-d_4, 25 ℃) spectrum of **21**

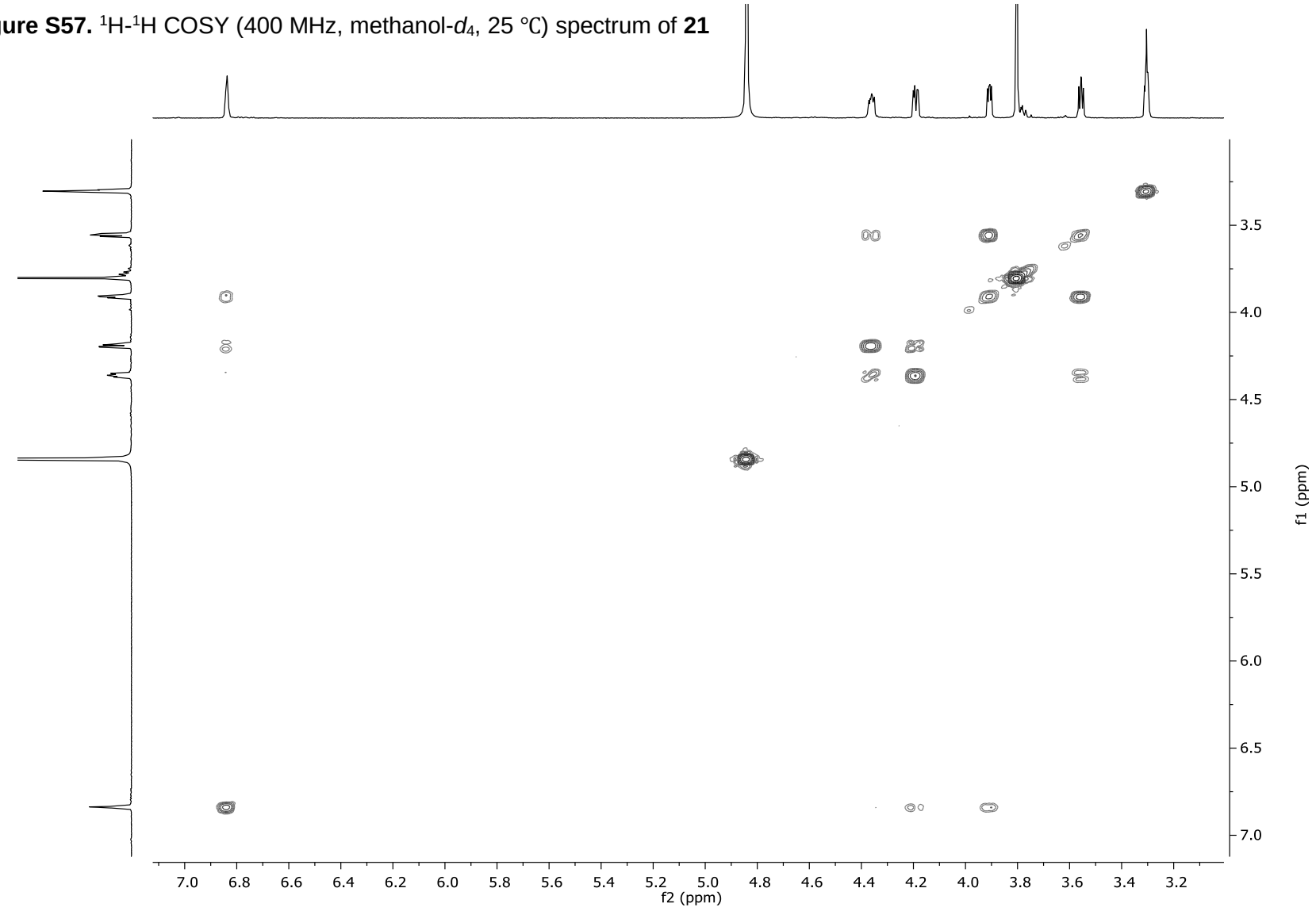

Figure S58. HSQC (400 MHz, methanol-d_4, 25 ℃) spectrum of **21**

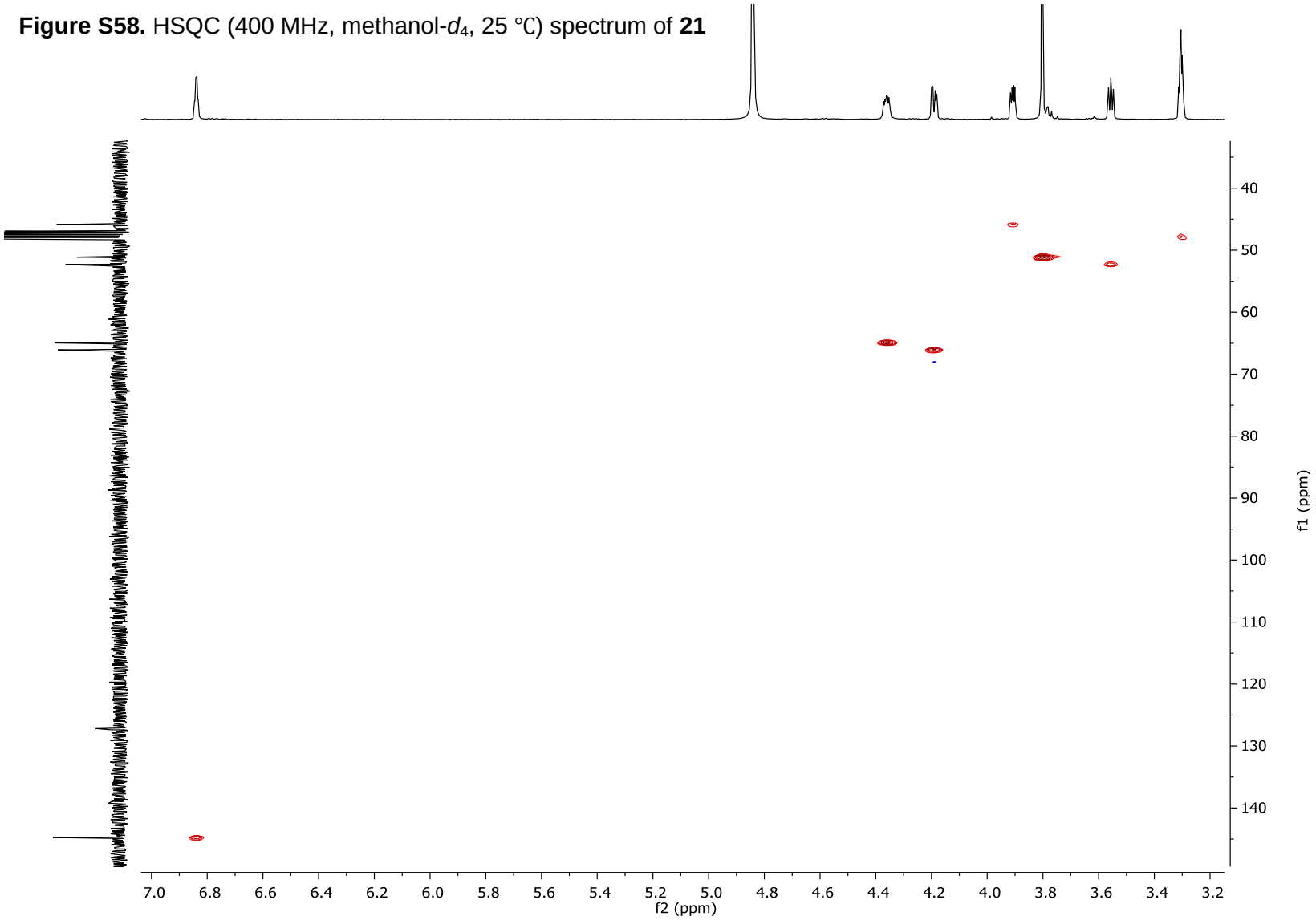

Figure S59. ^{1}H NMR (500 MHz, methanol-d_4, 25 °C) spectrum of **22**

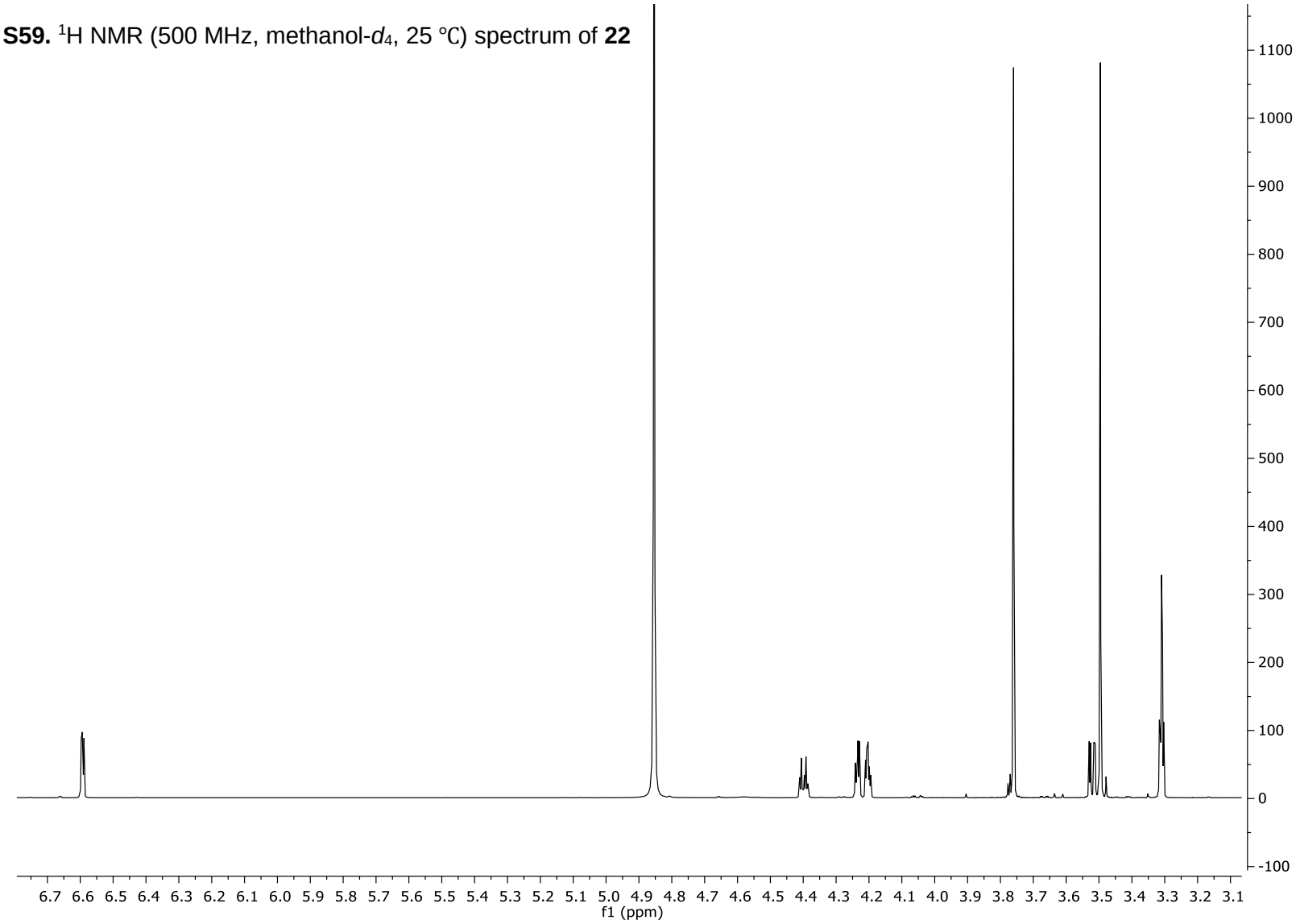

Figure S60. ^{13}C NMR (125 MHz, methanol-d_4, 25 °C) spectrum of **22**

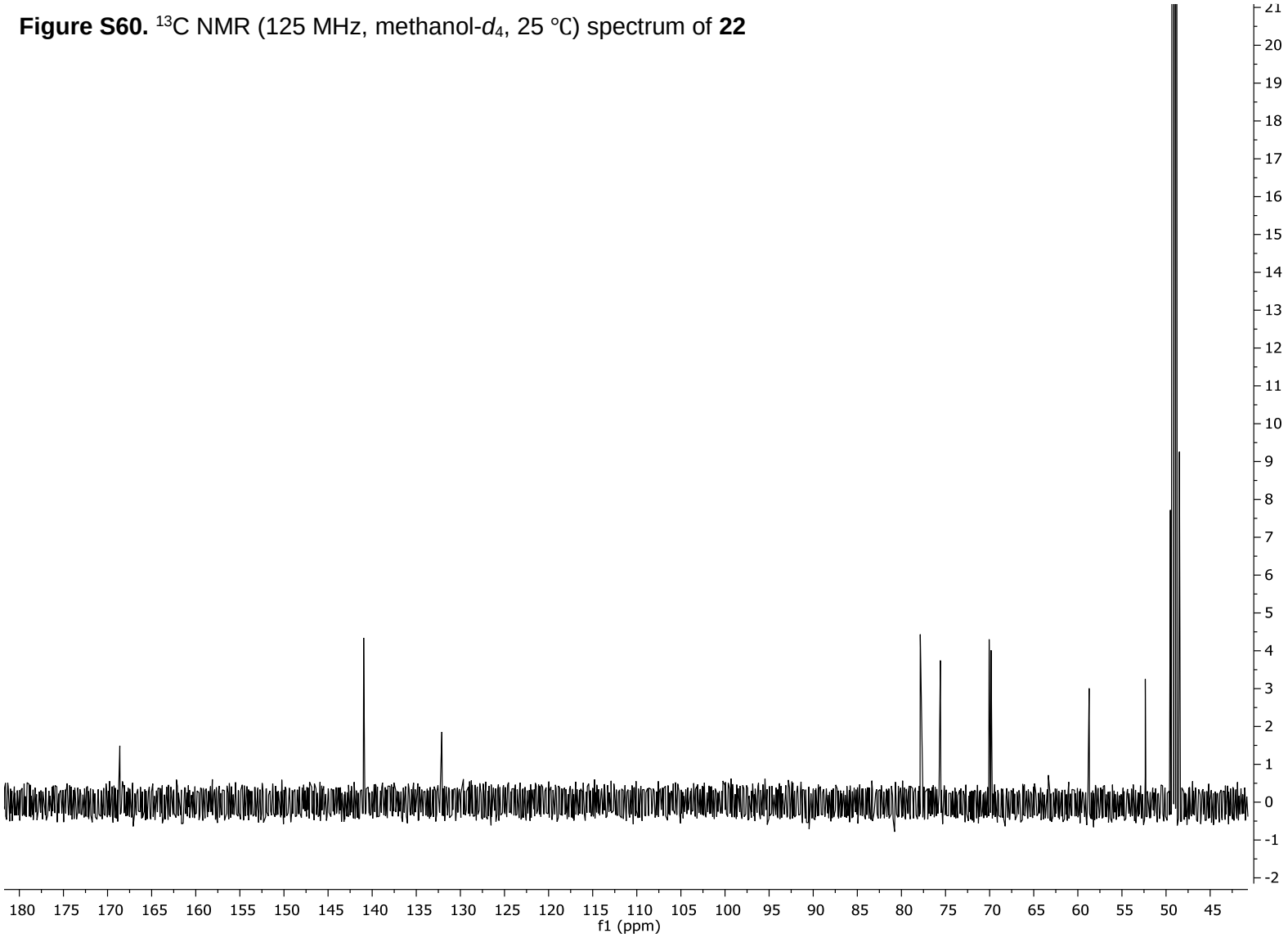

Figure S61. ^{1}H-^{1}H COSY (500 MHz, methanol-d_4, 25 ℃) spectrum of **22**

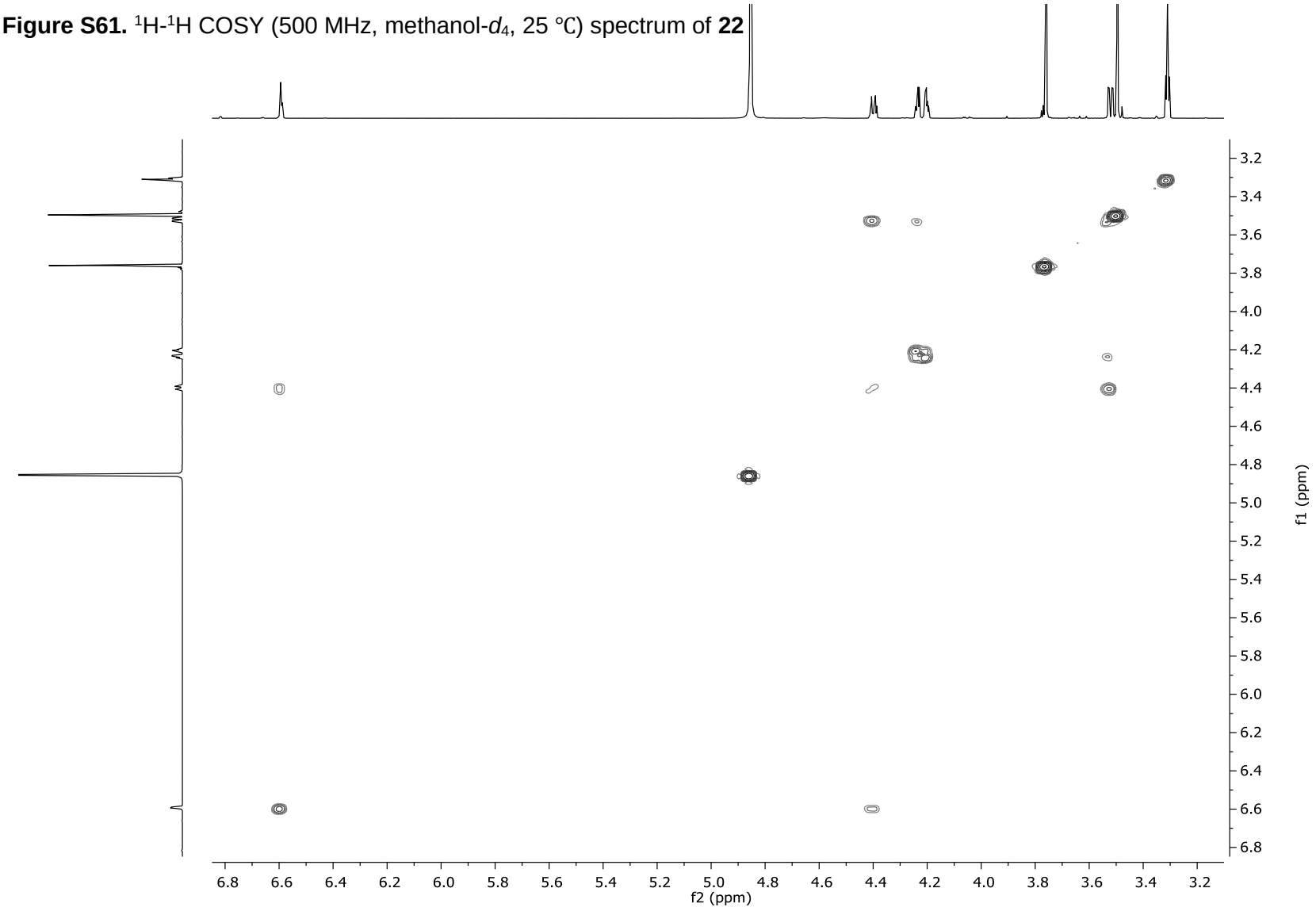

Figure S62. HSQC (500 MHz, methanol-d_4, 25 ℃) spectrum of **22**

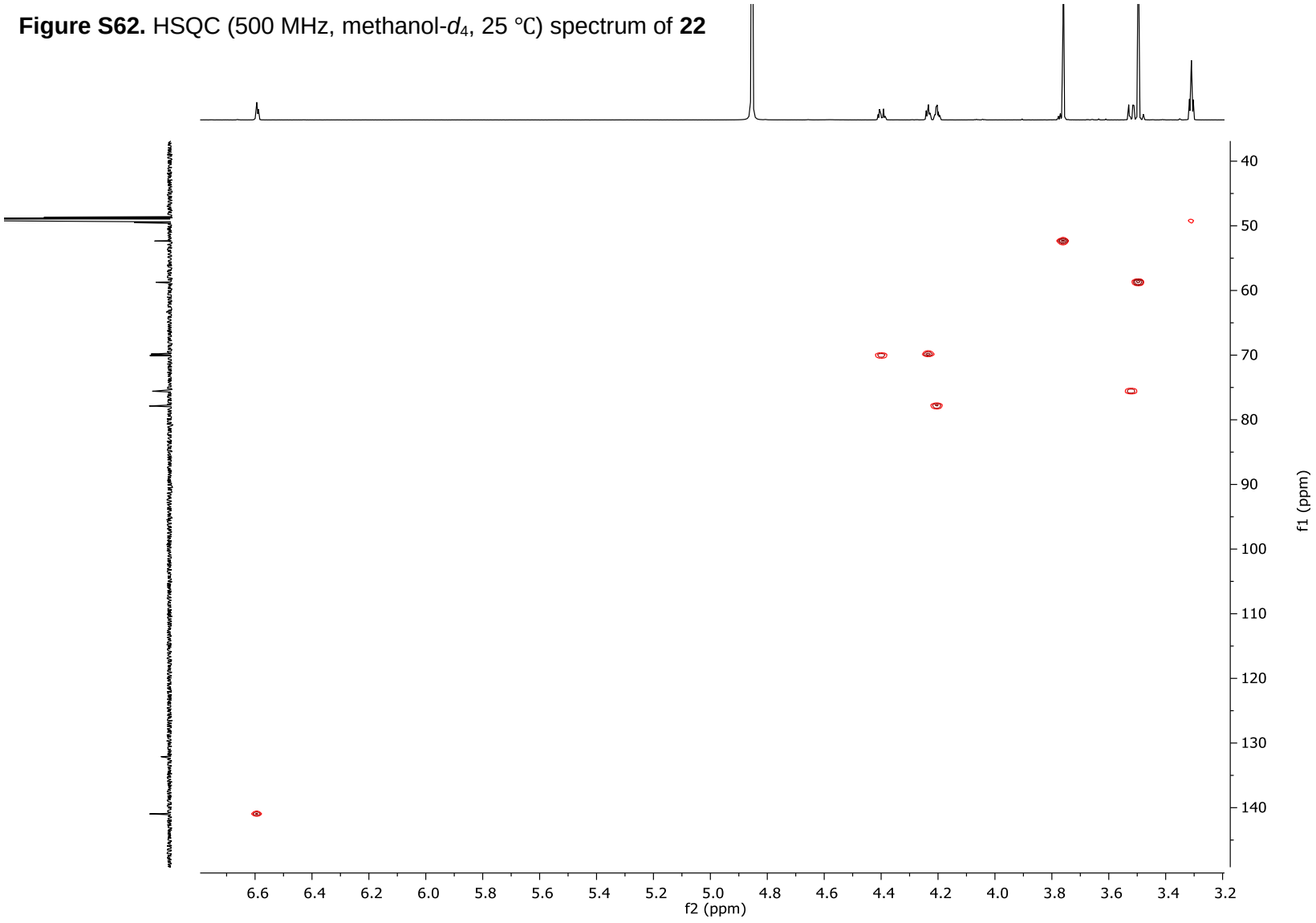

Figure S63. ^{1}H NMR (400 MHz, methanol-d_4, 25 ℃) spectrum of **23**

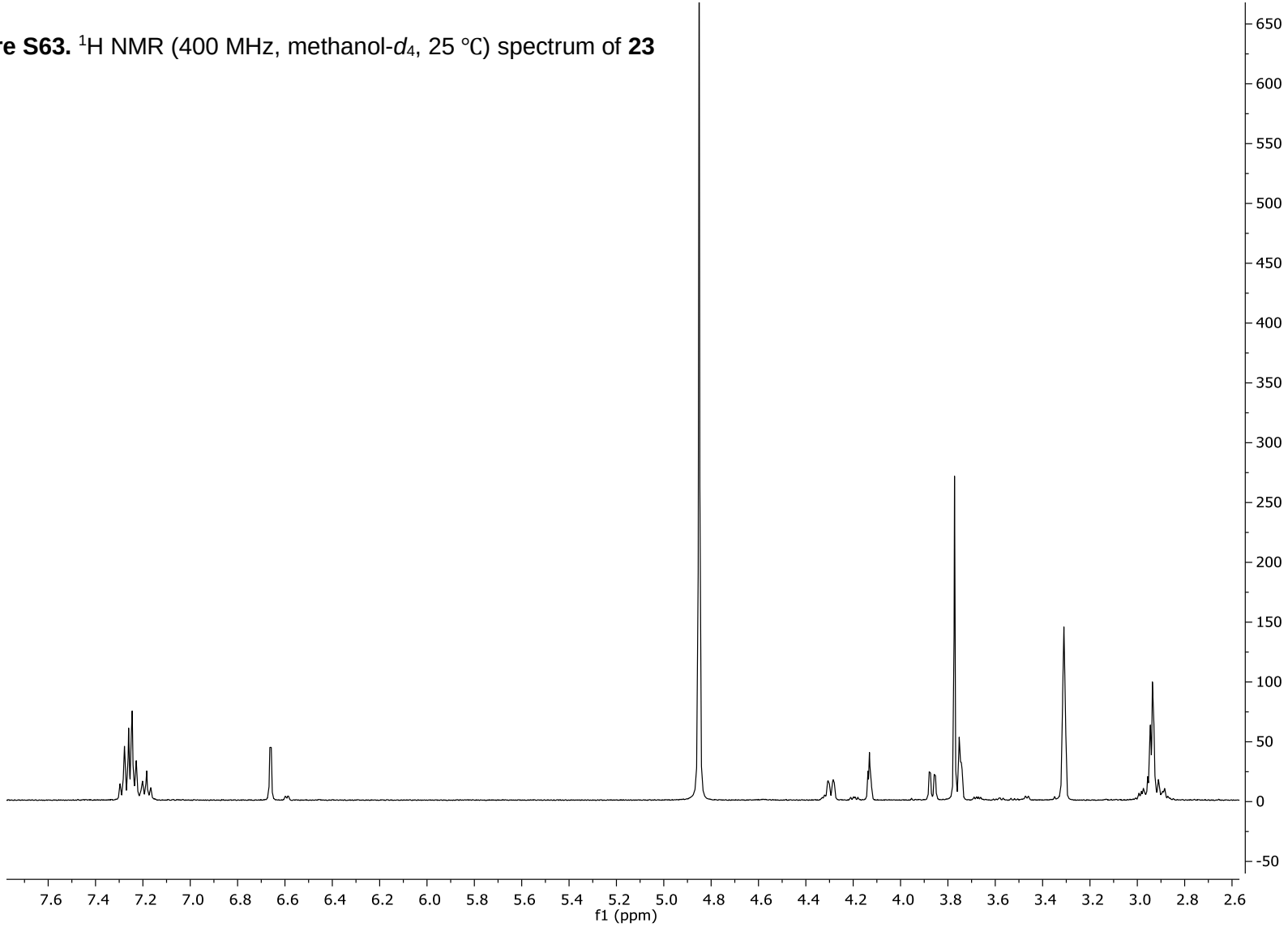

Figure S64. ^{13}C NMR (100 MHz, methanol-d_4, 25 ℃) spectrum of **23**

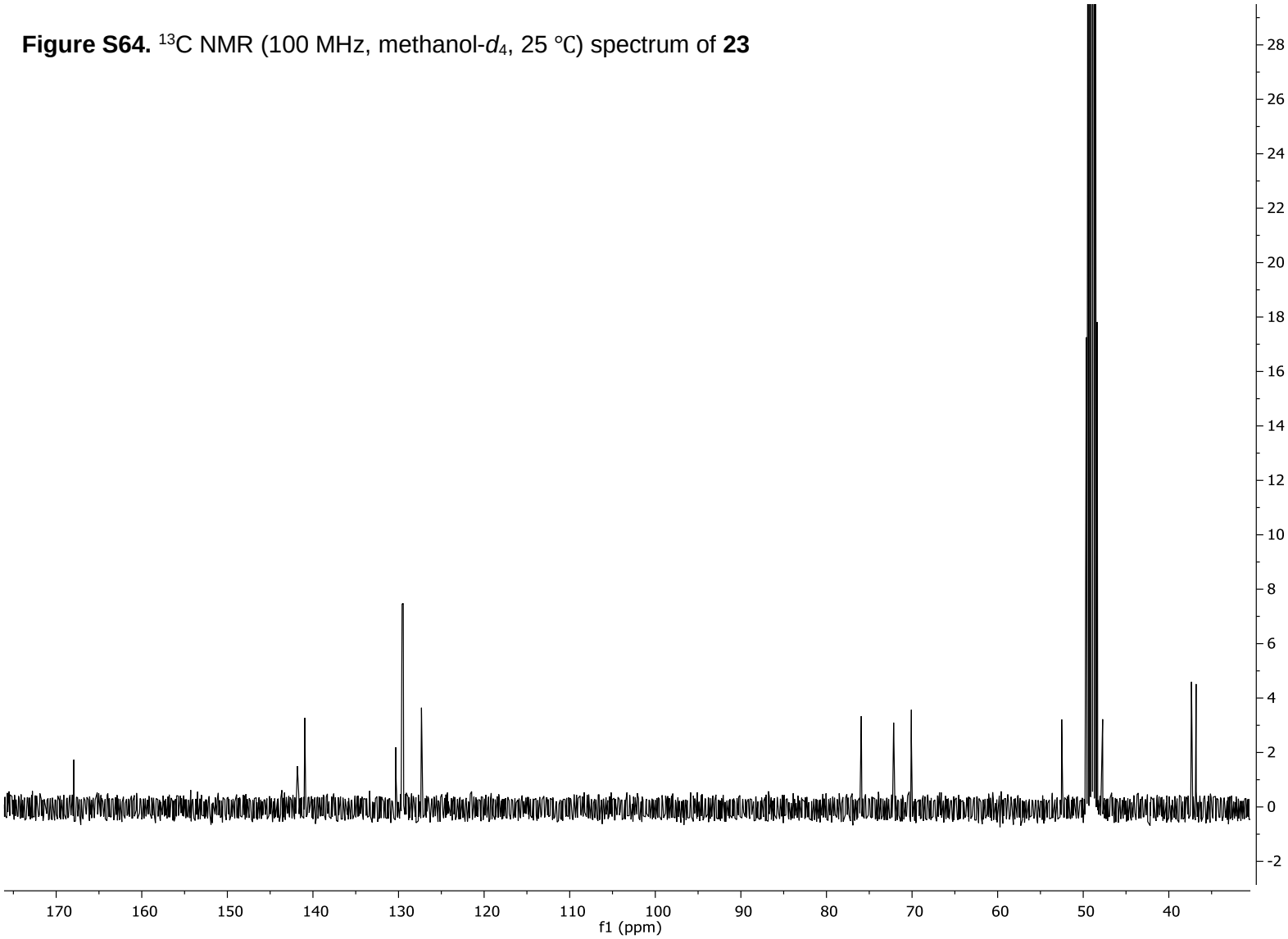

Figure S65. ^{1}H-^{1}H COSY (400 MHz, methanol-d_4, 25 ℃) spectrum of **23**

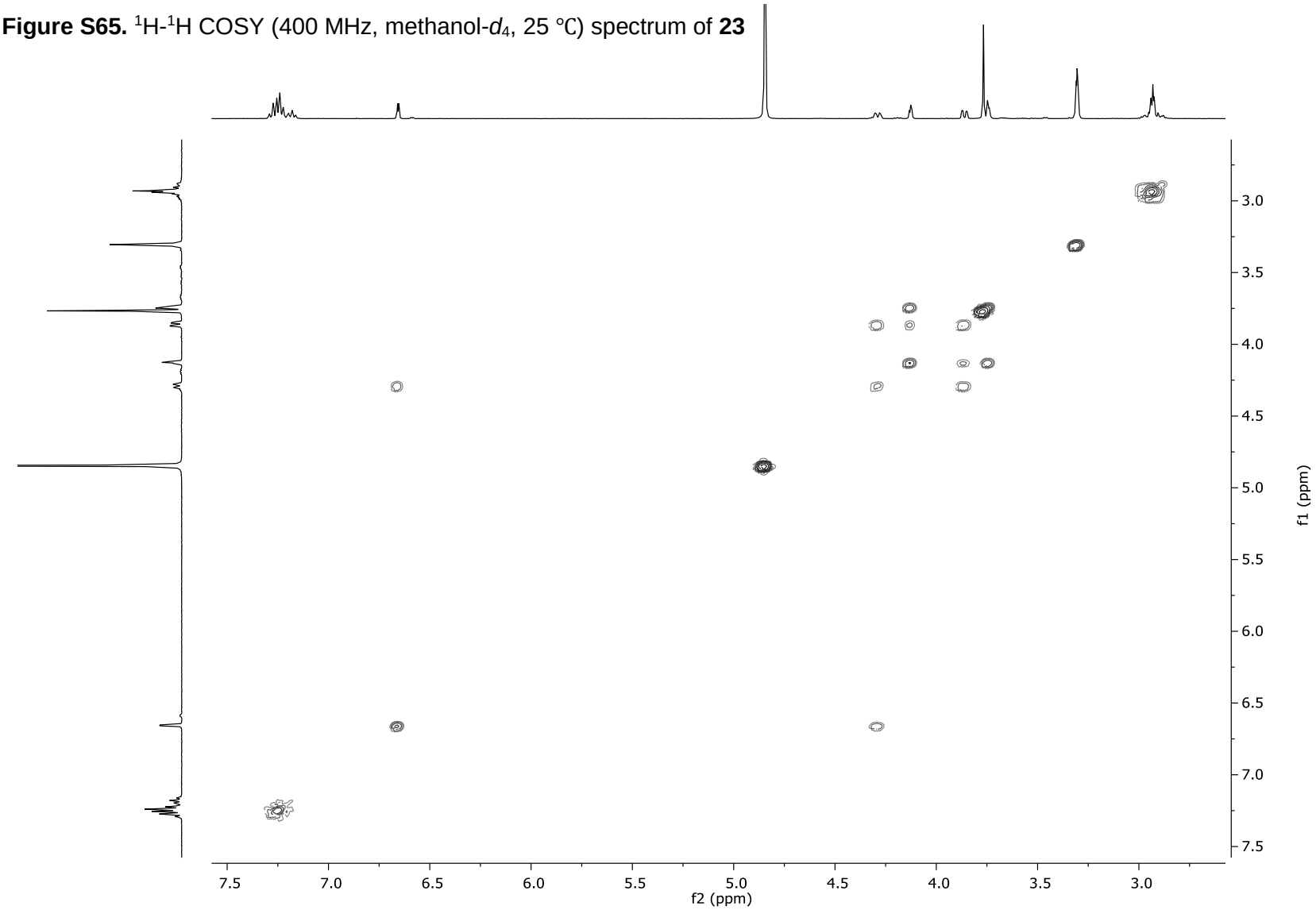

Figure S66. HSQC (400 MHz, methanol-d_4, 25 °C) spectrum of **23**

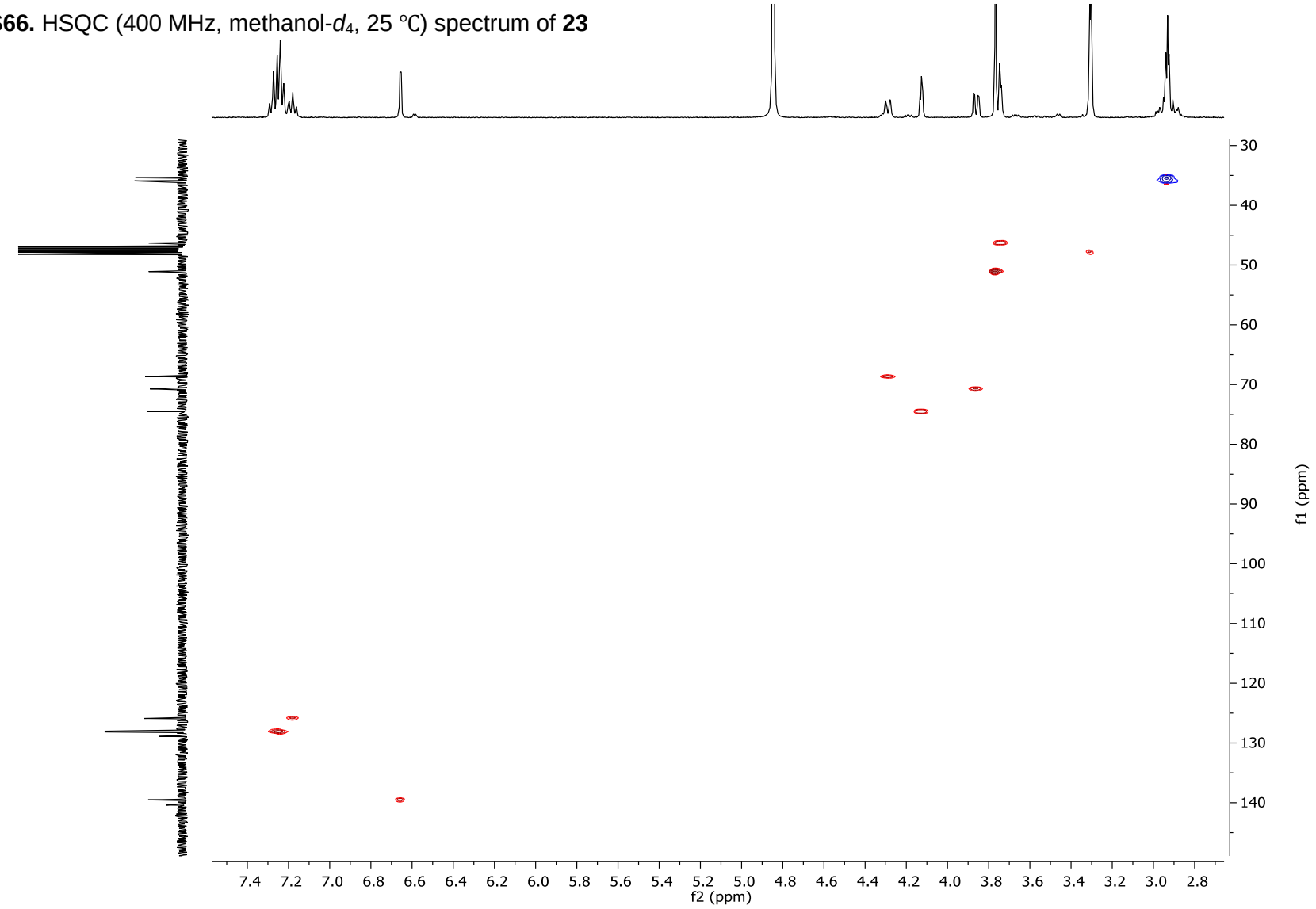

Figure S67. ^{1}H NMR (400 MHz, methanol-d_4, 25 ℃) spectrum of **24**

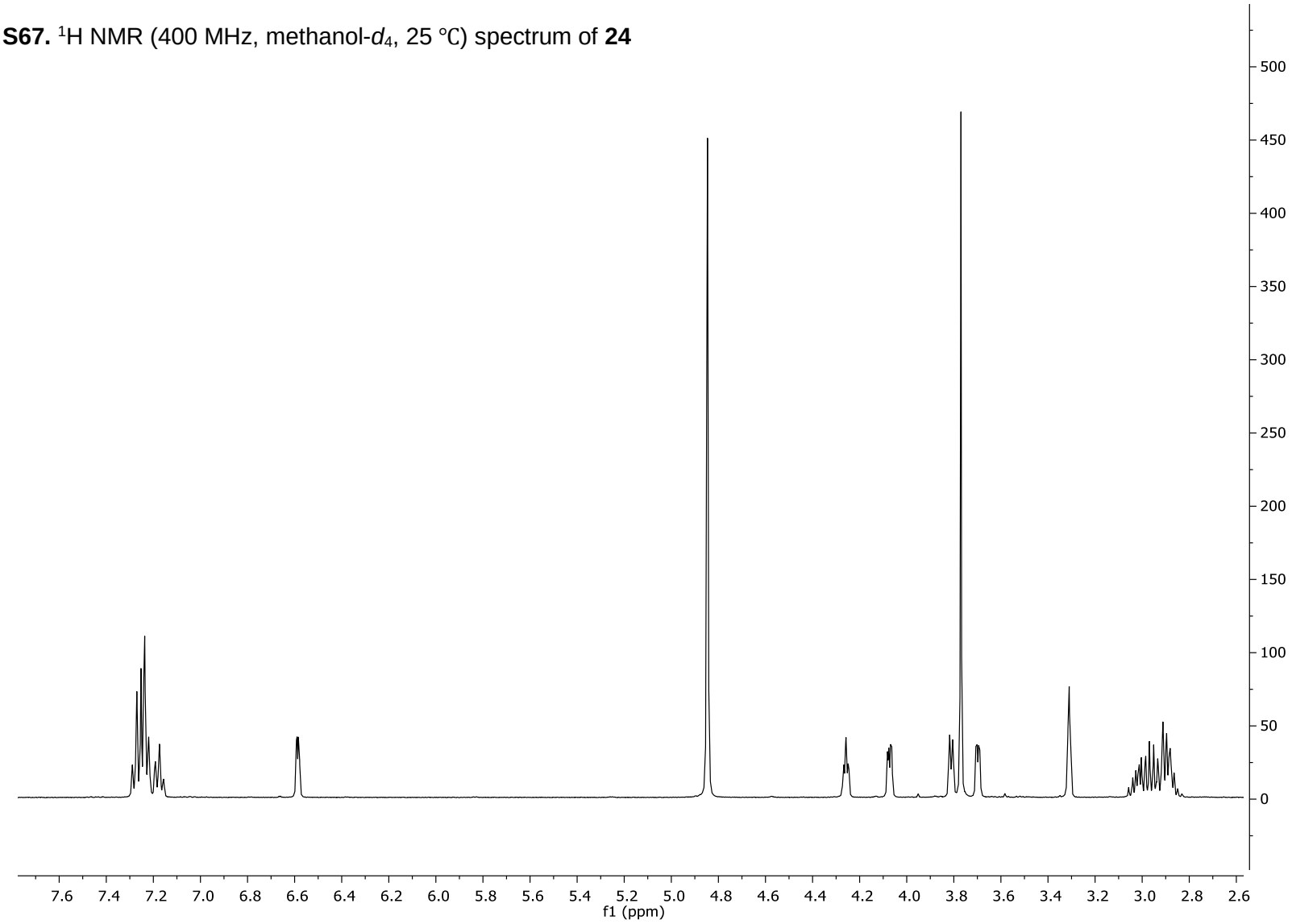

Figure S68. ^{13}C NMR (100 MHz, methanol-d_4, 25 °C) spectrum of **24**

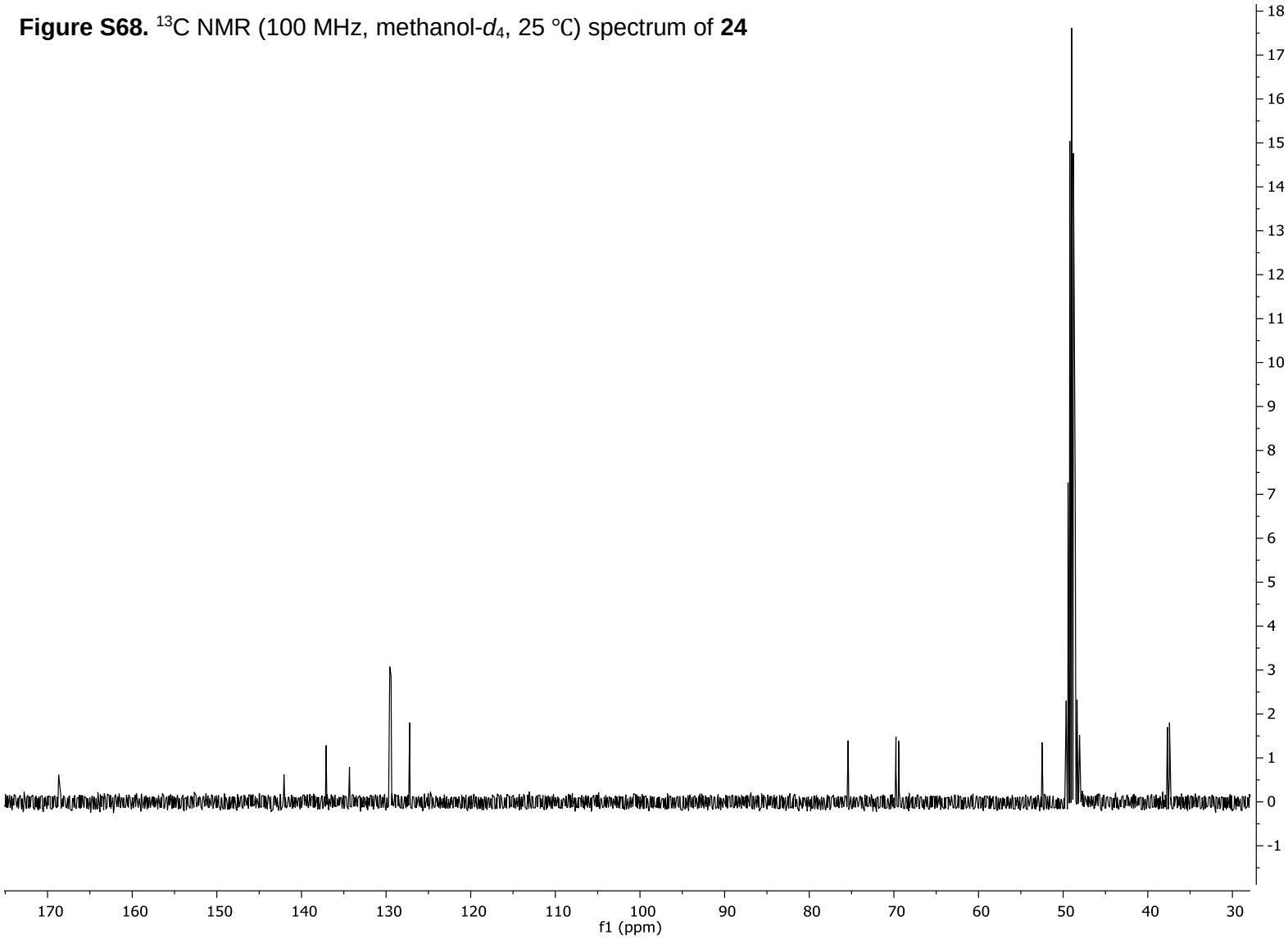

Figure S69. ^{1}H-^{1}H COSY (400 MHz, methanol-d_4, 25 ℃) spectrum of **24**

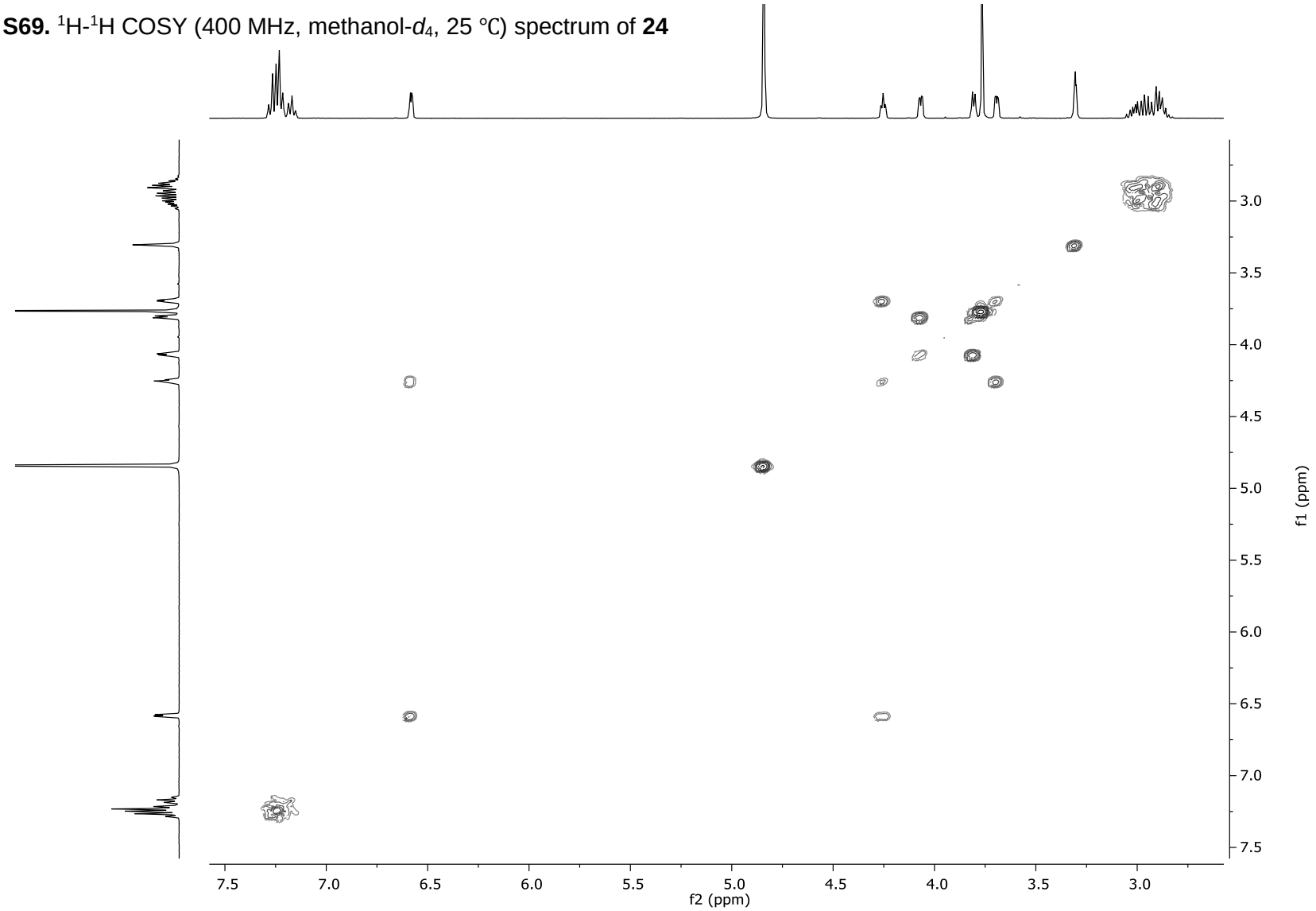

Figure S70. HSQC (400 MHz, methanol-d_4, 25 ℃) spectrum of **24**

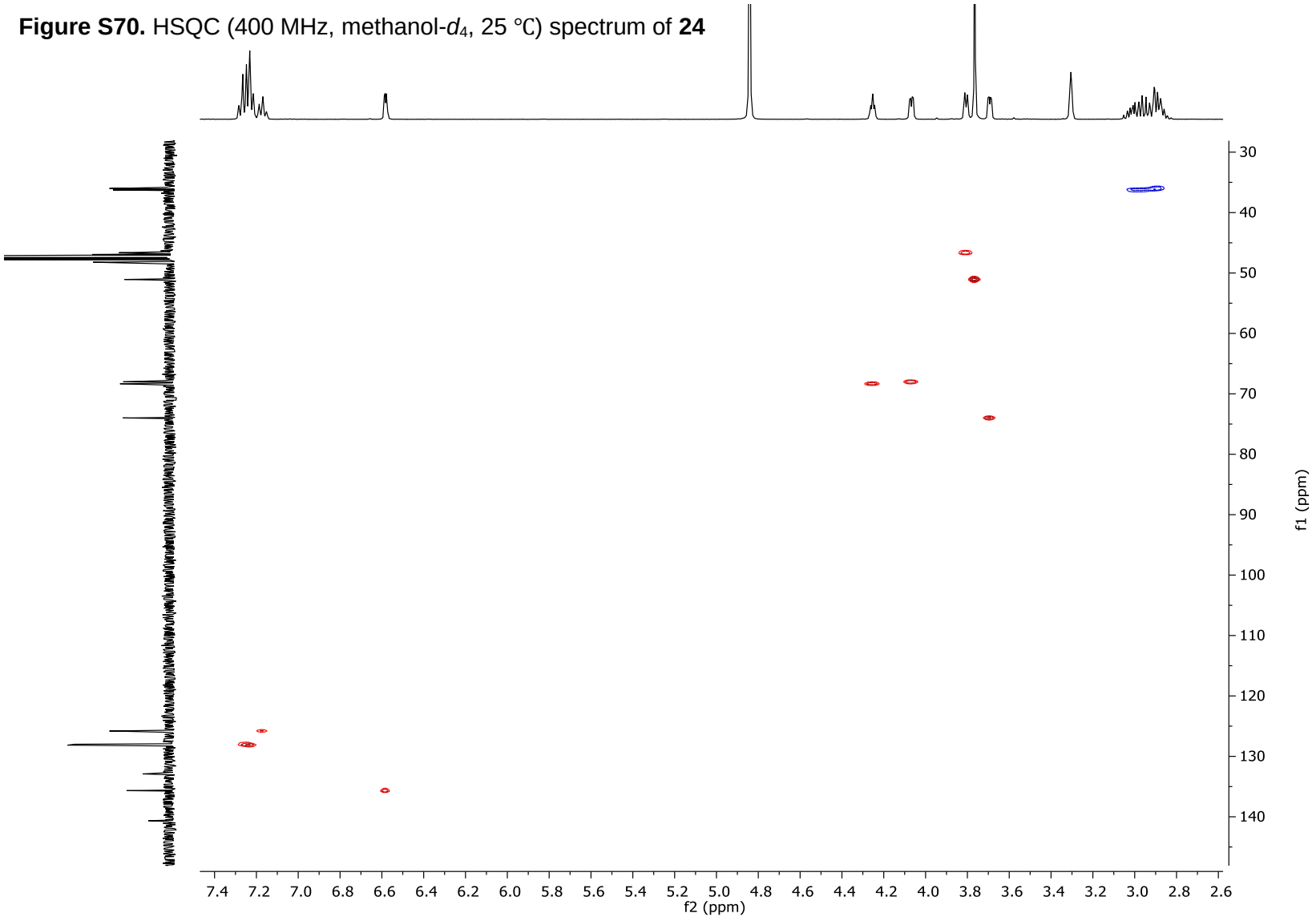

Figure S71. ^{1}H NMR (400 MHz, methanol-d_4, 25 ℃) spectrum of **25**

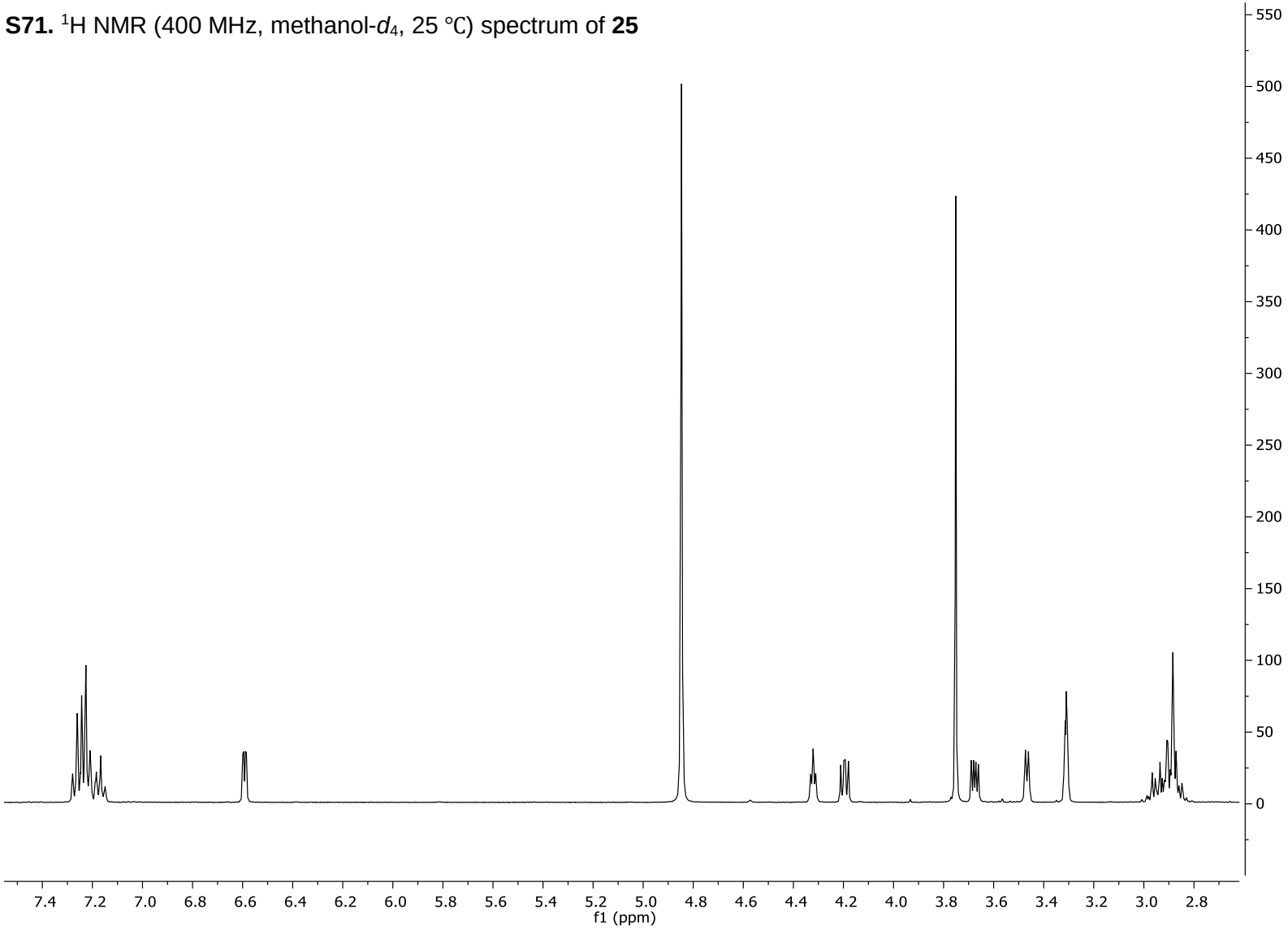

Figure S72. ^{13}C NMR (400 MHz, methanol-d_4, 25 °C) spectrum of **25**

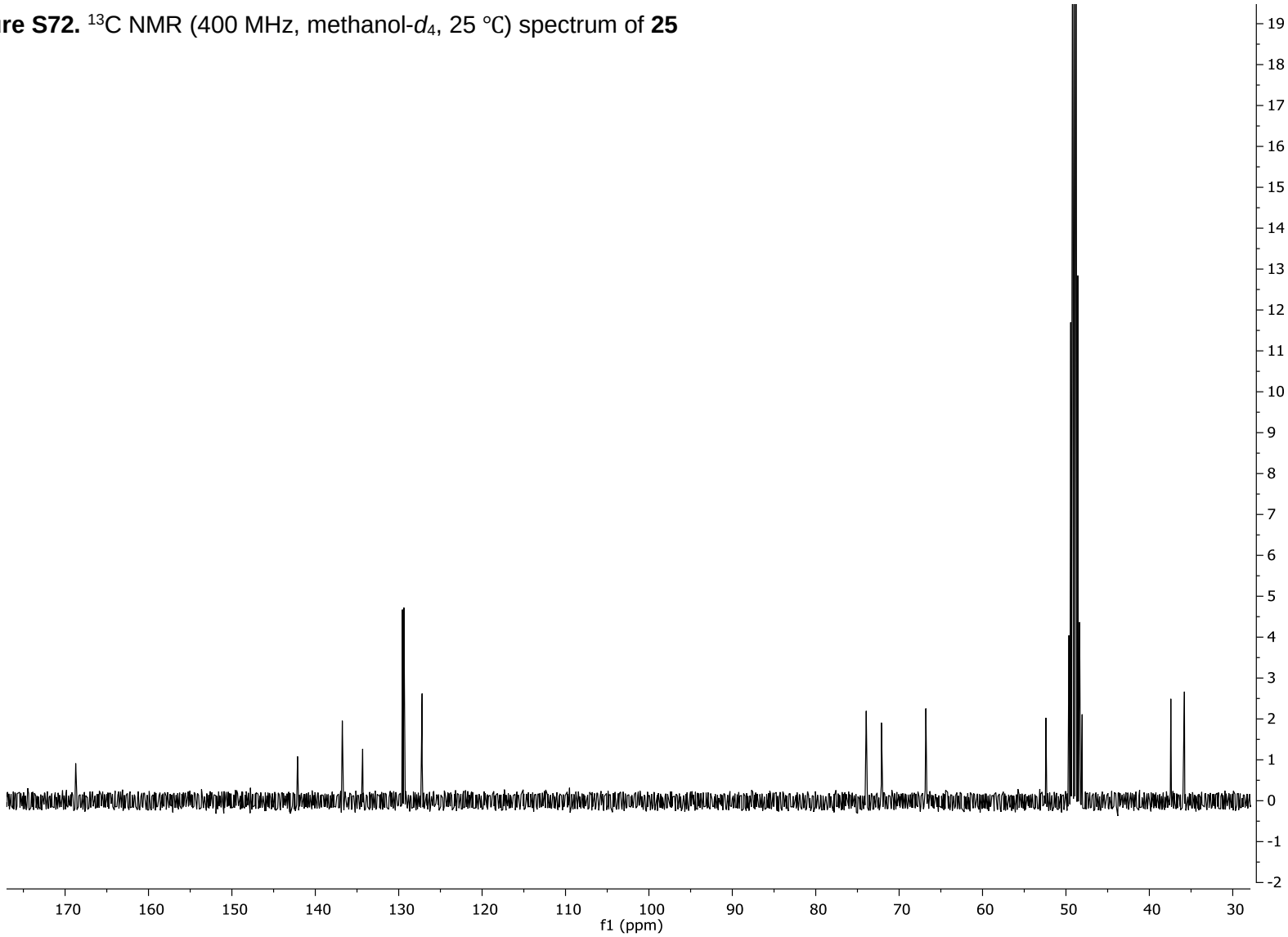

Figure S73. ^{1}H-^{1}H COSY (400 MHz, methanol-d_4, 25 ℃) spectrum of **25**

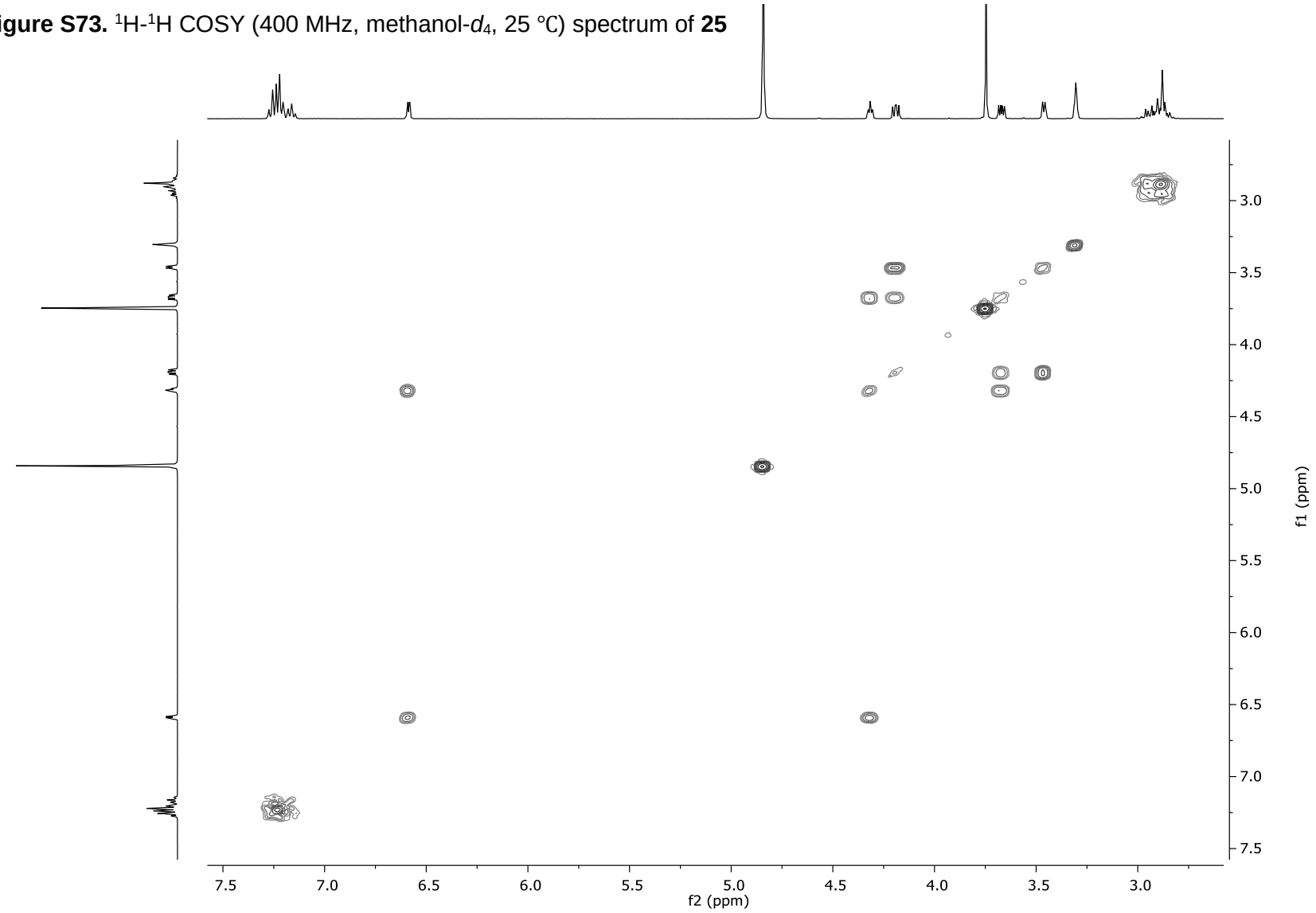

Figure S74. HSQC (400 MHz, methanol-d_4, 25 ℃) spectrum of **25**

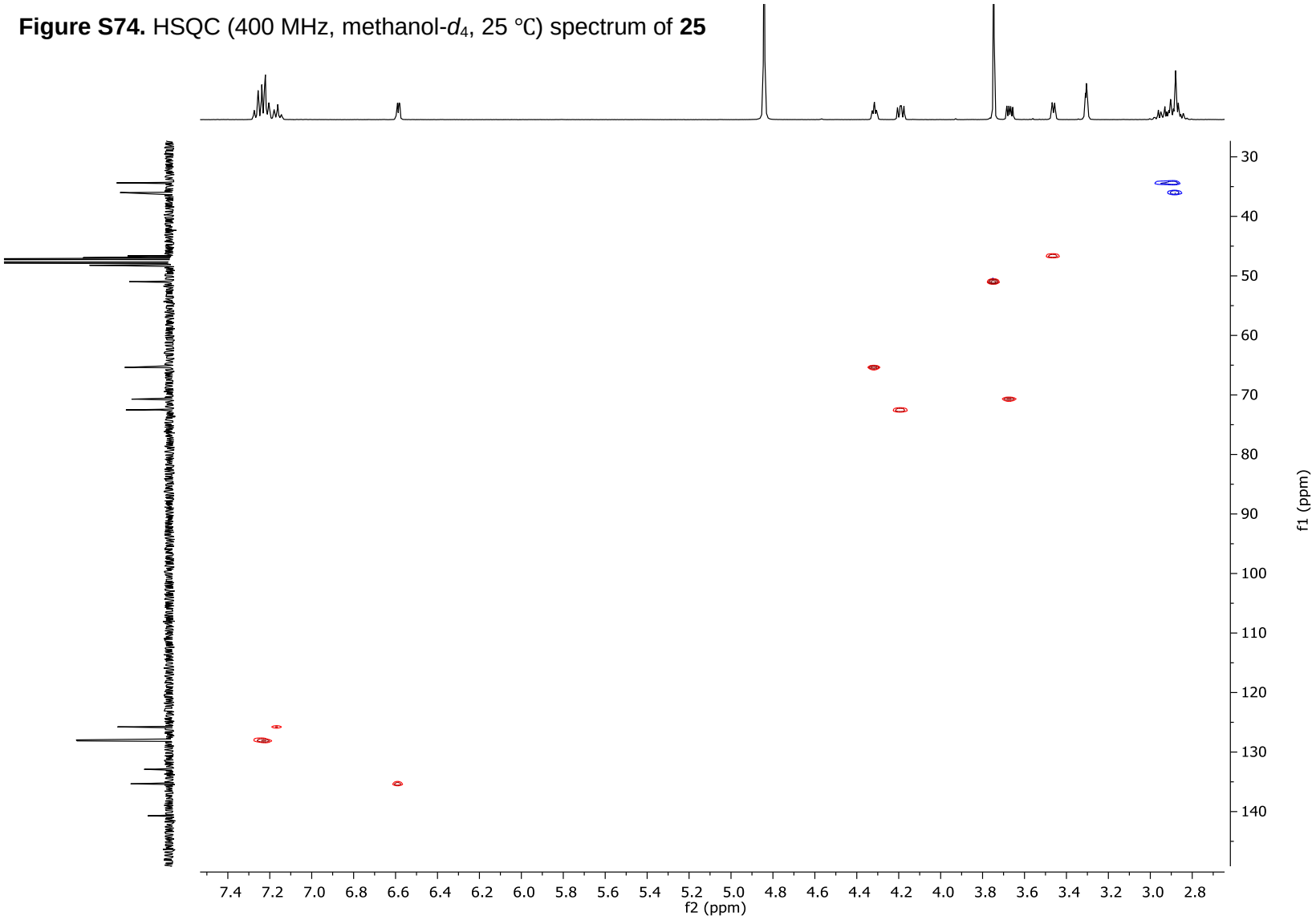

Figure S75. ^{1}H NMR (400 MHz, methanol-d_4, 25 ℃) spectrum of **26**

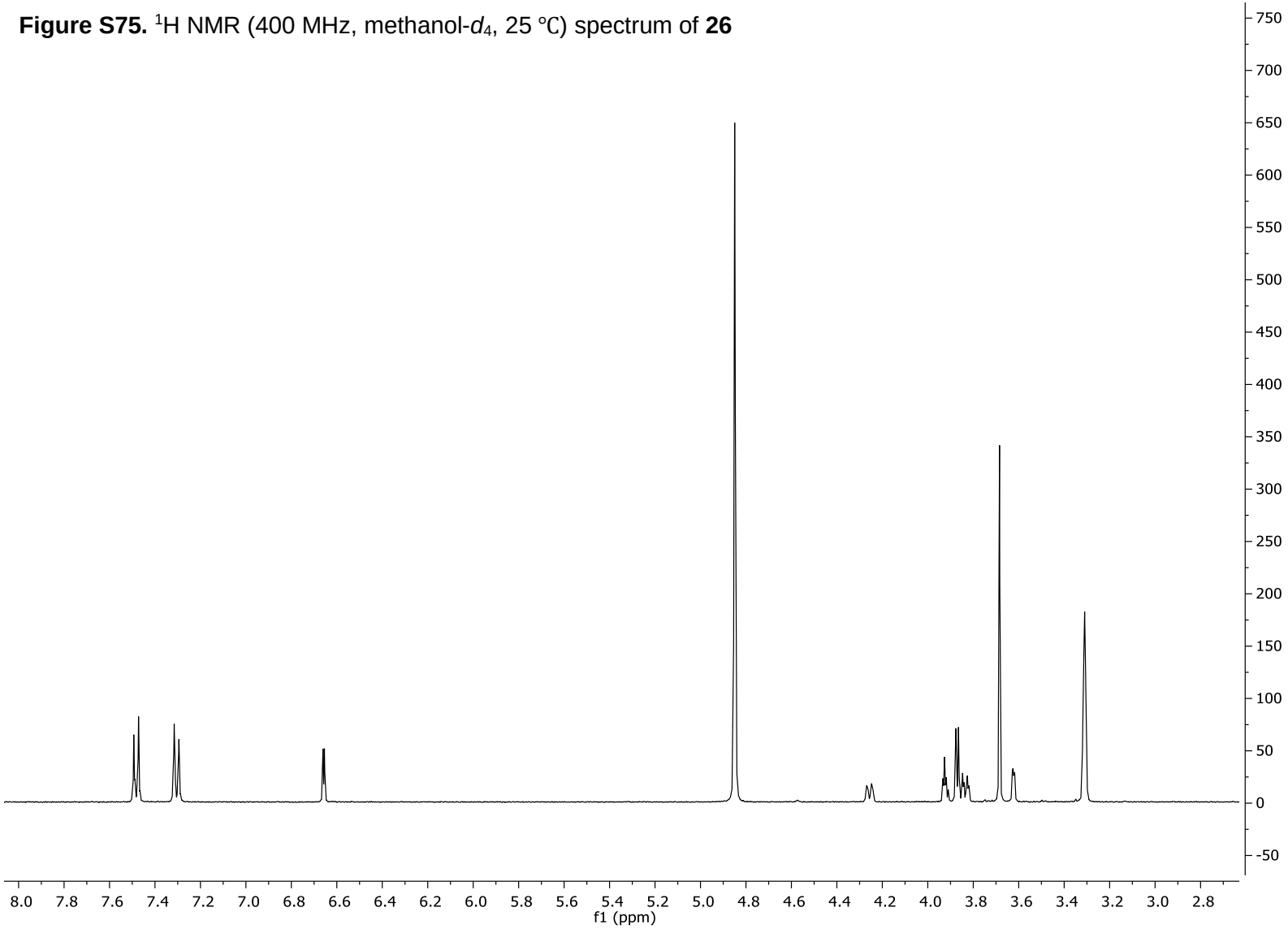

Figure S76. ^{13}C NMR (100 MHz, methanol-d_4, 25 °C) spectrum of **26**

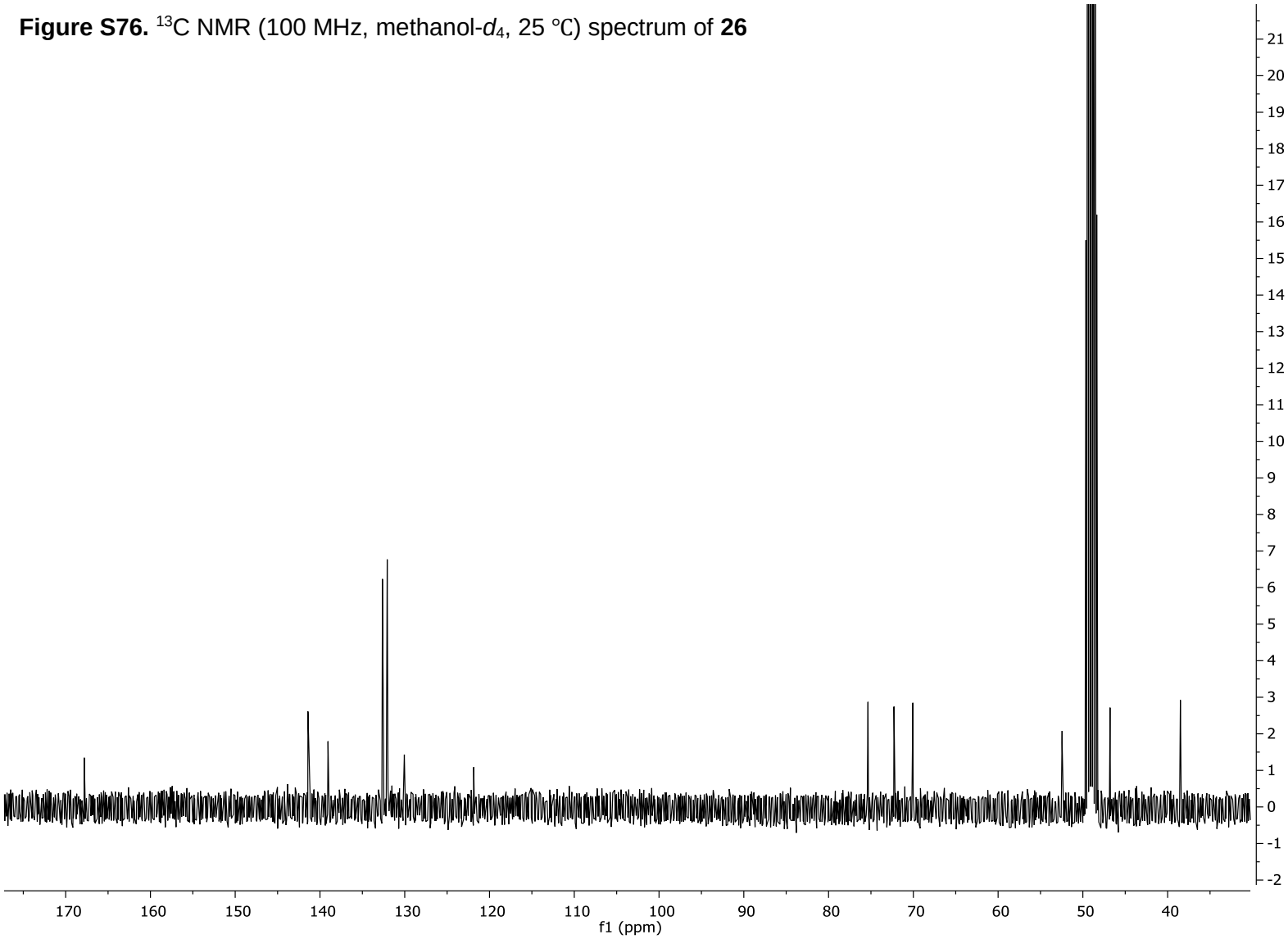

Figure S77. ^{1}H-^{1}H COSY (400 MHz, methanol-d_4, 25 ℃) spectrum of **26**

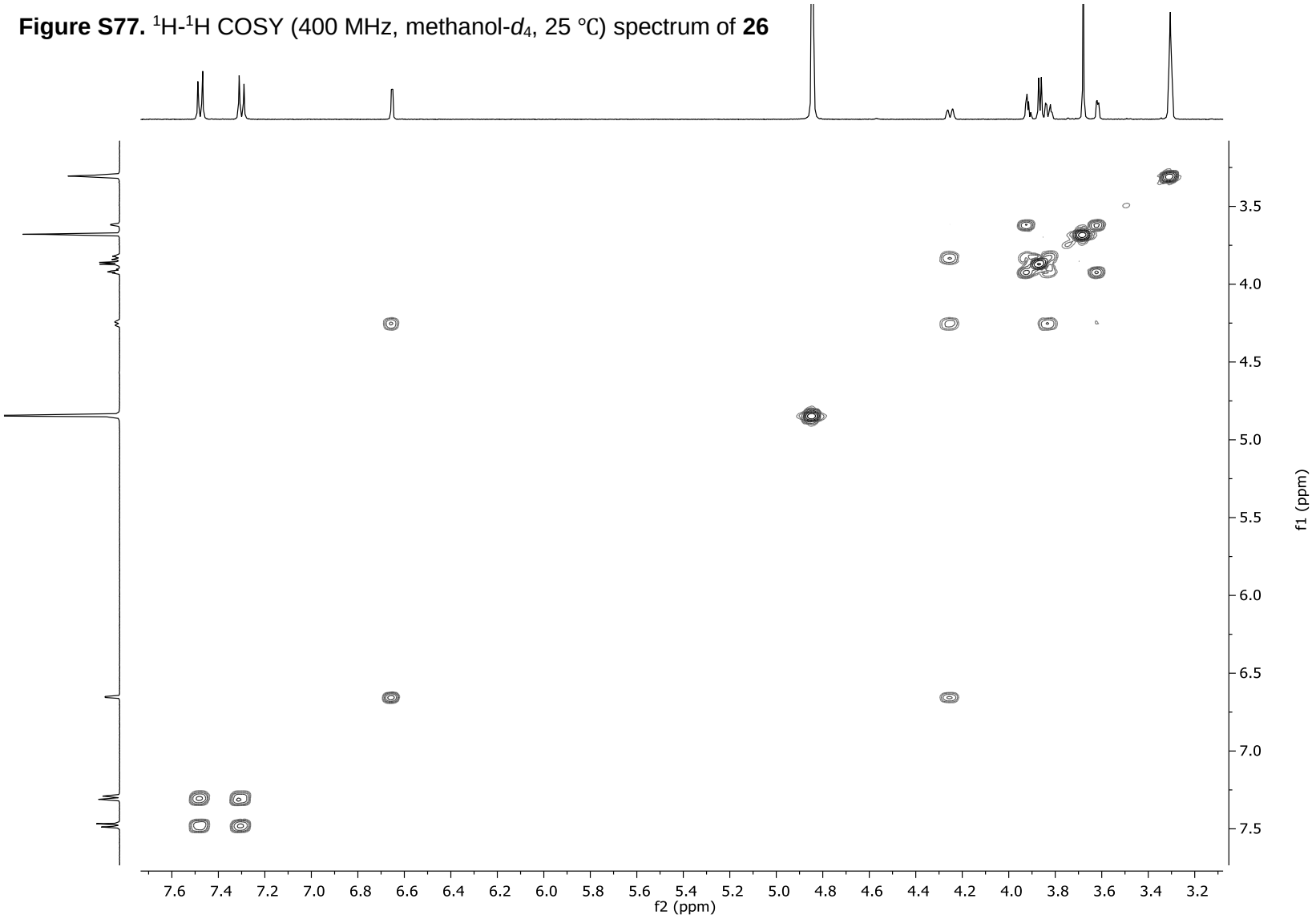

Figure S78. HSQC (400 MHz, methanol-d_4, 25 ℃) spectrum of **26**

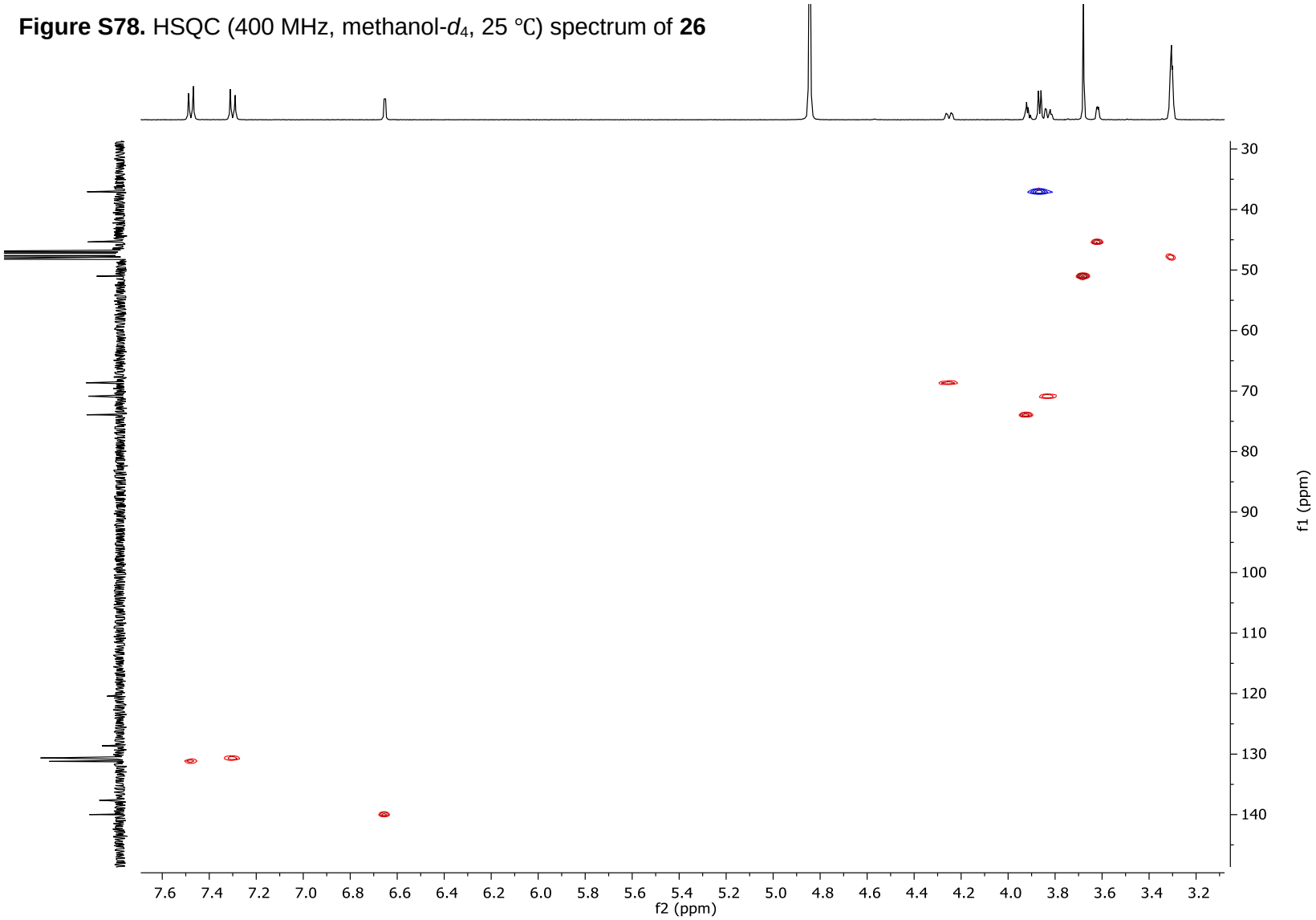

Figure S79. ^{1}H NMR (400 MHz, methanol-d_4, 25 ℃) spectrum of **27**

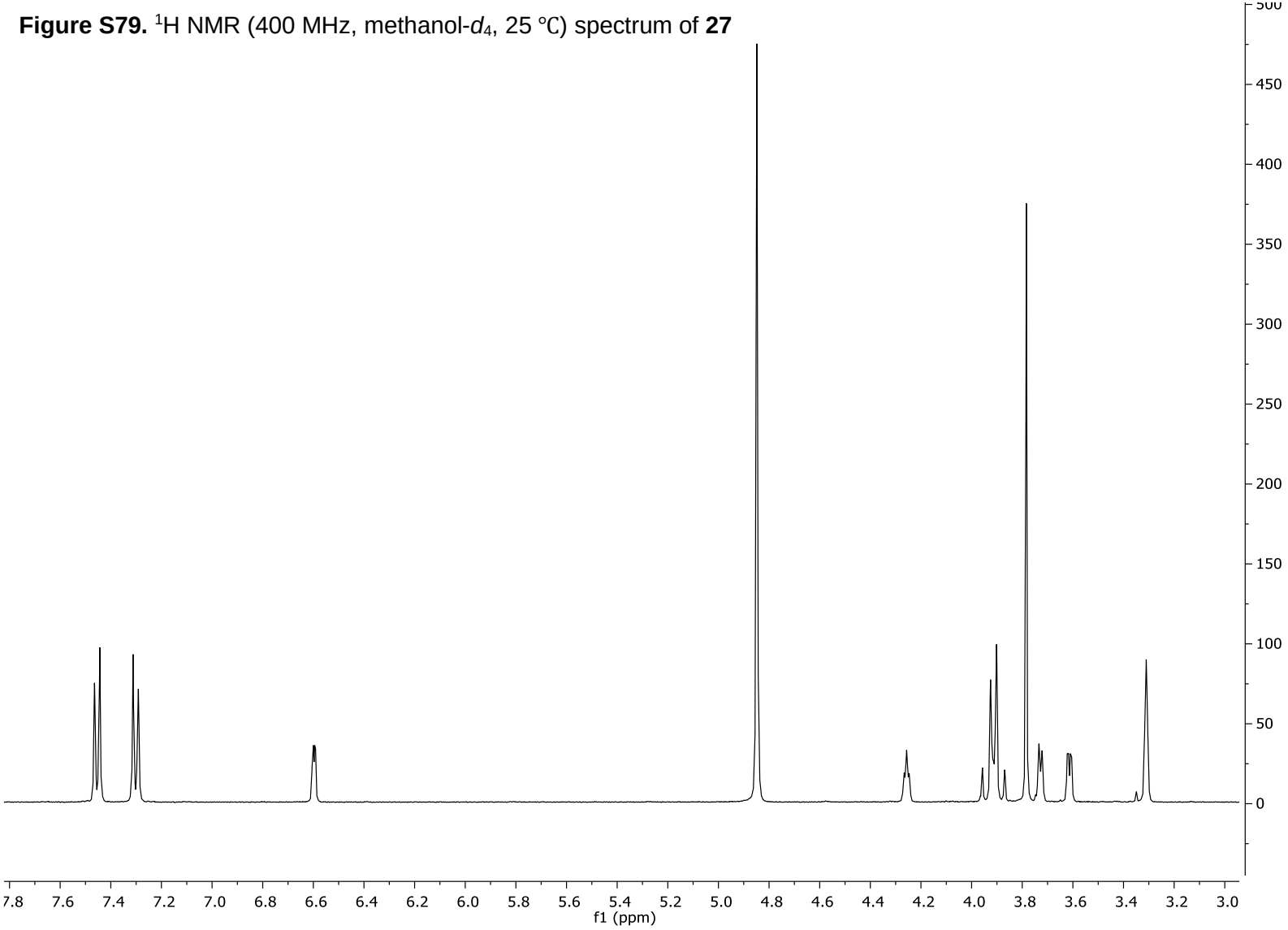

Figure S80. ^{13}C NMR (100 MHz, methanol-d_4, 25 °C) spectrum of **27**

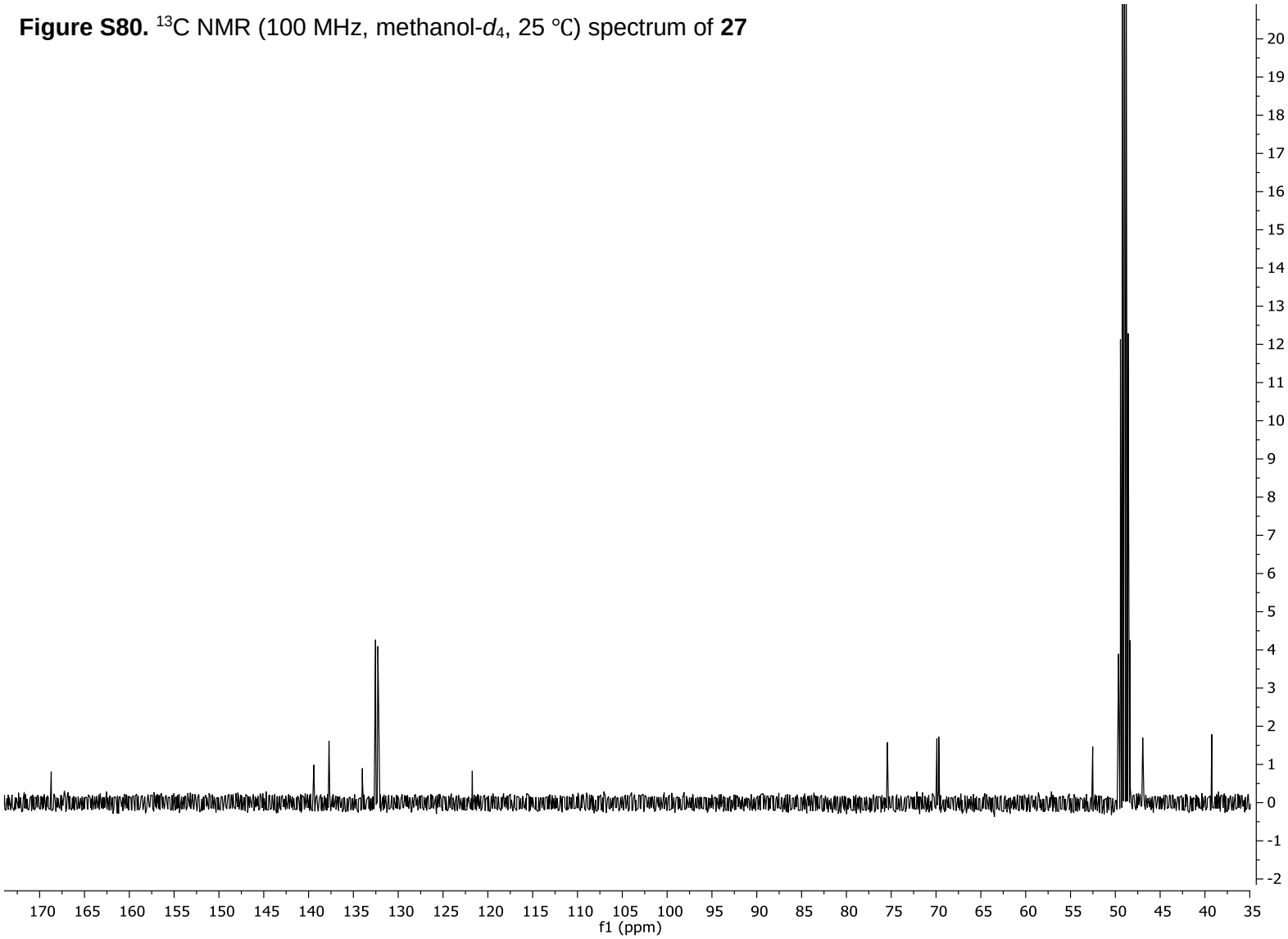

Figure S81. ^{1}H-^{1}H COSY (400 MHz, methanol-d_4, 25 ℃) spectrum of **27**

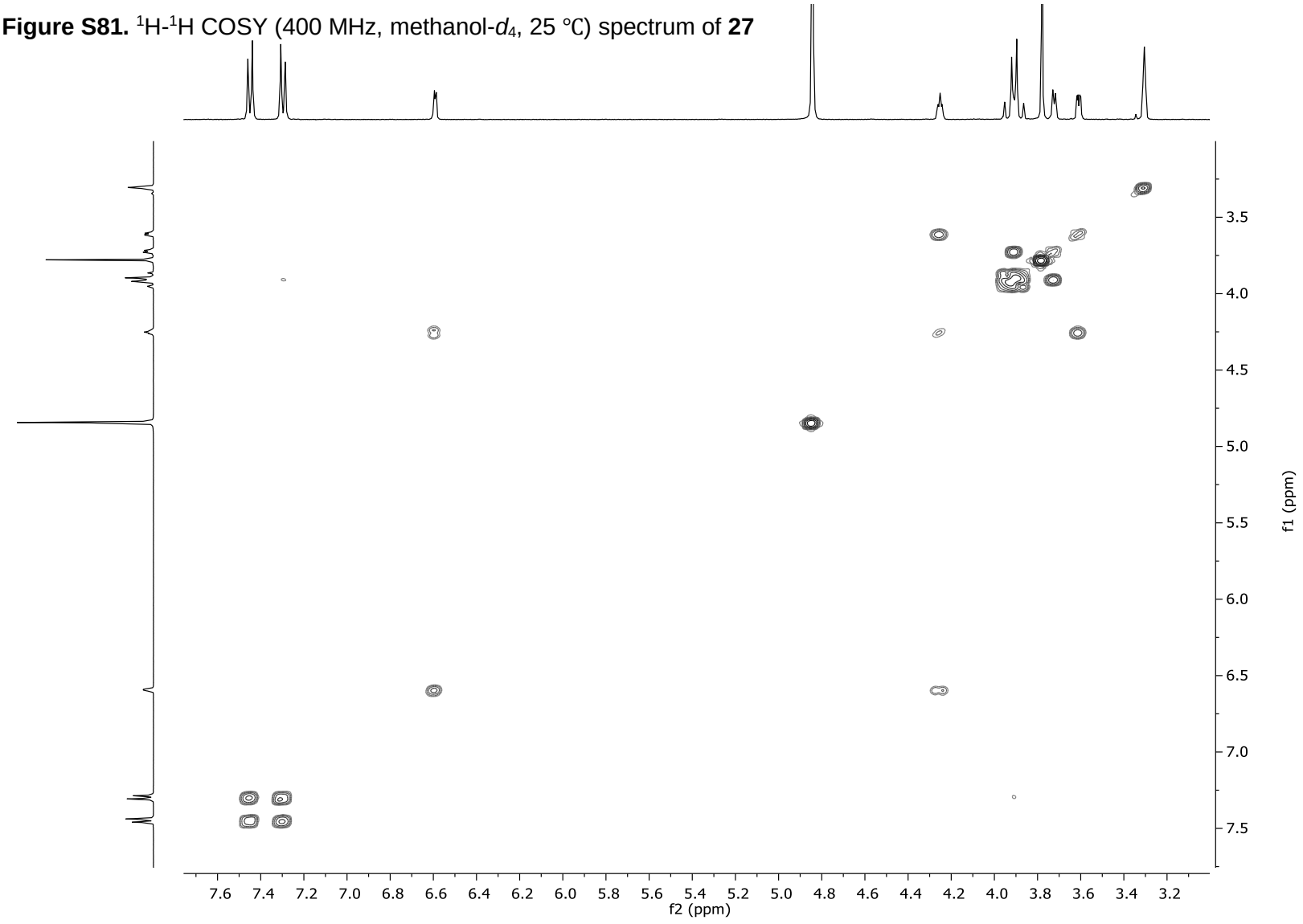

Figure S82. HSQC (400 MHz, methanol-d_4, 25 ℃) spectrum of **27**

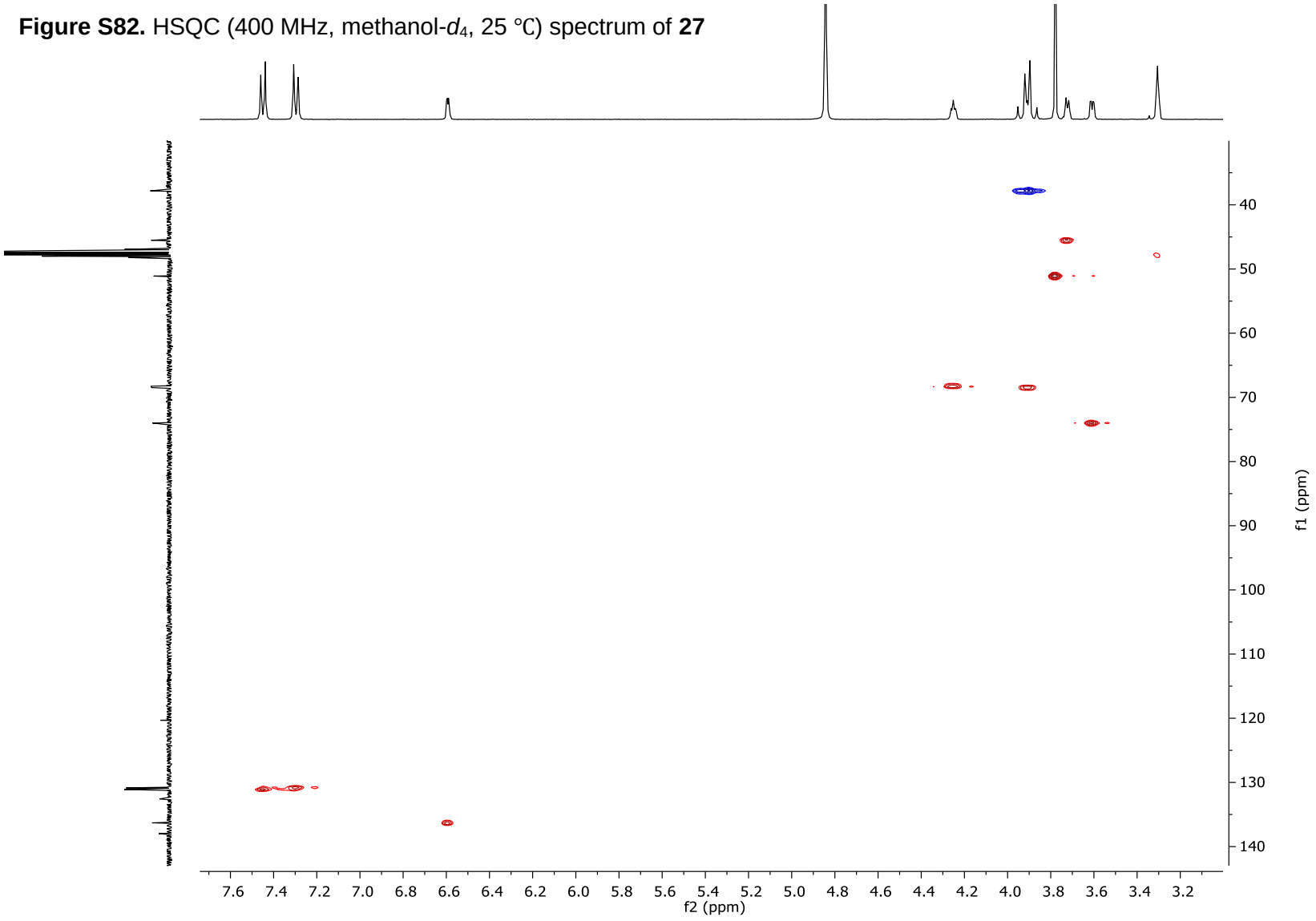

Figure S83. ^{1}H NMR (400 MHz, methanol-d_4, 25 ℃) spectrum of **28**

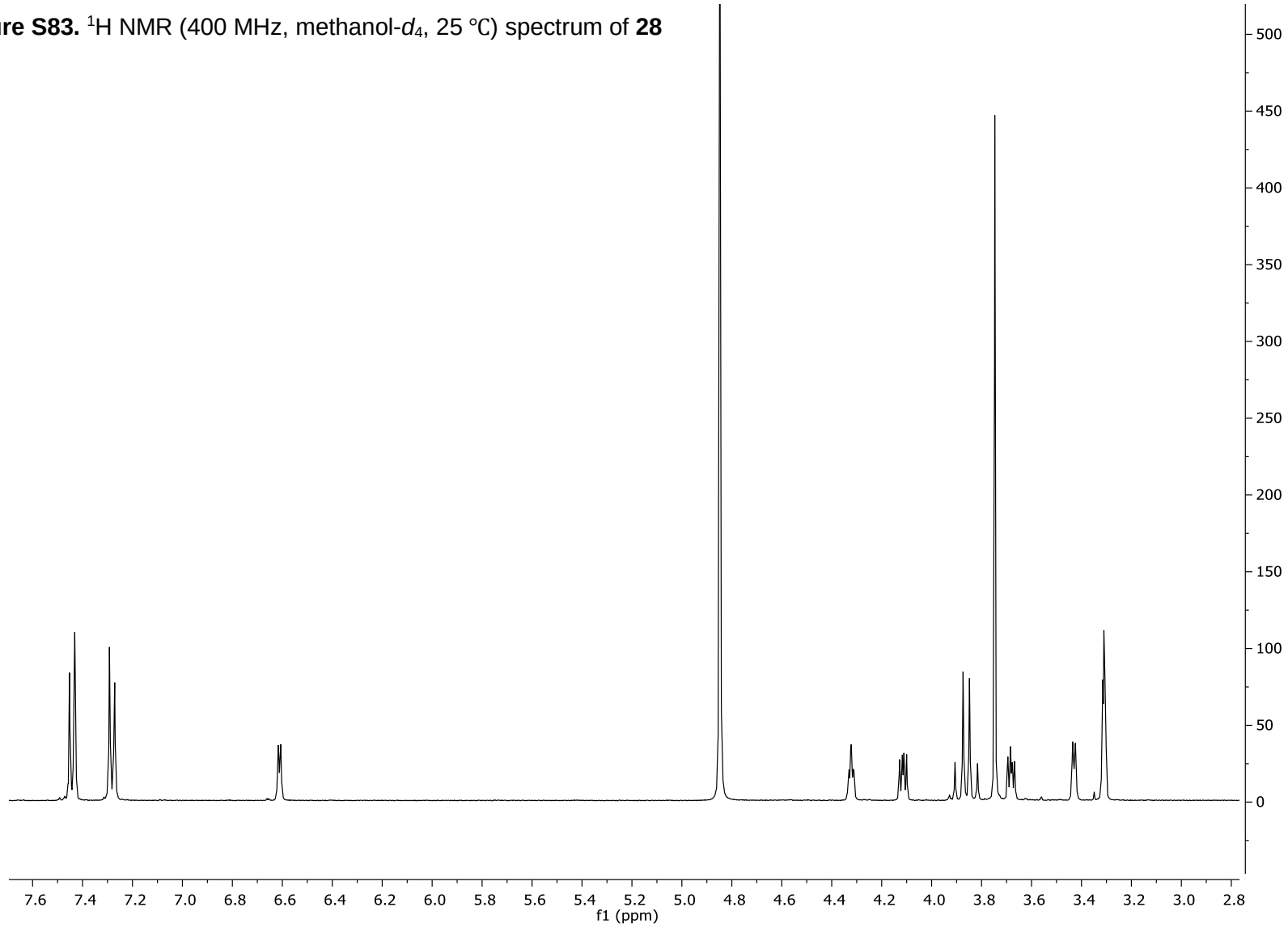

Figure S84. ^{13}C NMR (100 MHz, methanol-d_4, 25 °C) spectrum of **28**

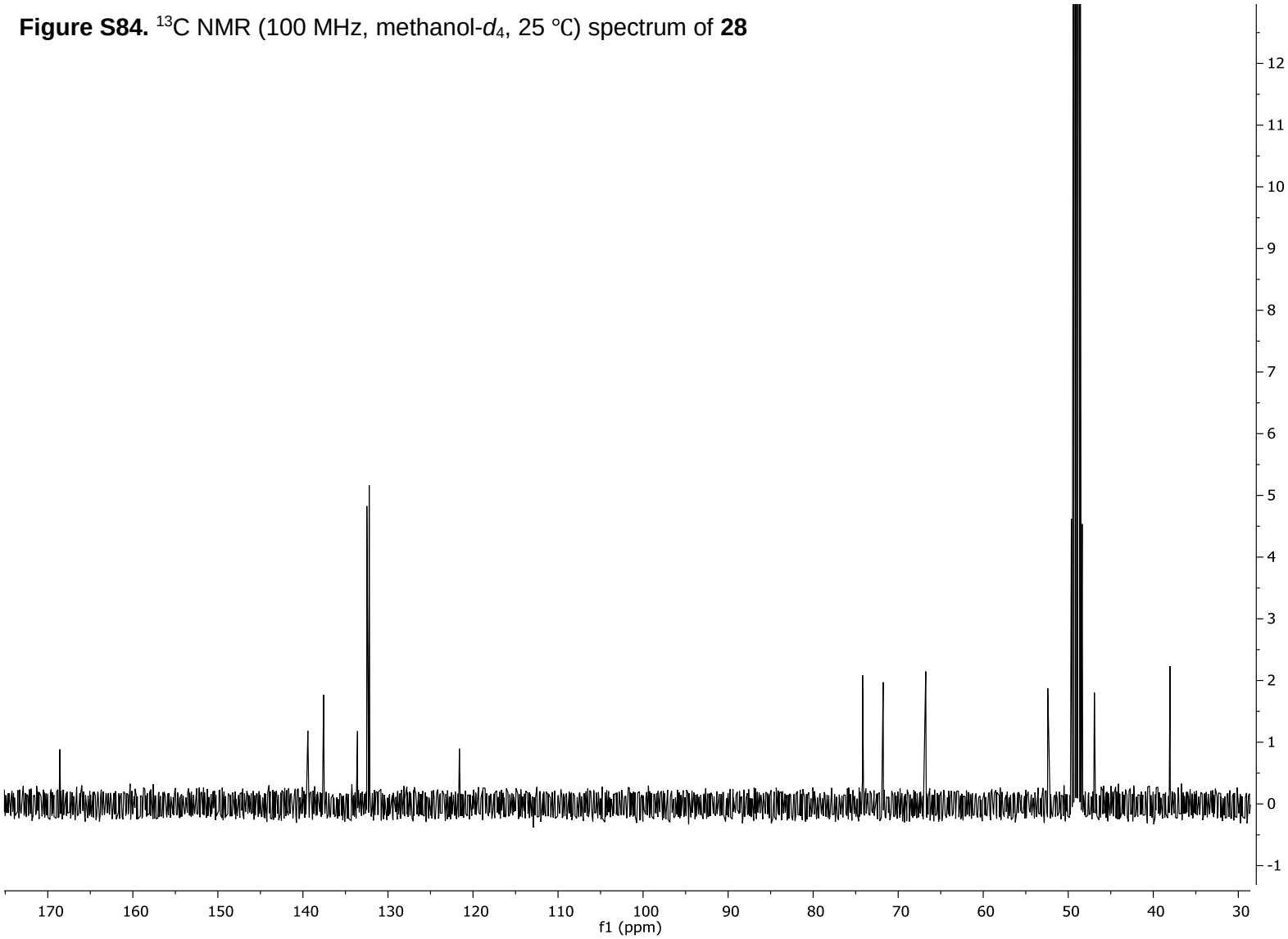

Figure S85. ^{1}H-^{1}H COSY (400 MHz, methanol-d_4, 25 ℃) spectrum of **28**

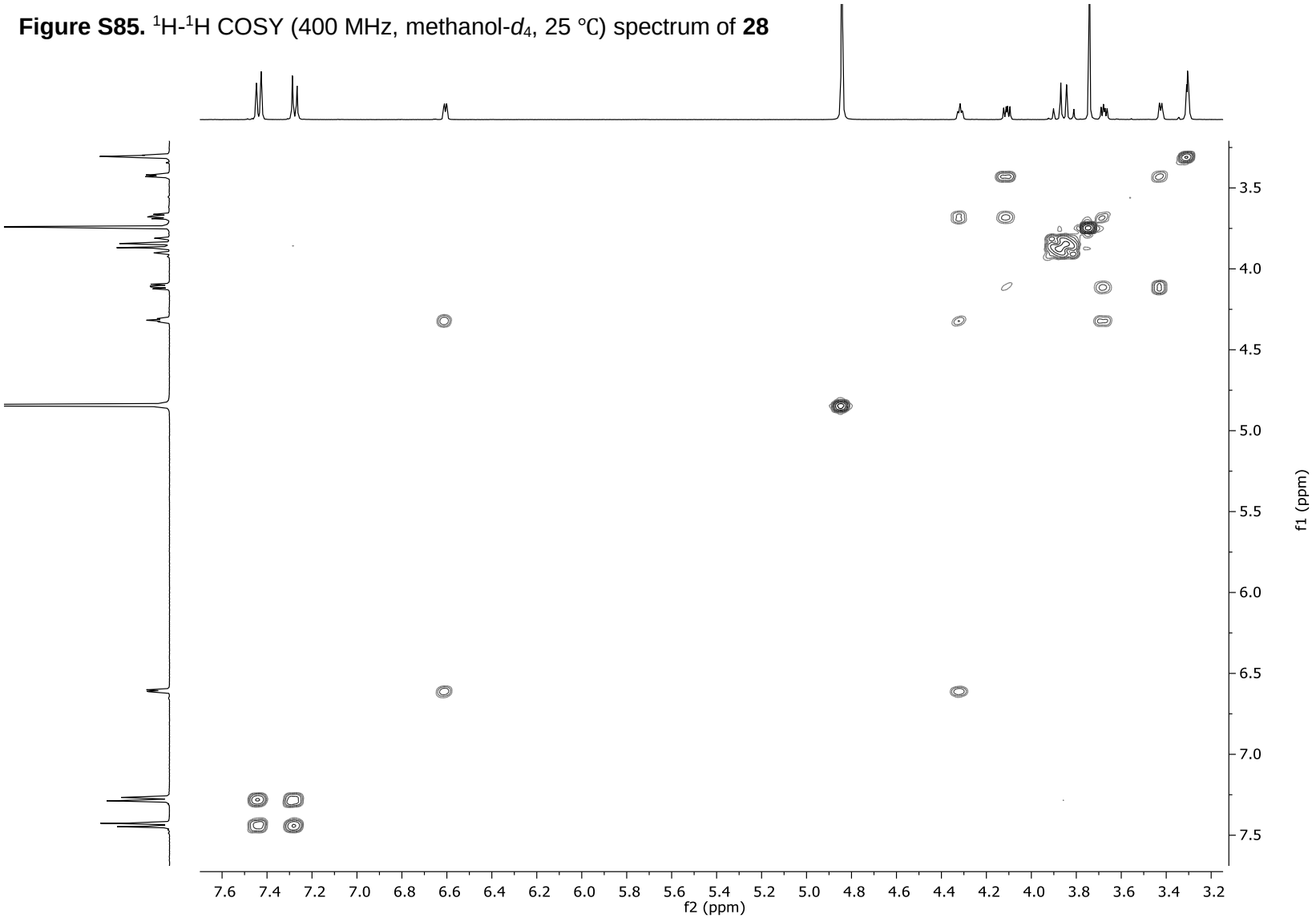

Figure S86. HSQC (400 MHz, methanol-d_4, 25 ℃) spectrum of **28**

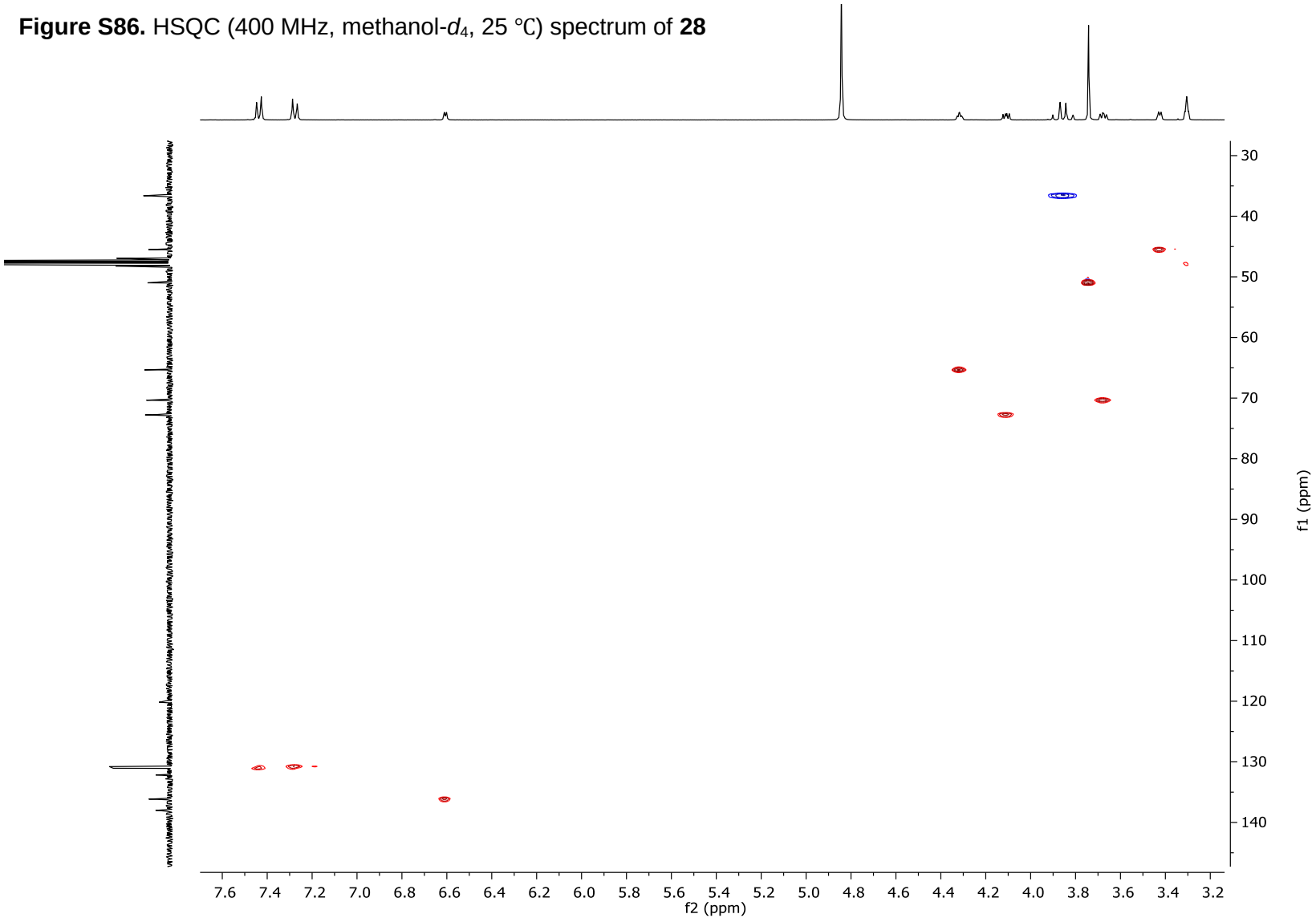

Figure S87. ^{1}H NMR (500 MHz, methanol-d_4, 25 ℃) spectrum of **30**

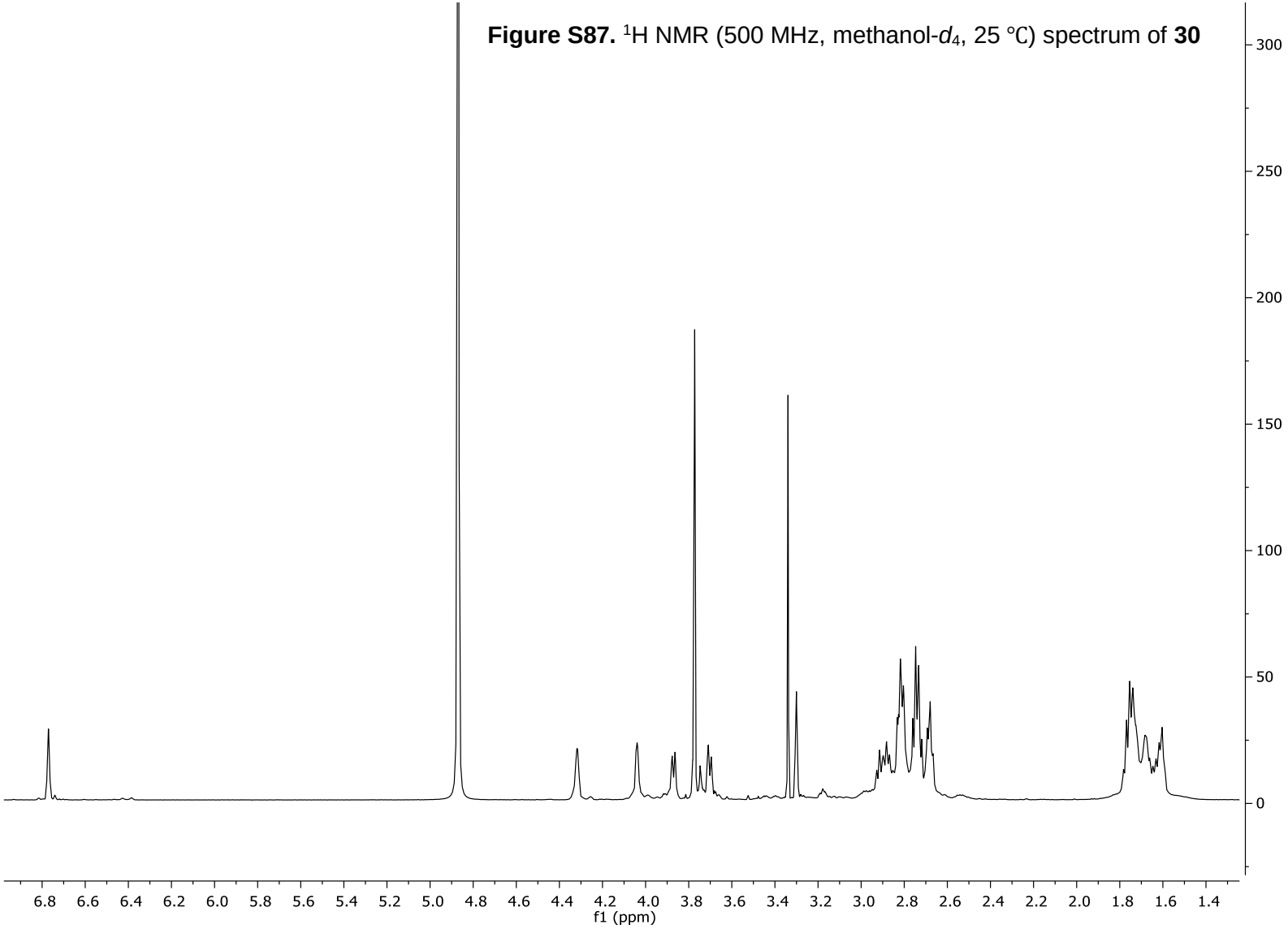

Figure S88. ^{13}C NMR (100 MHz, methanol-d_4, 25 °C) spectrum of **30**

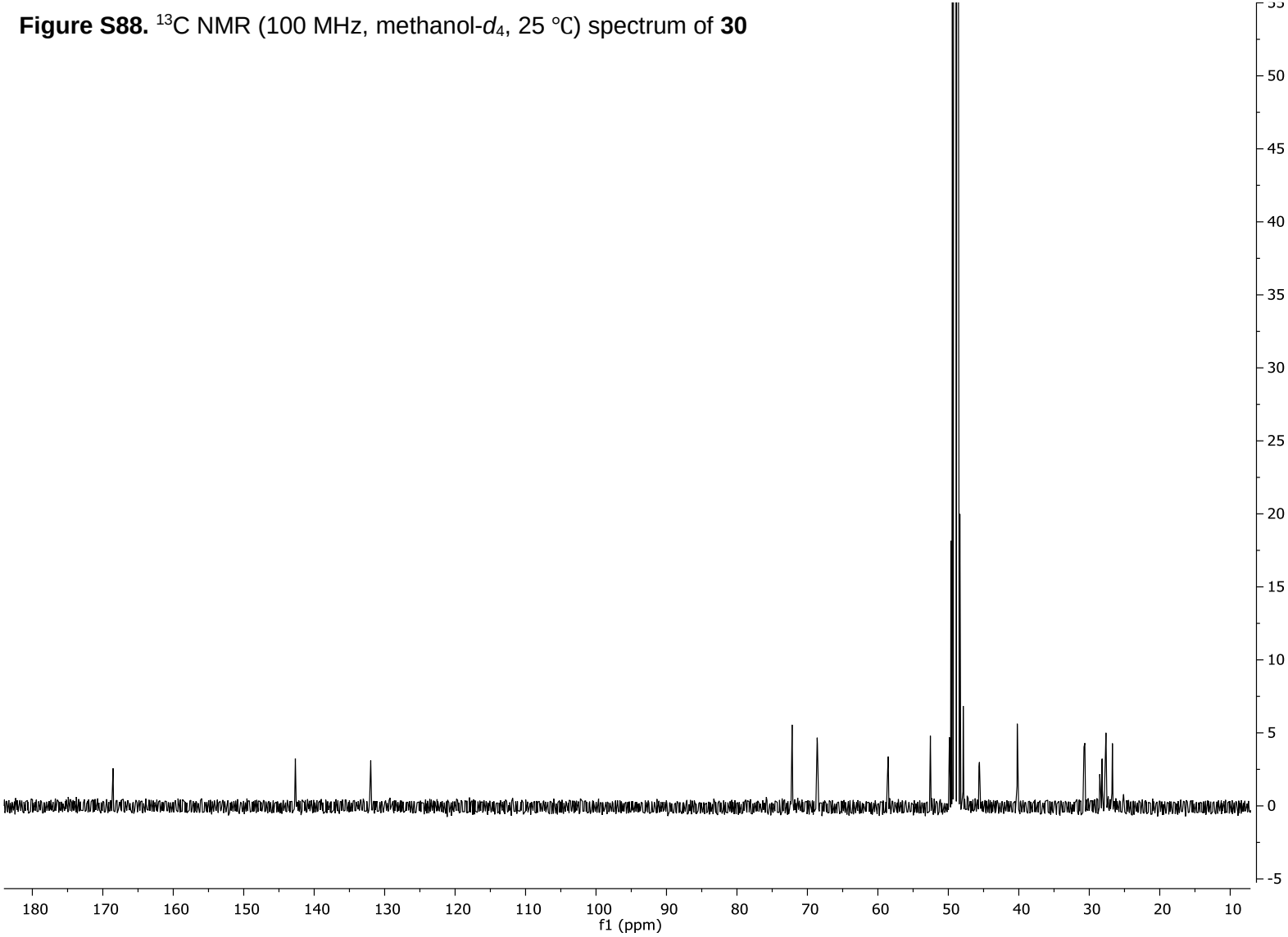

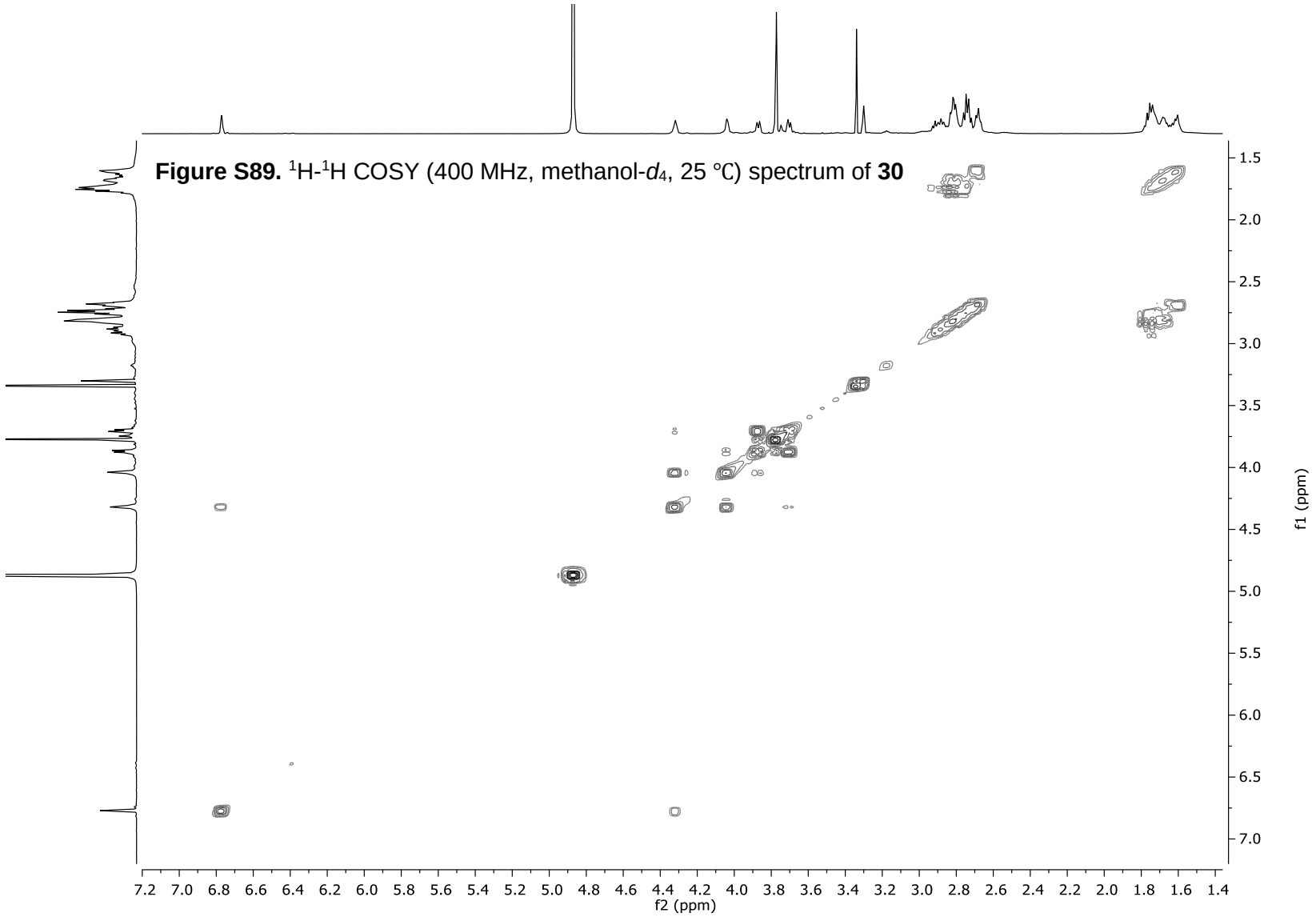

Figure S89. ^{1}H-^{1}H COSY (400 MHz, methanol-d_4, 25 ℃) spectrum of **30**

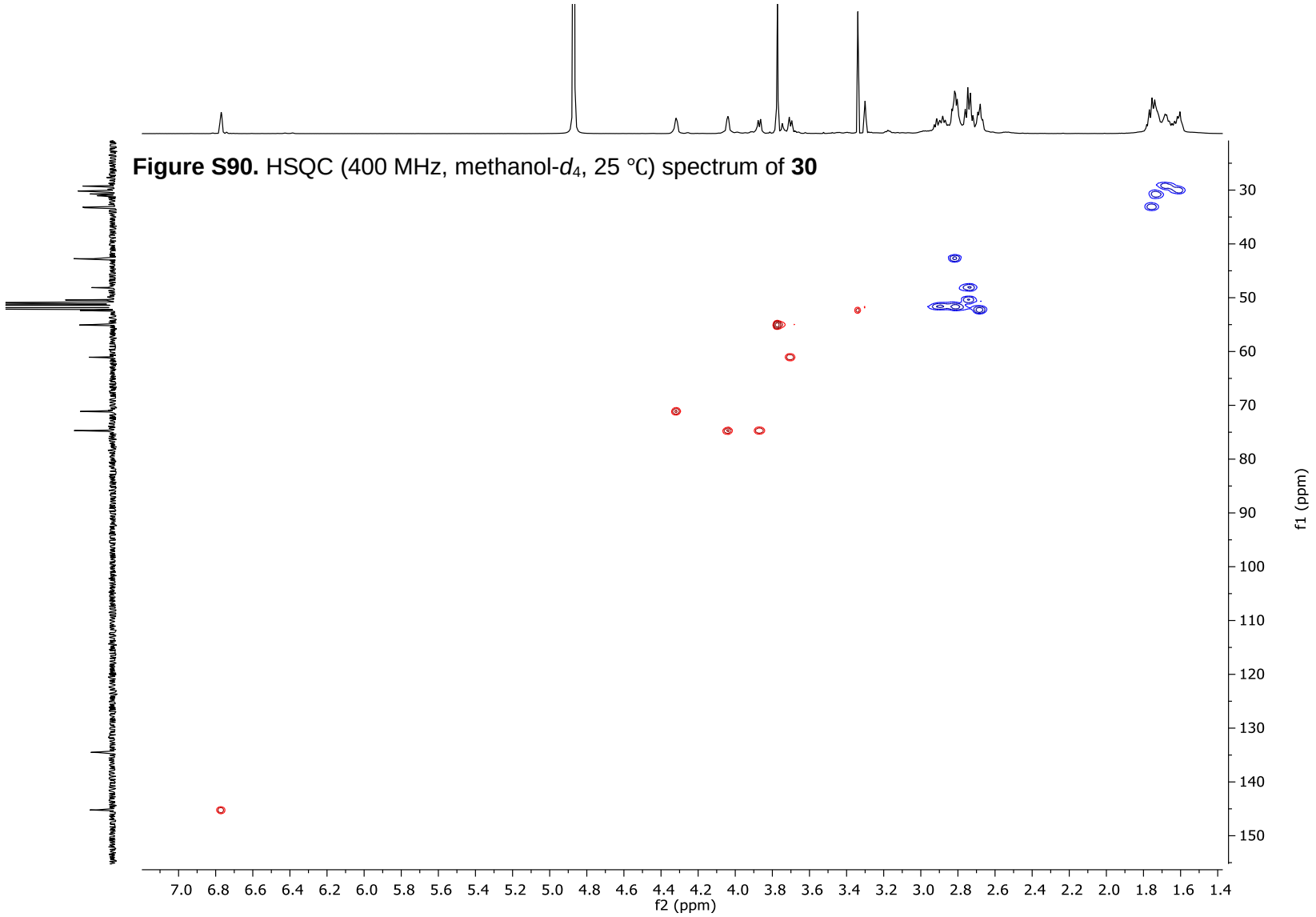

Figure S90. HSQC (400 MHz, methanol-d_4, 25 ℃) spectrum of **30**

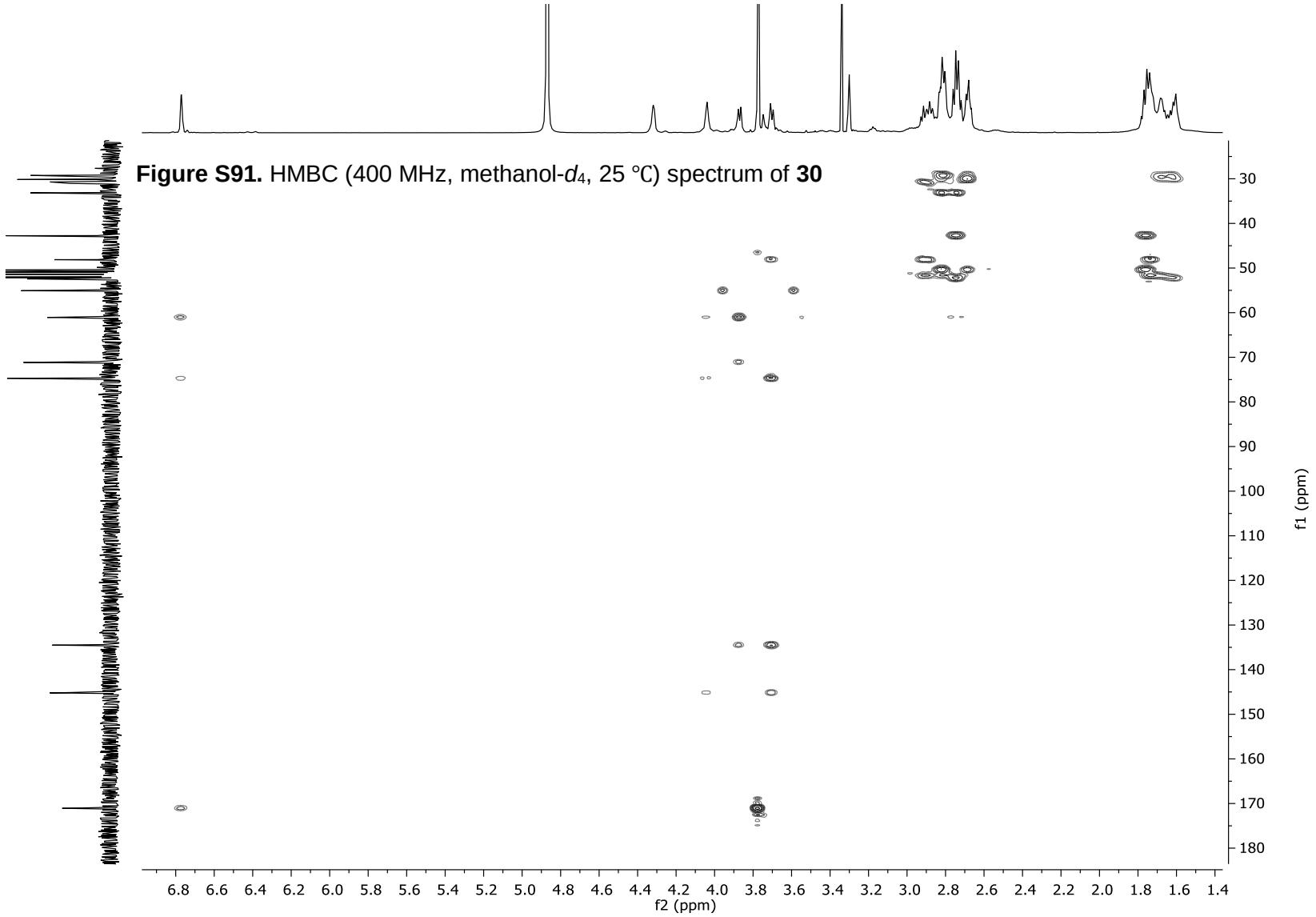

Figure S91. HMBC (400 MHz, methanol-d_4, 25 ℃) spectrum of **30**

Figure S92. ^{1}H NMR (400 MHz, methanol-d_4, 25 ℃) spectrum of TFA-**30**

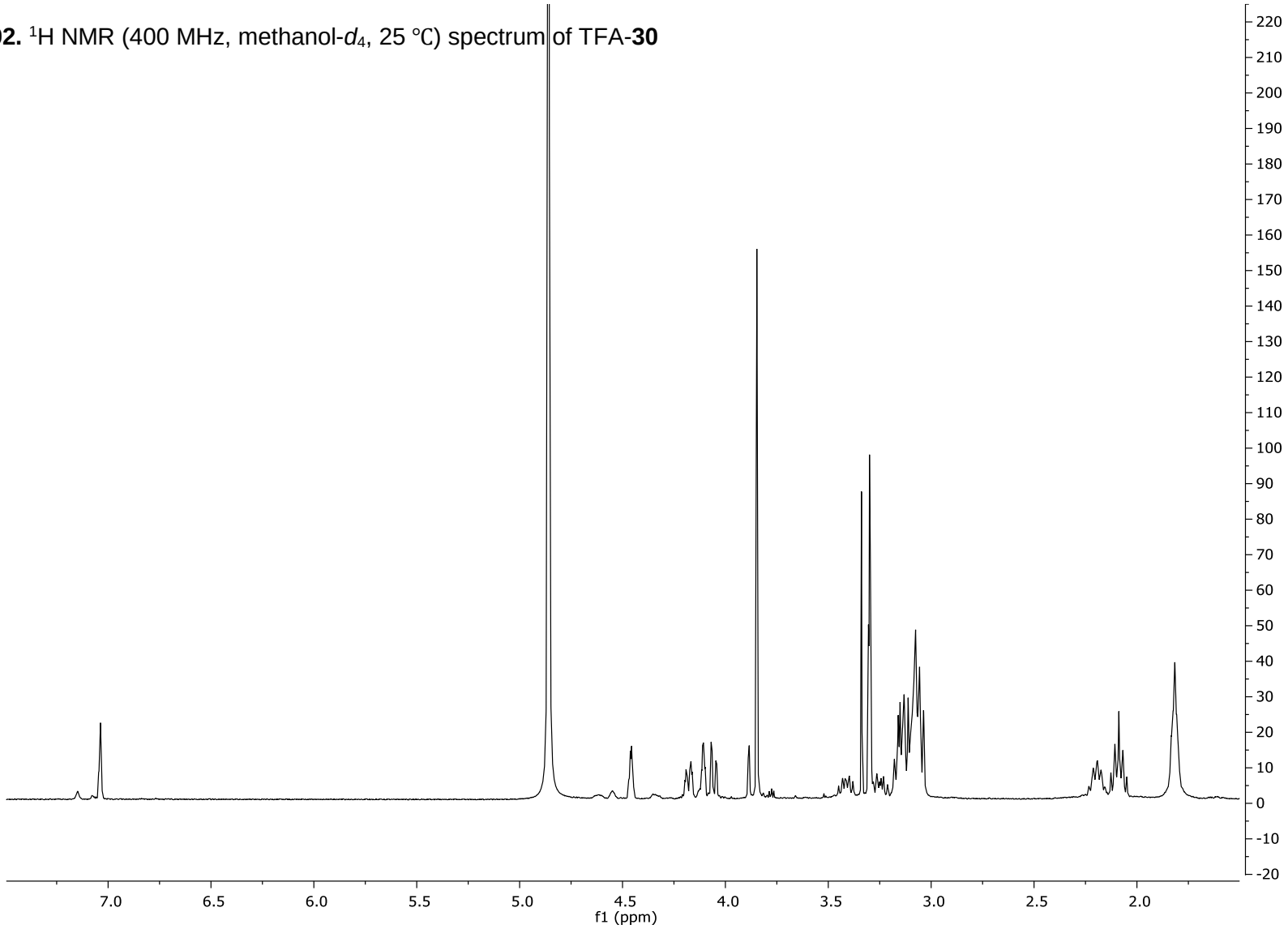

Figure S93. ^{13}C NMR (100 MHz, methanol-d_4, 25 °C) spectrum of TFA-**30**

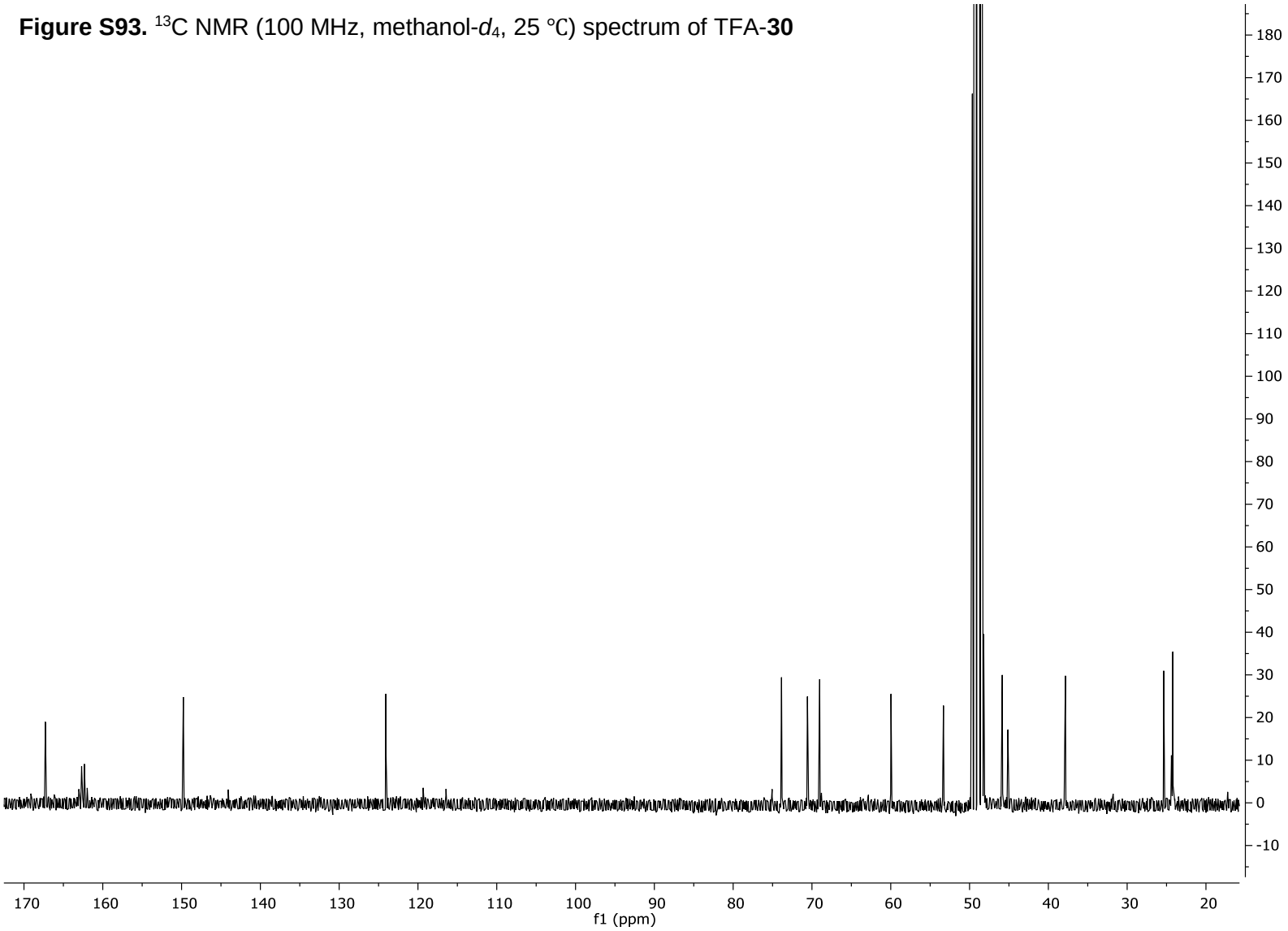

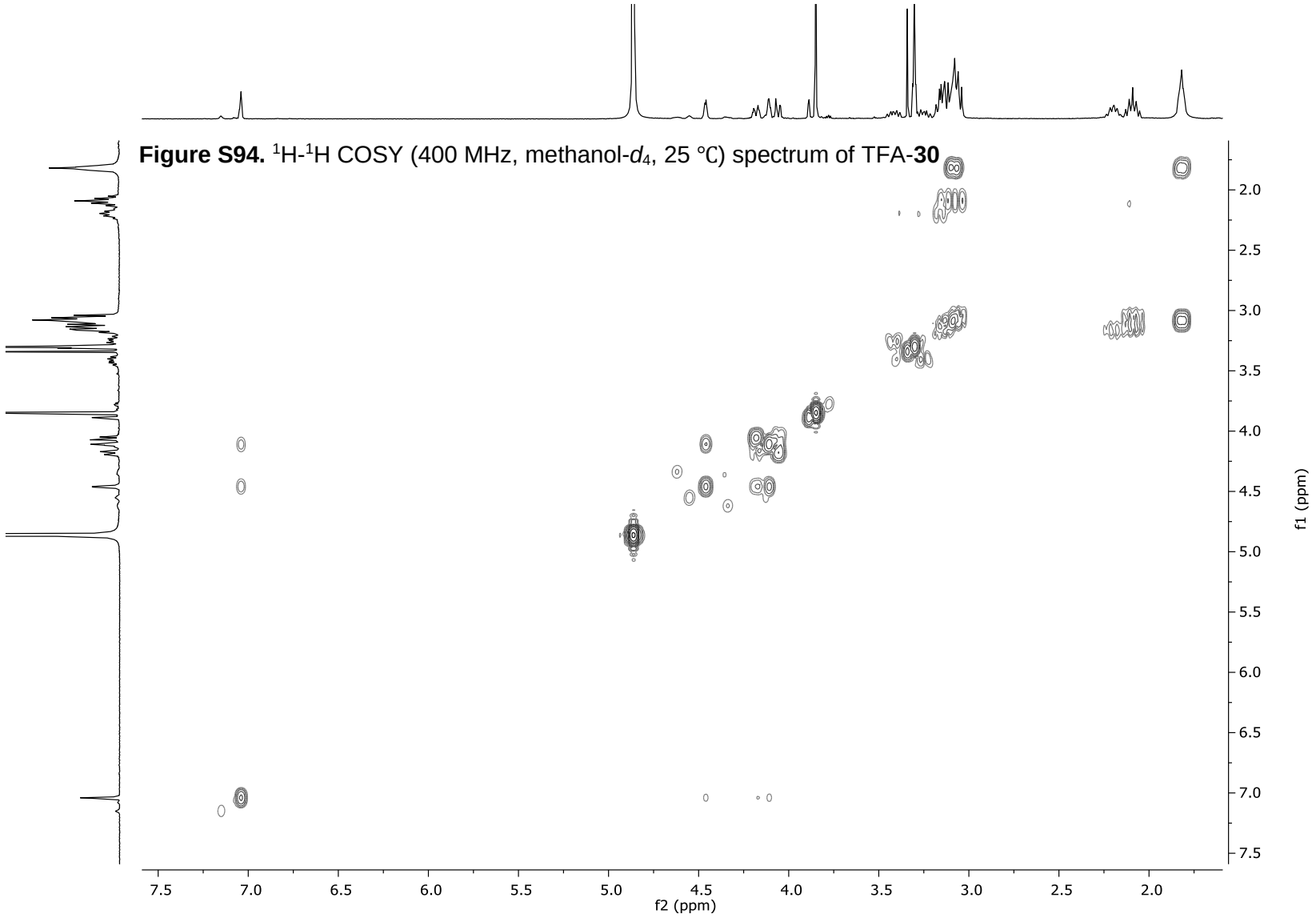

Figure S94. ^{1}H-^{1}H COSY (400 MHz, methanol-d_4, 25 ℃) spectrum of TFA-**30**

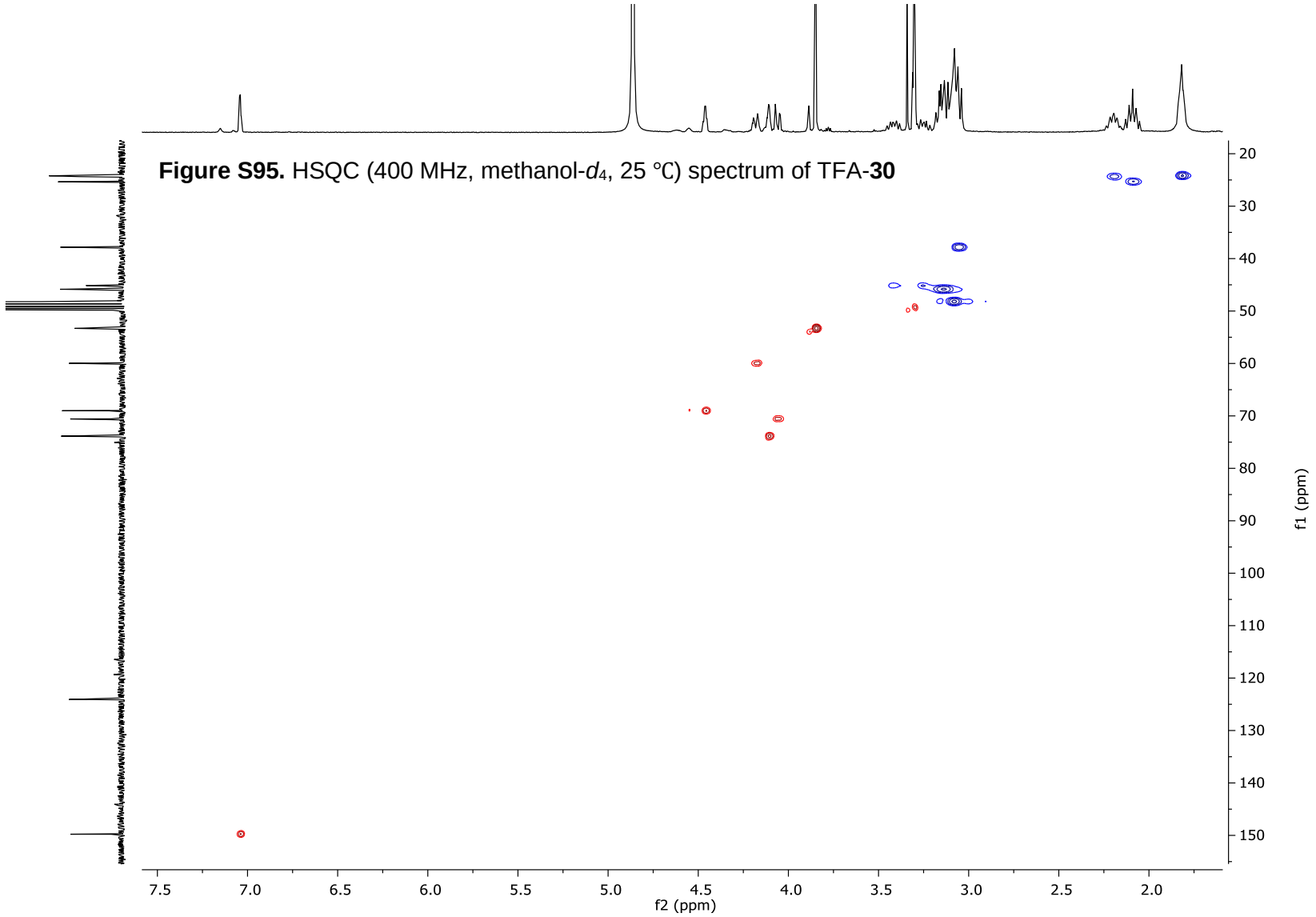

Figure S95. HSQC (400 MHz, methanol-d_4, 25 ℃) spectrum of TFA-**30**

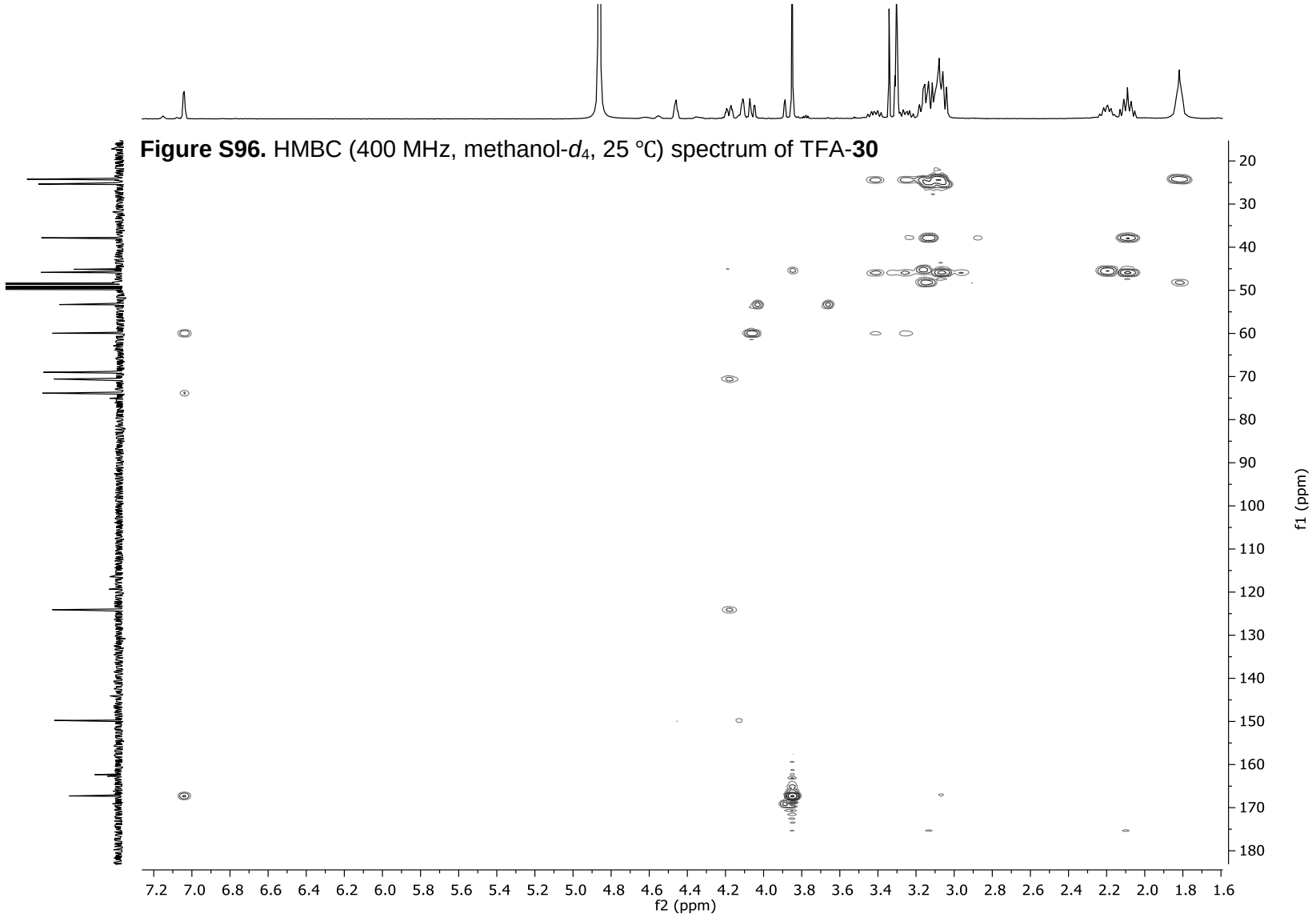

Figure S96. HMBC (400 MHz, methanol-d_4, 25 ℃) spectrum of TFA-**30**

Figure S97. ^{13}C NMR (100 MHz, methanol-d_4, 25 °C) spectrum of [^{13}C]-labeled **30**

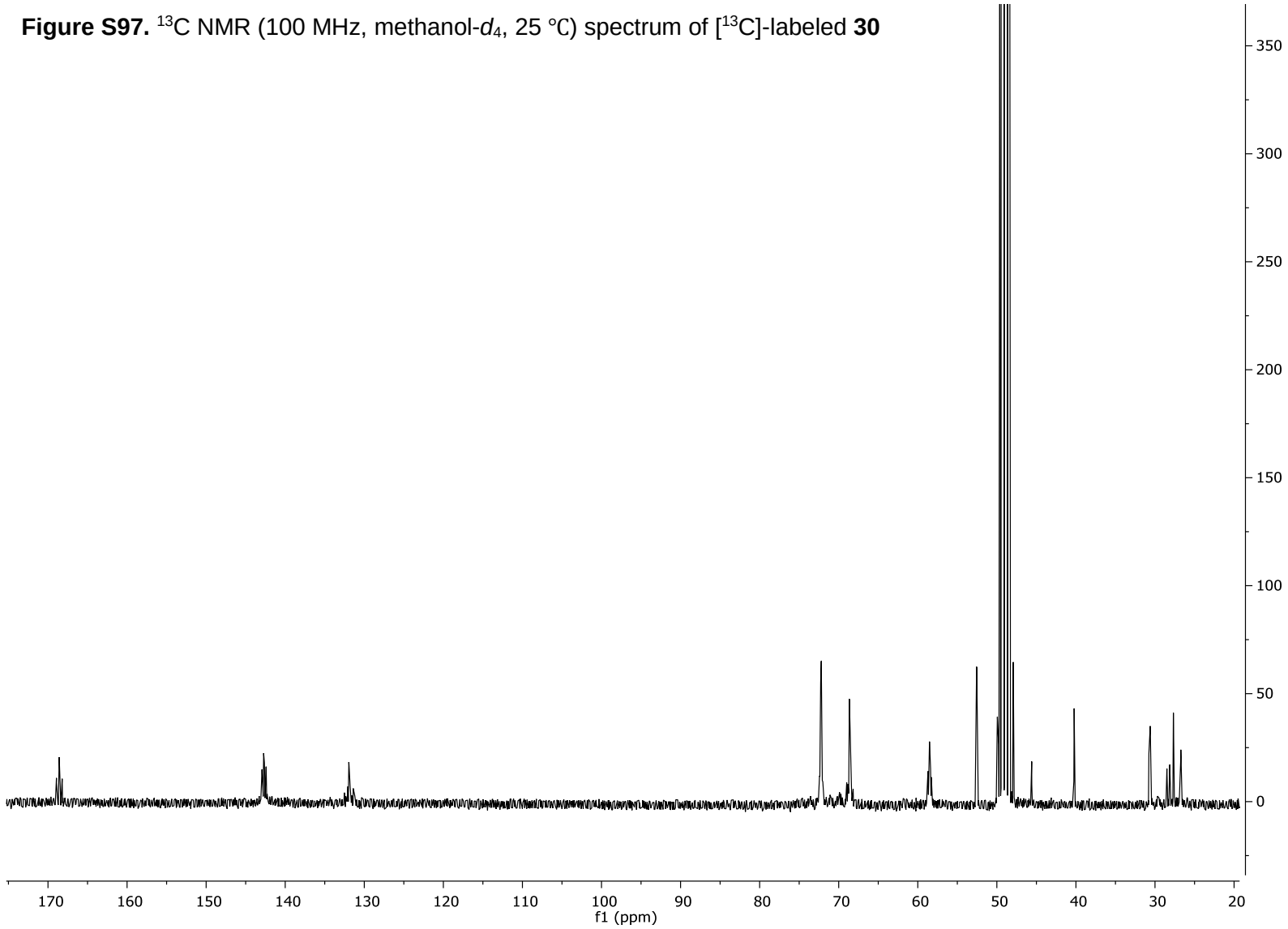

Figure S98. ^{1}H NMR (400 MHz, $CDCl_3$, 25 ℃) spectrum of **31**

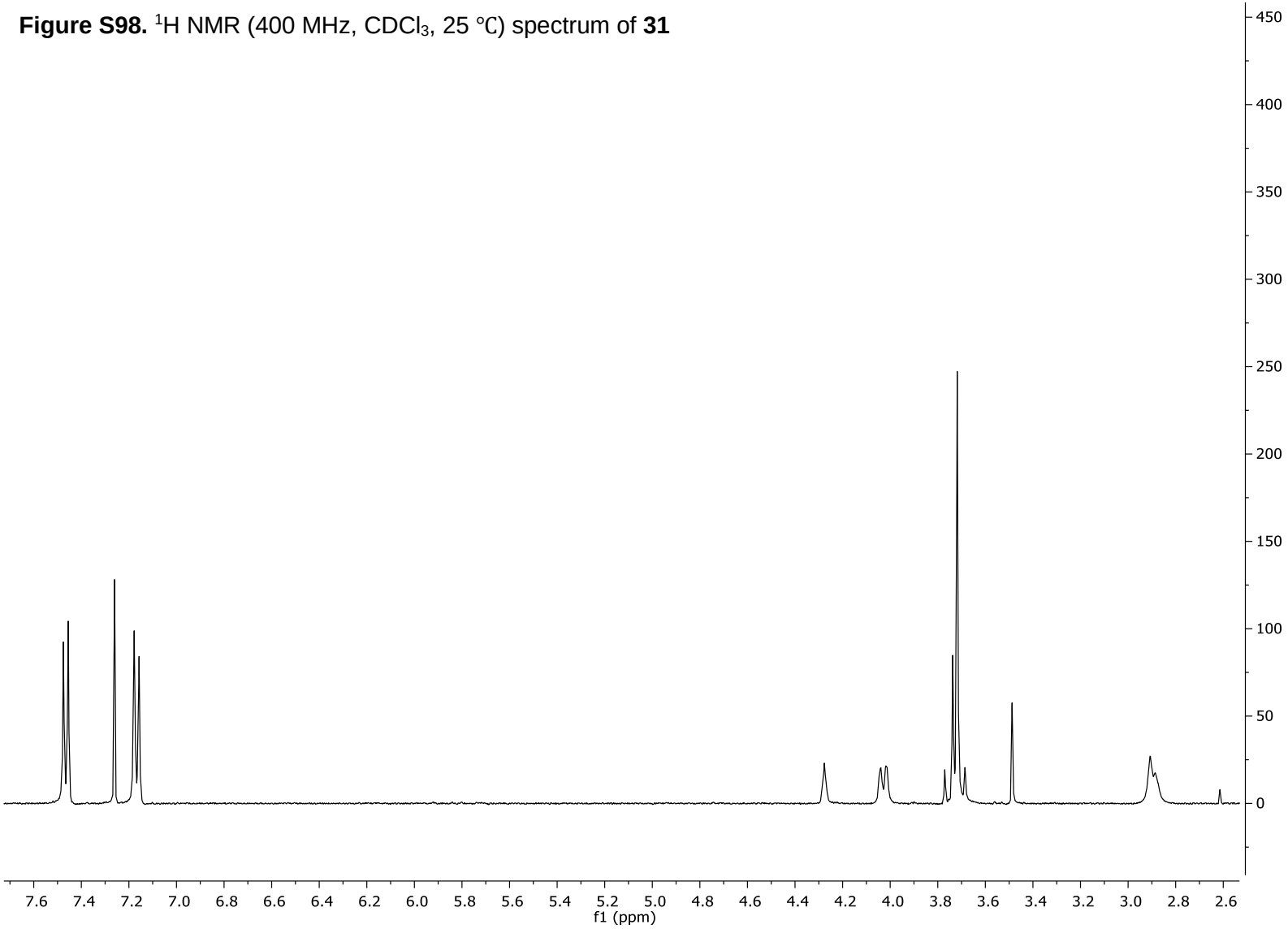

Figure S99. ^{13}C NMR (100 MHz, $CDCl_3$, 25 ℃) spectrum of **31**

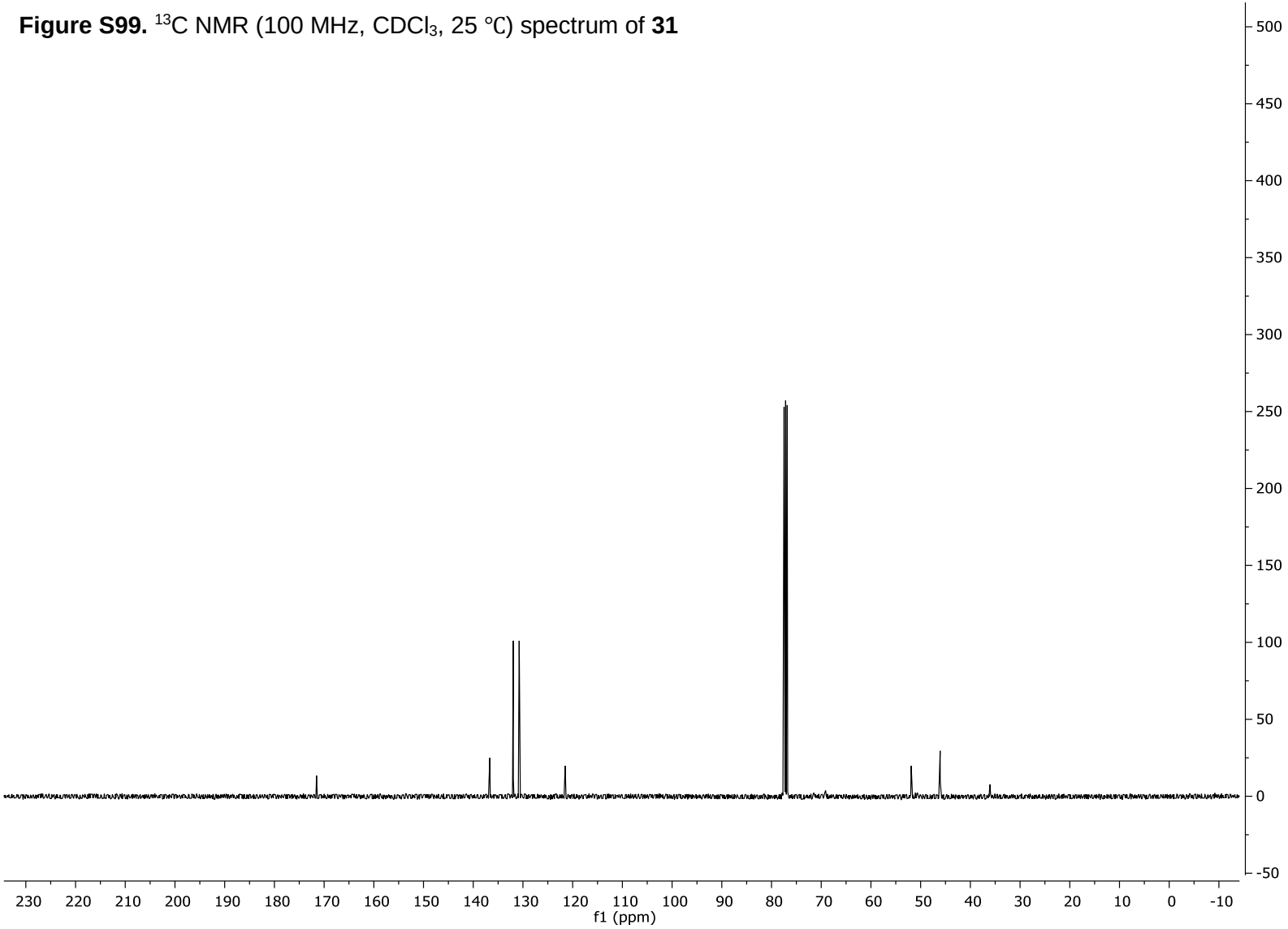

Figure S100. ^{1}H-^{1}H COSY (400 MHz, $CDCl_3$, 25 ℃) spectrum of **31**

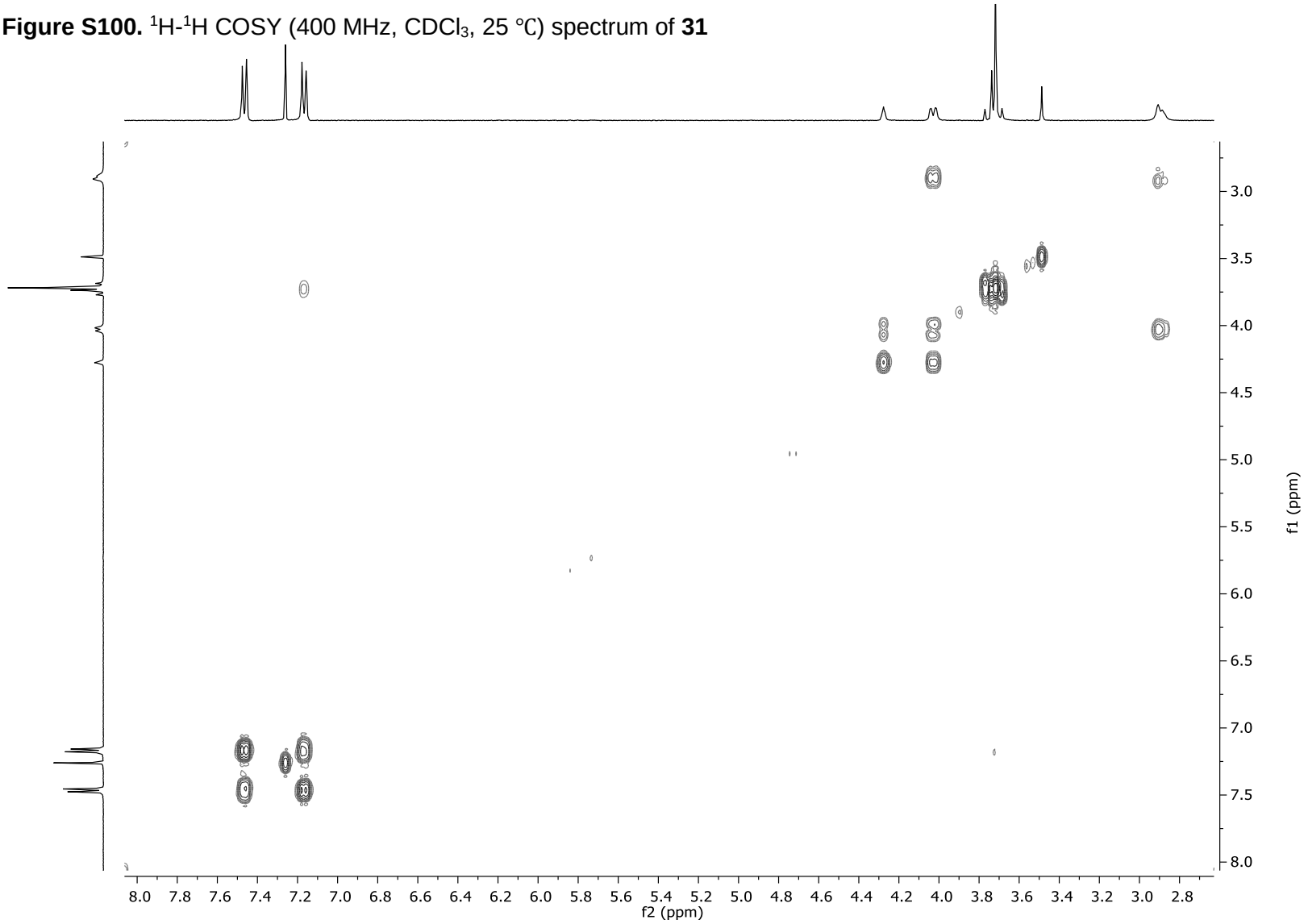

Figure S101. HSQC (400 MHz, $CDCl_3$, 25 ℃) spectrum of **31**

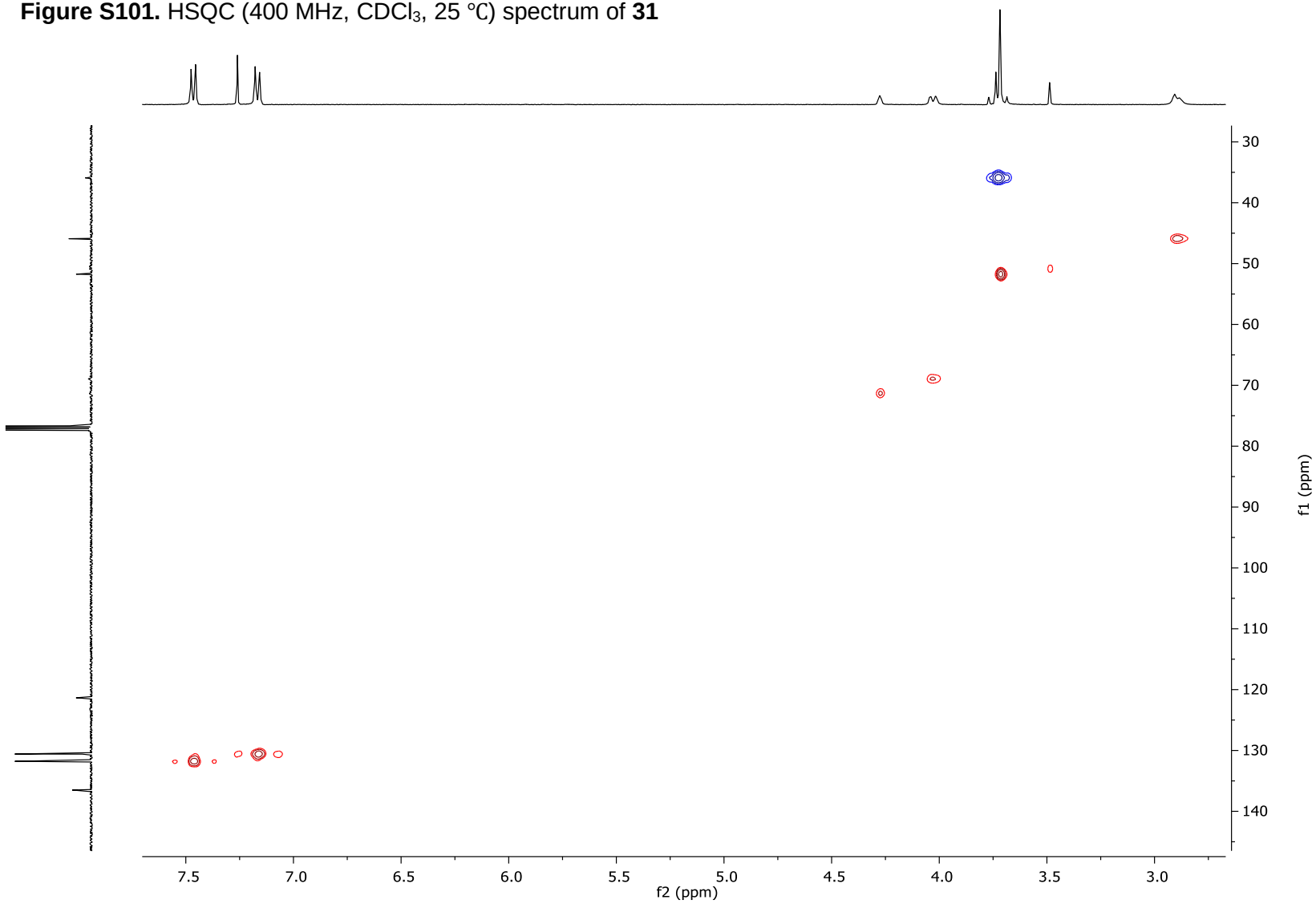

Figure S102. HMBC (400 MHz, $CDCl_3$, 25 ℃) spectrum of **31**

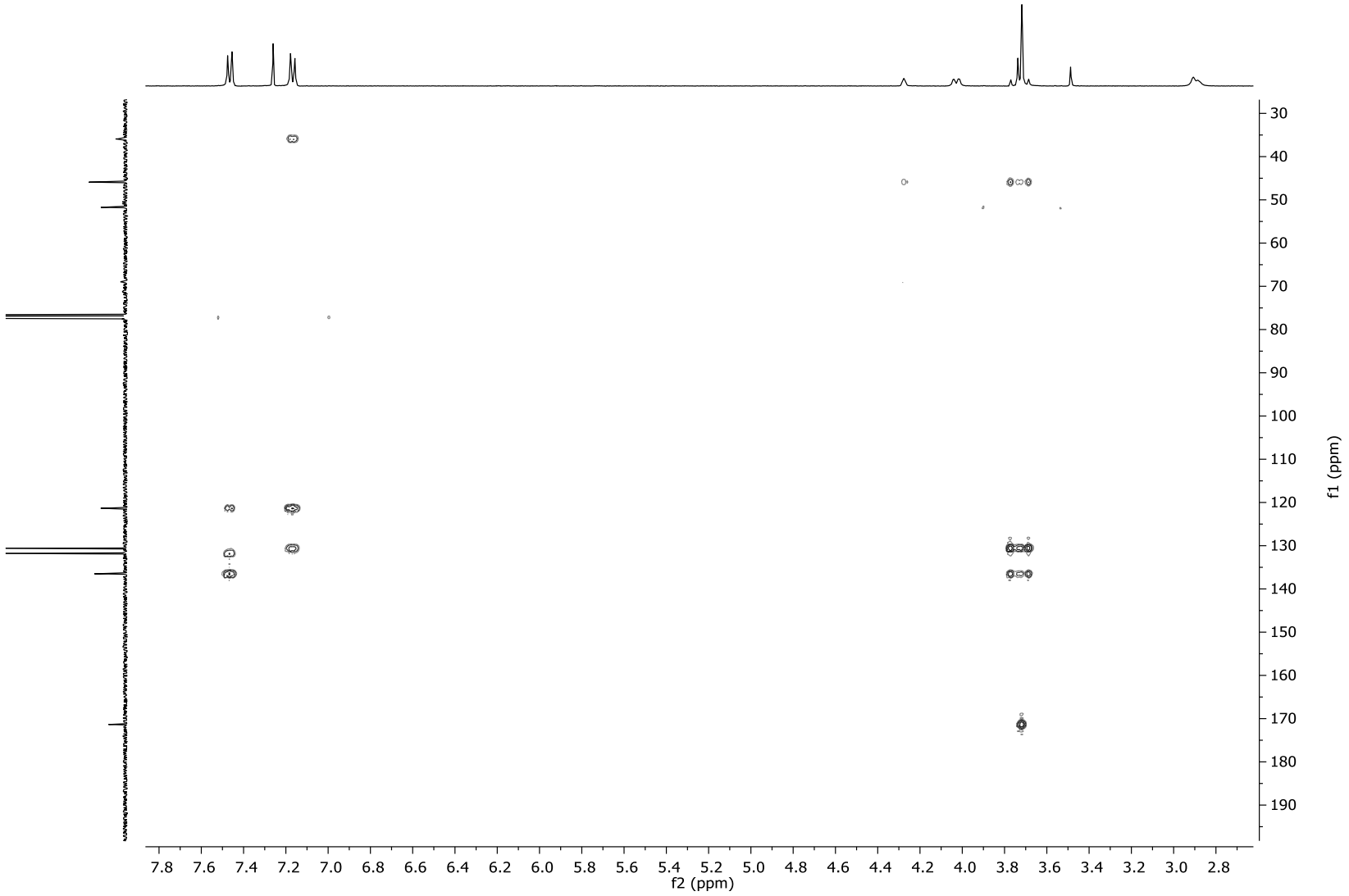

Figure S103. ^{1}H NMR (500 MHz, DMSO-d_6, 25 ℃) spectrum of **31**

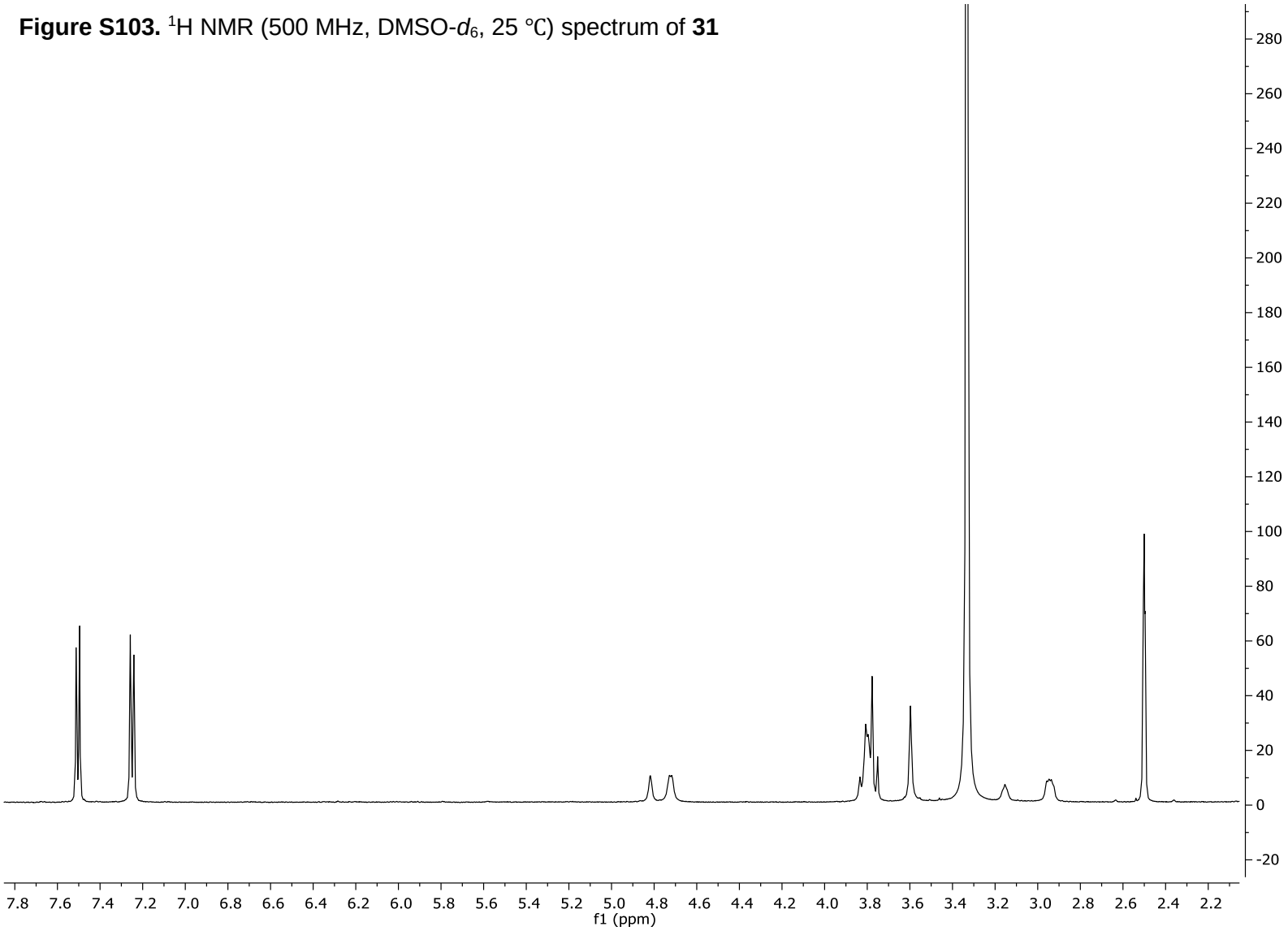

Figure S104. ^{1}H-^{1}H COSY (500 MHz, DMSO-d_6, 25 ℃) spectrum of **31**

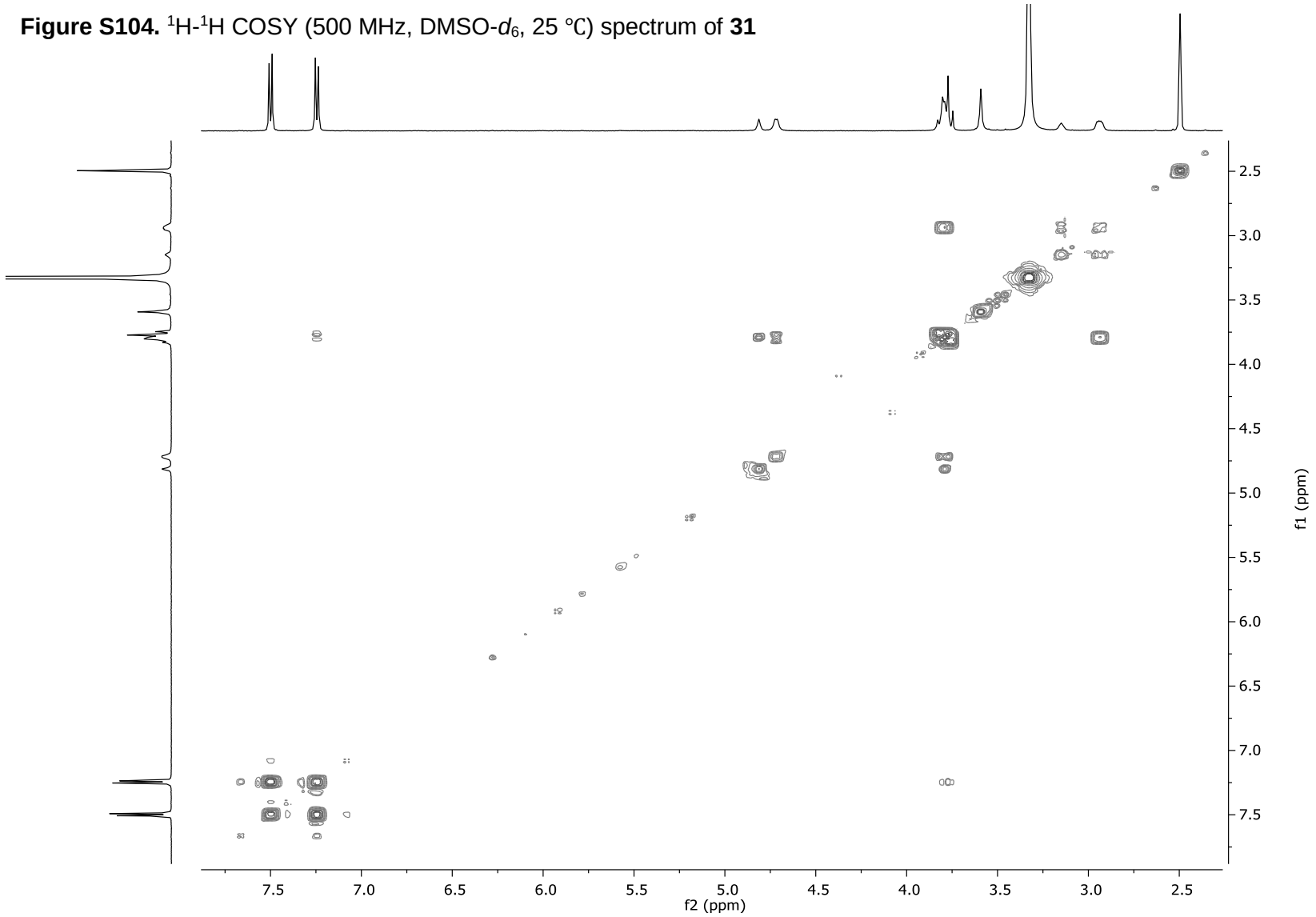

Figure S105. HSQC (500 MHz, DMSO-d_6, 25 ℃) spectrum of **31**

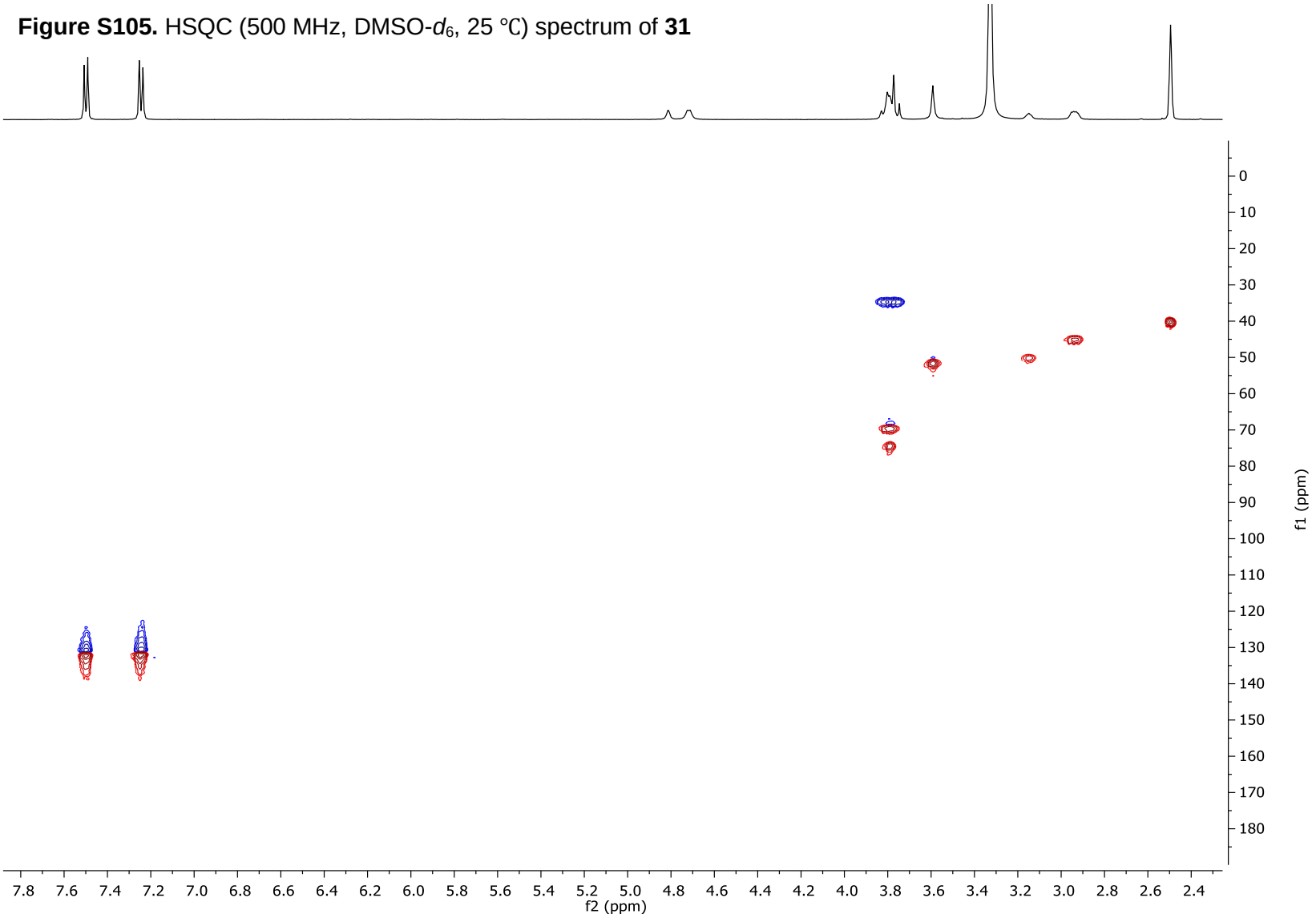

References

[1] L. Du, J. You, K. M. Nicholas, R. H. Cichewicz, *Angew Chem Int Ed Engl* **2016**, *55*, 4220-4225.

[2] Y. Usami, M. Ohsugi, K. Mizuki, H. Ichikawa, M. Arimoto, *Org Lett* **2009**, *11*, 2699-2701.

[3] a) E. S. Zhang, T. L. Xu, D. J. Wang, T. K. Huang, M. Yuan, J. Li, Y. Zou, *Rsc Adv* **2014**, *4*, 10022-10027; b) E. Valecchi, A. Tacchi, D. Prosperi, F. Compostella, L. Panza, *Synlett* **2004**, 2529-2532.

[4] K. Mizuki, K. Iwahashi, N. Murata, M. Ikeda, Y. Nakai, H. Yoneyama, S. Harusawa, Y. Usami, *Org Lett* **2014**, *16*, 3760-3763.

[5] a) Y. Usami, K. Mizuki, H. Ichikawa, M. Arimoto, *Tetrahedron-Asymmetr* **2008**, *19*, 1461-1464; b) Y. Usami, M. Ohsugi, K. Mizuki, H. Ichikawa, M. Arimoto, *Organic Letters* **2009**, *11*, 2699-2701.

[6] Y. Usami, K. Mizuki, *J Nat Prod* **2011**, *74*, 877-881.

[7] a) W. F. Wood, C. O. Fisher, G. A. Graham, *J Chem Ecol* **1993**, *19*, 837-841; b) W. F. Wood, *J Chem Ecol* **1990**, *16*, 2057-2065; c) W. F. Wood, C. G. Morgan, A. Miller, *J Chem Ecol* **1991**, *17*, 1415-1420.